Stable states in an unstable landscape: microbial resistance at the front line of climate change

Authors: Dylan Cronin[1†], Hannah Holland-Moritz[2†], Derek Smith[3†], Samuel T. N. Aroney[4†], Suzanne Hodgkins[1], Mikayla Borton[5], Yueh-Fen Li[1], Kieran Healy[6], IsoGenie Field & Analytic Teams 2010-2017, EMERGE Institute Coordinators, Malak M. Tfaily[7], Patrick Crill[8], Carmody K. McCalley[9], Kelly Wrighton[5], Ruth Varner[2], Gene W. Tyson[4*], Ben Woodcroft[4*], Sarah C. Bagby[3*], Jessica Ernakovich[2*], Virginia I. Rich[1*].

† These authors contributed equally to this work, * Corresponding authors

[1]The Ohio State University, Columbus, OH; [2]University of New Hampshire, Durham, NH; [3]Case Western Reserve University, Cleveland, OH; [4]Queensland University of Technology, Brisbane, AU; [5]Colorado State University, Fort Collins, CO; [6]Duke University, Durham, NC; [7]University of Arizona, Tucson, AZ; [8]Stockholm University, Stockholm, SE; [9]Rochester Institute of Technology, Rochester, NY

One Sentence Summary

In a warming permafrost peatland, microbiome shifts are concerted and correspond to habitat change, rather than proceeding gradually with rising temperature, with multiple lines of evidence indicating that this microbiome ecological resistance is linked to functional redundancy and high dispersal.

Abstract

Microbiome responses to warming may amplify or ameliorate terrestrial carbon loss and thus are a critical unknown in predicting climate outcomes. We quantified microbial warming response over seven years in a thawing permafrost peatland, using large-scale multi-omics data. We integrated analyses of organisms (via taxonomy), functions (via metabolic pathways and proteins), and community organization (via network structure and ecological assembly) to deeply characterize response mechanisms. This revealed unexpected and comprehensive microbiome stability. This resistance to change appeared bolstered by habitat-specific dispersal and community-level functional redundancy, particularly via versatile carbon generalists. Our findings challenge widespread assumptions of significant soil microbiome alteration with climate change, and reveal key genome-inferred processes that underlie microbiome stability. This suggests that future research should reorient towards critical habitat transitions.

Main Text

Introduction

Arctic permafrost peatlands, warming at a rate four times faster than the global average (*1*), contain globally significant reserves of soil organic carbon (*2*). This carbon's fate and flux dynamics as carbon dioxide (CO_2) or methane (CH_4) will determine these systems' feedbacks to climate change (*3*–*5*). Soil microbiota play a critical role in controlling these dynamics (*6*). While rising Arctic temperatures trigger cascading changes that alter microbial community structure, assembly, and metabolism (*7*–*9*), underlying mechanisms of microbial change remain elusive (*10*). Resolving whether gradual or concerted change dominates, and at what scale, is vital for establishing how climate models should represent these critical ecosystems (*11*, *12*). Furthermore, modeling microbial responses to climate change remains a highly consequential, active area of research (*13*).

One prevailing assumption is that climate change will significantly alter belowground microbiome community and structure, yet previous studies reveal that microbial responses are dependent on disturbance intensity, timeframe, and ecological conditions. This variation in response could be driven by differences in study design and disturbance intensity (observation vs. manipulation (*14*)), timeframe (few- vs. many-year (*15*, *16*); see supplemental textS1), and environmental setting (with the impact of weather, soil properties and depth, plant communities, and hydrology potentially outweighing climate warming impacts (*17*–*22*)). These differences may mask a broad pattern of gradual microbiome response to climate change or alternatively, may indicate unexpected microbiome stability, with infrequent observations of concerted change. Stability may arise from community resistance or resilience (supplemental textS2), potentially driven by functional stability and metabolic flexibility (*23*, *24*). This stability, in turn, could create a pattern of concerted rather than gradual change, with potential for profoundly different outcomes in climate-critical systems.

A landscape in transition

Here we address the consequences of permafrost thaw on belowground microbiomes at Stordalen Mire, a discontinuous permafrost peatland in northern Sweden (68° 21' N, 19° 20' E; supplemental textS3) that has been intensively studied over decades. As permafrost thaws, dry elevated palsas collapse to form partially thawed bogs and then fully thawed fens, whose extent has doubled over the past 50 years (*5*). Thaw changes redox conditions from predominantly oxic to anoxic, significantly altering plant, microbial, and viral community compositions (*5*, *7*, *9*, *25*–*27*) and increasing anaerobic microbial lineages and metabolisms, including methanogenesis (*9*, *26*). While thaw-driven habitat conversion in Arctic peatlands is highly visible and its microbial impacts are well documented (*5*, *7*, *9*, *25*–*27*), it is unknown if rising temperatures also induce gradual within-habitat changes in microbiome composition, structure, and function or if microbiomes are broadly stable outside of concerted habitat transitions.

To address this gap, we quantified community change in Stordalen's habitats through three genome-resolved lenses: *organisms* (across taxon ranks ranging from phylum to strain), *functions* (encoded metabolic pathways and proteins), and community *organization* (community network structure and mechanisms of ecological assembly). Our dataset of 199 metagenomes

(2.37 Tbp) and 66 metatranscriptomes (1.87 Tbp) captures seven years of progressive ~0.7°C/yr belowground warming for each habitat (2011-2017, Fig1A) at peak growing season in palsas, bogs, and fens (figS1). This period included significant interannual fluctuations in air temperature and water table depth (figS2) and encompassed four of the planet's hottest years (*28*). Given the strength of these study site fluctuations, due to widespread assumptions in the literature we expected that warming would induce gradual year-over-year changes detectable through all three lenses within each habitat. Contrary to our expectation, we consistently observed within-habitat microbiome stability and resistance to climatic changes across taxon ranks, metabolic functions, and community organization.

Microbiomes are resistant to increasing ground temperature

Microbiome composition and function resisted change over time

To evaluate microbiome changes, we reconstructed 13,290 metagenome-assembled genomes (MAGs) that represent 1,806 species-level taxa (i.e., clustered at 95% average nucleotide identity, Fig1A). Together these MAGs captured 73% of the community sequencing reads at genus-level [see Methods], which is high for natural systems. Read-mapping-based abundances revealed that microbial diversity and composition were resistant to change over seven years within habitat and depth (down to 39 cm) (Fig1A and Fig1B; tableS1). Very little variation in community composition could be accounted for by sample year at any level of resolution (strain: ≤3.0%, $p = 0.03$; genus: 1.6%, $p = 0.03$; phylum: 1.6%, $p = 0.005$) evaluated by distance-based redundancy analyses on single-copy marker genes (figS3; figS4). Similarly, in 75% of habitats and depths, genome-resolved community composition was not explained by time (p-value range: 0.22-0.79 Fig1B and Fig1C; figS5; figS6) and interannual fluctuation was significant only at certain depths in the fen (for 0-9, 20-29, and 30-39 cm, respectively: R^2: 0.35, 0.62, 0.81; p-value: 0.036, 0.048, 0.048; figS7). Only the deeper fen (30-39 cm) samples exhibited both significant non-directional inter-annual fluctuation (figS7) and directional change ($R^2 = 0.50$, $p = 0.012$) in community composition with time (Fig1C), and only 8 of 1,806 species were significantly correlated to time (Spearman rho ranging from -0.7 to 0.91, $p < 0.05$ figS8). The stability observed across a range of taxonomic granularities suggests that the microbial community is compositionally resistant over time and the rebounding of the fen community to its original state after 2013 suggests resilience (see supplemental textS4).

Encoded microbiome functions were similarly consistent within habitats over time (Fig1B&C). Beta diversity of community-wide protein clusters (a metric unconstrained by functional annotation), as well as manually-curated genome-resolved pathways of carbon, nitrogen, and sulfur metabolism did not significantly change over time within 92% of habitats and depths (Fig1C; figS9); the sole exception was 30-39 cm in the fen (R^2: 0.49-0.55, PERMANOVA, $p < 0.05$ Fig1B and Fig1C**;** figS9; figS10). At the finest level of functional annotation (MAG-specific specialization), individual functional guilds of organisms (e.g., methanogens, homoacetogens, fermenters, and macromolecule degraders) maintained similar abundances through time (figS11). (Expressed microbiome function was not used for temporal analysis due to discontinuity in the metatranscriptomic time series.) Thus, within the majority of Stordalen Mire habitats and depths, we observed both compositional and functional resistance to change over time across multiple levels of granularity.

Our third lens, microbial community organization, was also stable over time within habitat and depth. We used two distinct genome-resolved network approaches to understand the influence of soil biogeochemical conditions (weighted genome correlation network analysis (WGCNA)) and inter-microbe interactions (multilayer temporal networks (MTN)) on the organizational structure of the community with time. Habitat-specific WGCNA modules showed no linear correlation of community composition to time (Pearson, $p<0.05$) (table S3). MTN microbial co-occurrence networks indicated variability in specific organisms over time, yet the overall community network was resistant to change across different resolutions of network structure (Fig1C, Fig2B, figS12) ranging from coarse (whole network degree distribution) to fine (Jaccard similarity of triangles), suggesting that keystone taxa are stable (*29*). To understand if subcommunities of microbes were resilient over time, we calculated the temporal persistence of MTN subcommunities by categorizing each by the number of years it persisted (figS13). Persistent subcommunities (occurring in ≥ four of the seven years) accounted for a conservative estimate of 40% of the abundance-weighted community with time (depending on the interannual relax rate; figS14) indicating that while not all microbe-microbe interactions were stable from year to year, persistent clusters contributed extensively to community composition.

Finally, we sought to understand what ecological mechanisms may underlie the apparent stability in community organization and to ask if they were changing over time. We used beta-null modeling (*30*) to determine whether stochastic (dispersal and ecological drift) or deterministic (abiotic or biotic selection) processes drove community structure (figS15; figS16). A change in community assembly mechanisms over time could indicate a shift in the ecological pressures shaping the community (for example, increased selection due to changing ground temperature). Instead, beta-null modeling showed that while each habitat was governed by distinct assembly mechanisms (homogenizing selection in the palsa, homogenizing dispersal in the water-logged habitats), the ratio between deterministic and stochastic assembly processes within each habitat did not change with time (Mantel, $p > 0.05$) (Fig1B and Fig2C).

Microbiome composition and function had weak susceptibility to temperature

Finally, we explored the possibility that organisms, functions, and organization of the communities were being shaped by subtle or non-monotonic changes in abiotic drivers. Below we focus on temperature; see figS17 for other abiotic factors. After accounting for covariation between temperature and depth (strongest in palsa; figS18), genome-resolved community composition was slightly, but significantly, linearly correlated to ground temperature in bog and fen (Fig 1C, Bray-Curtis dissimilarity: partial mantel rho = 0.152 and 0.24, $p < 0.001$, respectively; tableS2) but not palsa. However, non-linear generalized additive models revealed that inclusion of habitat and depth removed any predictive relationship between community composition and temperature ($p = 0.4$; supplemental textS5), suggesting that the effect of temperature was weak. Ground temperature had no significant effect on carbon, nitrogen, or sulfur pathways in the palsa or bog, and on only xyloglucan degradation in the fen (supplemental textS5). While some WGCNA modules were significantly (Pearson, $p < 0.05$) correlated with temperature, all but one of these modules (figS19) were more strongly correlated with depth, echoing results from the models of community composition. Instead, WGCNA

174 modules were much more strongly correlated to carbon cycling metrics (e.g., $\delta^{13}C_{CO2}$, $\delta^{13}C_{CH4}$,
175 $\alpha_{CO2-CH4}$ (figS20; figS21)), consistent with previous work at the site (*9*, *26*, *27*, *31*, *32*), and other
176 features (e.g., pH and total nitrogen; figS22). No community assembly mechanisms were
177 related to ground temperature or air temperature (day-of-sampling or prior four weeks) (Mantel,
178 $p > 0.05$), implying that even with lag effects, temperature was not a strong selective or
179 stochastic force on community formation. As with temporal change, microbiome sensitivity to
180 temperature was strongest in the fen but weak overall and overshadowed by other abiotic
181 factors (depth, pH, and nutrient availability).
182
183 **Metabolic connections maintain stability**
184 *Carbon generalists are highly prevalent, and macromolecule degradation is widespread*
185 Microbiome capacity to degrade available organic matter determines the rate and form
186 of peat carbon loss to the atmosphere; therefore we sought to understand the prevalence and
187 ecological role of these organisms. Carbon generalists, which we defined as MAGs encoding ≥
188 3 alternative CAZyme pathways and ≥ 3 sugar degradation pathways (supplemental textS6;
189 figS23; figS24), were >80% of the community and taxonomically diverse across all three thaw
190 stages and nearly all depths. The prevalence of these metabolic generalists produced
191 community-level functional redundancy (figS37), with each CAZyme pathway encoded by a
192 median of 531 carbon generalists, and each sugar degradation pathway by a median of 253.
193 Macromolecule and sugar degradation dominated encoded and expressed pathways,
194 particularly in the palsa and bog where >84% of the abundance-weighted community encoded
195 and >50% expressed these pathways (Fig3A; Fig3C; figS9; figS25; figS26). Fermentation
196 pathways were also highly abundant (47-93% cumulative relative abundance) (Fig3A; figS9).
197 These sorts of acquisition-oriented carbon generalists are typical of cold peatlands and other
198 wetlands (*24*, *33*, *34*) and we hypothesize that these generalists confer resilience. As thaw
199 alters organic matter profiles and shifts redox conditions (*35*), functionally redundant carbon
200 generalists enable the community to continue exploiting changing carbon sources, yielding more
201 consistent downstream metabolites (e.g. for methanogenesis) even as environmental conditions
202 shift.
203
204 *Chitin degradation and nitrogen fixation offer alternative pathways to nitrogen acquisition*
205 Access to nitrogen is a fundamental constraint on microbial growth in northern peatlands
206 (figS27), where nitrogen is frequently limiting (*36*, *37*). We found organisms extensively used
207 two complementary nitrogen-acquisition pathways—nitrogen fixation and chitin degradation—
208 that may buffer a lack of preferred low-molecular-weight organic nitrogen compounds (*38*, *39*).
209 Nitrogen fixation increases the bioavailable nitrogen pool, benefiting diazotrophs directly and the
210 community indirectly (*40*). Up to 25% of the community encoded nitrogen fixation (compared to
211 ~0.3% in marine microbiomes (*41*)), and > 75% of encoding MAGs showed pathway expression
212 (figS28).
213
214 Pathways for degrading chitin ($(C_8H_{13}O_5N)_n$), the second most abundant biopolymer in
215 nature (*42*), were even more widespread. Chitin is insoluble so mobilization of this nitrogen pool
216 requires extracellular enzymes and many degradation pathways exist (figS29). At Stordalen
217 Mire, multiple chitin degradation pathways were ubiquitously encoded (abundance weighted

218 median 73%, range 45%–94%) and expressed (median 95% of encoding cells, range 59–100%
219 with one outlier sample at 5% (figS29)). Furthermore, organisms containing these functions
220 were closely linked to key environmental outputs (as Variable Importance in Projection (VIP)
221 members of WGCNA modules related to carbon and nitrogen cycling (figS20; figS21; figS22)).
222 In many aquatic and terrestrial environments, including peatlands, extracellular chitin
223 degradation products can facilitate commensal and cross-feeding interactions (*42*–*45*), which
224 may promote community stability (*46*) while buffering against fluctuations in low-molecular-
225 weight nitrogen availability. The ubiquity of both nitrogen fixation and chitin degradation
226 pathways, may confer resilience to nutrient fluctuations in these habitats.
227
228 *Active sulfur cycling and sulfur-containing polysaccharide degradation might be a critical control*
229 *on organic matter degradation*
230 Despite small environmental pools of sulfur species (*32*, *47*), sulfur cycling can control
231 organic matter degradation rates, particularly in the bog (*48*). We observed a range of sulfur
232 transformations across the thaw gradient (Fig3A). Habitat-wide expression of dissimilatory sulfur
233 oxidation and sulfate reduction (encoded pathway relative abundances ~25% and up to 10%,
234 respectively; figS30; figS31) suggest the presence of cryptic sulfur cycling, which can profoundly
235 influence system biogeochemistry (*49*). Interestingly, although all microbes require sulfur for
236 growth, we detected assimilatory sulfate reduction in only 25% (fen) to 50% (palsa, bog) of the
237 population (figS32). Our analysis of carbohydrate degradation suggests a novel hypothesis: that
238 community members may instead meet their sulfur requirements through CAZyme degradation
239 of sulfur-containing polysaccharides (figS33), known to be preferentially consumed from plant
240 organic matter (*32*). This novel linkage between the carbon and sulfur cycles in permafrost
241 peatlands is analogous to some marine isolates' ability to degrade sulfur polysaccharides and
242 thereby increase H_2, acetate, and sulfide concentrations (*50*, *51*).
243
244 *The flexible community of carbon generalists supports methanogenesis in the bog and fen*
245 Despite being markedly less metabolically flexible than carbon generalists (supplemental
246 textS6), several methanogens persisted through seven years of thaw-induced change
247 (Fig3C&D; supplemental textS7). Consistent with previous reports (*9*), methanogenesis—
248 primarily hydrogenotrophic—was encoded by a handful of MAGs (< 1%) in the bog and fen and
249 was highly expressed there (Fig3A). Acetoclastic and methylotrophic methanogenesis were
250 uncommon, with the former present only in the fen (Fig3A; figS25). Despite low abundances,
251 methanogens have an outsized impact on ecosystem output. For example, the
252 hydrogenotrophic methanogen *Ca.* 'Methanoflorens' spp. is a strong predictor of $\alpha_{CO2\text{-}CH4}$ (*9*, *26*),
253 which is an isotopic indicator of CH_4 metabolic pathways. Strikingly, WGCNA not only confirmed
254 this relationship but also identified thirteen non-methanogens (including multiple
255 *Acidimicrobiales*, *Terracidiphilus* and *Ca*. Acidiflorens) that were highly predictive of (VIP > 1.5)
256 and correlated to $\alpha_{CO2\text{-}CH4}$ (Spearman's rho, $p < 0.005$). These correlations were comparable to
257 or higher than that of *Ca.* 'M. stordalenmirensis' itself (Fig3C), suggesting that these
258 predominantly carbon-generalist, nitrogen-flexible lineages may be gatekeepers for
259 methanogenic carbon flux. For example, several of the *Ca*. 'Acidiflorens' spp. may supply H_2
260 and formate to *Ca.* 'M. stordalenmirensis' (*9*). Further, the MTN analysis showed *Ca*. 'M.
261 stordalenmirensis' is persistently associated with eight MAGs—all VIPs for [CO_2], $\delta^{13}C_{CO2}$, $\alpha_{CO2\text{-}}$

$_{CH4}$ and/or nitrogen content—from the same WGCNA module (Fig3D). These MAGs included the Dormibacterota *Ca*. 'Changshengia' spp., which was previously identified as highly correlated with the fraction of carbon mineralized to CO_2 vs. CH_4 in the bog (*9*). These diverse metabolic partnerships may increase stability by reducing substrate limitation for methanogens, as was seen in aquatic microbial communities (*52*, *53*).

From close analysis of the metabolic capabilities of methanogen-associated lineages, we propose a novel hypothesis that trading and acquisition of both nitrogen and carbon underlies these relationships. We observed that highly connected methanogens important to network structure (e.g., *Ca*. 'M. stordalenmirensis') typically lacked recognizable nitrogen-fixation or other nitrogen-linked decomposition pathways (supplemental textS7). Conversely, methanogens encoding and expressing nitrogen-fixation have fewer connections and appear to be more independent (see supplemental textS7; figS34; figS35; figS36). In other systems, methanogenesis expression (*54*) and CO_2 and CH_4 production increase with addition of chitin, which methanogens do not themselves degrade (*44*, *55*, *56*). Here, all eight persistent methanogen partners (Fig3D) encode and express chitin degradation. Furthermore, we identify a potential new linkage between methanogens and their partners through the reductive glycine pathway. This energy-conserving and amine-recycling carbon-fixation pathway, capable of producing methanogenesis substrates (pyruvate, acetate, and formate) and bioavailable nitrogen (as ammonia) (*57*, *58*), is encoded and expressed by five of the eight methanogen partners. These observations suggest a previously unrecognized role for nitrogen in metabolic interactions supporting methanogen persistence and activity in these ecosystems.

Habitat-specific microbiome resistance arises from functional redundancy and dispersal mediated by hydrologic connectivity

Stordalen Mire is warming, causing rapid permafrost thaw and habitat conversion (*5*), yet we observed within-habitat stability in microbiomes' organization, organisms, and functions. What ecological dynamics maintain the community's resistance and resilience to change (textS2)? We hypothesize that functional redundancy and homogenizing dispersal drive ecological resistance (Fig4).

Functional redundancy and functional similarity have been proposed to stabilize microbial communities (*59*). We saw strong signals of functional redundancy at both the community and the individual level: communities across the thaw gradient were dominated by diverse taxa encoding multiple alternative pathways for carbon and nitrogen acquisition (Fig3C; supplemental textS6; figS37; figS38; figS39). It is unclear if such abundance of versatile resource generalists is unusual or typical (*60*) (supplemental textS6). We argue that a "portfolio effect" (*61*, *62*) should operate at the individual as well as community level to smooth ecosystem outputs: under changing conditions, just as one lineage's decrease in efficiency may be compensated for by another's increase, maintaining community function, so can a metabolically versatile cell (i.e. with a broad portfolio of carbon/nitrogen-handling pathways) redirect metabolic flux under different conditions to maintain activity. Increased access via mobile genetic elements to genes providing metabolic versatility would further backstop these stabilizing forces (see companion paper by Guo et al.). If redundant pathways within redundant populations stabilize

communities, more narrowly distributed specialists (*24*) would be shielded from disturbance and the loss of taxa from critical functional groups.

Bog and fen microbiomes are likely further stabilized by homogenizing dispersal, i.e., dispersal high enough to result in a community that is more similar to a neighbor than would be expected by chance (Fig2c; Fig4; figS15; figS16). Dispersal dynamics are particularly important during disturbance, when dispersing organisms can determine ecosystem trajectory (*63*). Local dispersal can promote community resistance and resilience by “rescuing” disturbed communities, preventing cross-site divergence after local population reductions or extinctions (*23*, *64*). This is likely synergistic with functional redundancy and metabolic versatility, which improve the odds that dispersal will resupply organisms that fill key roles.

Conclusions

Ecological factors reinforce habitat resistance and resilience to gradual change (supplemental textS2), but enough disturbance can push communities into non-equilibrium dynamics and reassembly into a new community state (*64*–*66*). At Stordalen Mire, the surficial plant community reassembly makes habitat conversions detectable from space (Varner et al, co-submitted), but the dynamics of belowground change are unknown and not easy to remotely observe. Such knowledge gaps are a challenge in eco- and earth system climate models, which must calibrate the representation of microbial complexity (*11*) often in the absence of high-resolution datasets and parameter estimations (*13*, *67*). The analyses presented here demonstrate that, despite warming and landscape-scale change (*5*), habitat-specific microbiome complexity can be distilled to essential functions that are stable during peak growing season on a near-decadal timescale—supporting their representation in models.

Collectively, our findings challenge prevailing assumptions about microbial responses to climate change in critical permafrost ecosystems and offer new insights into processes underlying community stability. Our novel, integrated analysis over multiple levels of granularity for organismal ranks, metabolic functions, and community organization revealed little to no significant temporal change over seven years of progressive belowground warming. This analysis establishes a collection of metrics for assessing community response to environmental disturbance and a new standard of evidence that should be met before soil microbiome change is invoked. It also highlights that shorter-term or large disturbance experiments may incorrectly interpret fluctuating microbiome composition as longer-term temporal change. Critically, belowground microbial communities might be more resistant and resilient to temperature-induced climate change than previously thought, likely due to synergy between functional redundancy within communities and dispersal-mediated resupply of organisms encoding essential metabolic versatility.

Given that the three habitats’ microbiomes were stable and highly distinct over time—and across the landscape (Varner et al, co-submitted)—future sampling must target periods of habitat transition (figS2) when stabilizing capacity is exceeded. Further detailed study at spatial, temporal, and genetic resolutions not captured in this study may reveal other mechanisms of microbial response to changing conditions. For instance, spring and fall observations capturing

changing phenology may illuminate an erosion of stability driven by aboveground/belowground asynchronies. In addition, increased application of long-read sequencing may help resolve strain-level functional differences, including those mediated by the activity of mobile genetic elements. Despite these remaining unknowns, this work reveals the clear existence of stable habitats in a rapidly warming unstable Arctic landscape.

References and Notes

1. M. Rantanen, A. Y. Karpechko, A. Lipponen, K. Nordling, O. Hyvärinen, K. Ruosteenoja, T. Vihma, A. Laaksonen, The Arctic has warmed nearly four times faster than the globe since 1979. *Commun. Earth Environ.* **3**, 1–10 (2022).

2. E. A. G. Schuur, B. W. Abbott, R. Commane, J. Ernakovich, E. Euskirchen, G. Hugelius, G. Grosse, M. Jones, C. Koven, V. Leshyk, D. Lawrence, M. M. Loranty, M. Mauritz, D. Olefeldt, S. Natali, H. Rodenhizer, V. Salmon, C. Schädel, J. Strauss, C. Treat, M. Turetsky, Permafrost and Climate Change: Carbon Cycle Feedbacks From the Warming Arctic. *Annu. Rev. Environ. Resour.* **47**, 343–371 (2022).

3. G. Hugelius, J. Strauss, S. Zubrzycki, J. W. Harden, E. a. G. Schuur, C.-L. Ping, L. Schirrmeister, G. Grosse, G. J. Michaelson, C. D. Koven, J. A. O'Donnell, B. Elberling, U. Mishra, P. Camill, Z. Yu, J. Palmtag, P. Kuhry, Estimated stocks of circumpolar permafrost carbon with quantified uncertainty ranges and identified data gaps. *Biogeosciences* **11**, 6573–6593 (2014).

4. M. A. Kuhn, R. K. Varner, C. K. McCalley, C. R. Perryman, M. Aurela, S. A. Burke, J. P. Chanton, P. M. Crill, J. DelGreco, J. Deng, L. Heffernan, C. Herrick, S. B. Hodgkins, C. P. Jones, S. Juutinen, E. S. Kane, L. J. Lamit, T. Larmola, E. Lilleskov, D. Olefeldt, M. W. Palace, V. I. Rich, C. Schulze, J. H. Shorter, F. B. Sullivan, O. Sonnentag, M. R. Turetsky, M. P. Waldrop, Controls on Stable Methane Isotope Values in Northern Peatlands and Potential Shifts in Values Under Permafrost Thaw Scenarios. *J. Geophys. Res. Biogeosciences* **129**, e2023JG007837 (2024).

5. R. K. Varner, P. M. Crill, S. Frolking, C. K. McCalley, S. A. Burke, J. P. Chanton, M. E. Holmes, Isogenie Project Coordinators, S. Saleska, M. W. Palace, Permafrost thaw driven changes in hydrology and vegetation cover increase trace gas emissions and climate forcing in Stordalen Mire from 1970 to 2014. *Philos. Trans. R. Soc. Math. Phys. Eng. Sci.* **380**, 20210022 (2021).

6. J. K. Jansson, K. S. Hofmockel, Soil microbiomes and climate change. *Nat. Rev. Microbiol.* **18**, 35–46 (2020).

7. M. Hough, S. McCabe, S. R. Vining, E. Pickering Pedersen, R. M. Wilson, R. Lawrence, K.-Y. Chang, G. Bohrer, T. I. Coordinators, W. J. Riley, P. M. Crill, R. K. Varner, S. J. Blazewicz, E. Dorrepaal, M. M. Tfaily, S. R. Saleska, V. I. Rich, Coupling plant litter quantity to a novel metric for litter quality explains C storage changes in a thawing permafrost peatland. *Glob. Change Biol.* **28**, 950–968 (2022).

8. A. Persson, A. Hasan, J. Tang, P. Pilesjö, Modelling Flow Routing in Permafrost Landscapes with TWI: An Evaluation against Site-Specific Wetness Measurements. *Trans. GIS* **16**, 701–713 (2012).

9. B. J. Woodcroft, C. M. Singleton, J. A. Boyd, P. N. Evans, J. B. Emerson, A. A. F. Zayed, R. D. Hoelzle, T. O. Lamberton, C. K. McCalley, S. B. Hodgkins, R. M. Wilson, S. O. Purvine, C. D. Nicora, C. Li, S. Frolking, J. P. Chanton, P. M. Crill, S. R. Saleska, V. I. Rich, G. W. Tyson, Genome-centric view of carbon processing in thawing permafrost. *Nature* **560**, 49–54 (2018).

10. J. G. Ernakovich, R. A. Barbato, V. I. Rich, C. Schädel, R. E. Hewitt, S. J. Doherty, E. D. Whalen, B. W. Abbott, J. Barta, C. Biasi, C. L. Chabot, J. Hultman, C. Knoblauch, M. C. Y. L. Vetter, M. Leewis, S. Liebner, R. Mackelprang, T. C. Onstott, A. Richter, U. M. E. Schütte, H. M. P. Siljanen, N. Taş, I. Timling, T. A. Vishnivetskaya, M. P. Waldrop, M. Winkel, Microbiome assembly in thawing permafrost and its feedbacks to climate. *Glob. Change Biol.*, 5007–5026 (2022).

11. E. Kyker-Snowman, D. L. Lombardozzi, G. B. Bonan, S. J. Cheng, J. S. Dukes, S. D. Frey, E. M. Jacobs, R. McNellis, J. M. Rady, N. G. Smith, R. Q. Thomas, W. R. Wieder, A. S. Grandy, Increasing the spatial and temporal impact of ecological research: A roadmap for integrating a novel terrestrial process into an Earth system model. *Glob. Change Biol.* **28**, 665–684 (2022).

12. W. R. Wieder, G. B. Bonan, S. D. Allison, Global soil carbon projections are improved by modelling microbial processes. *Nat. Clim. Change* **3**, 909–912 (2013).

13. W. R. Wieder, S. D. Allison, E. A. Davidson, K. Georgiou, O. Hararuk, Y. He, F. Hopkins, Y. Luo, M. J. Smith, B. Sulman, K. Todd-Brown, Y. Wang, J. Xia, X. Xu, Explicitly representing soil microbial processes in Earth system models. *Glob. Biogeochem. Cycles* **29**, 1782–1800 (2015).

14. L. Wu, Y. Zhang, X. Guo, D. Ning, X. Zhou, J. Feng, M. M. Yuan, S. Liu, J. Guo, Z. Gao, J. Ma, J. Kuang, S. Jian, S. Han, Z. Yang, Y. Ouyang, Y. Fu, N. Xiao, X. Liu, L. Wu, A. Zhou, Y. Yang, J. M. Tiedje, J. Zhou, Reduction of microbial diversity in grassland soil is driven by long-term climate warming. *Nat. Microbiol.* **7**, 1054–1062 (2022).

15. J. Feng, C. Wang, J. Lei, Y. Yang, Q. Yan, X. Zhou, X. Tao, D. Ning, M. M. Yuan, Y. Qin, Z. J. Shi, X. Guo, Z. He, J. D. Van Nostrand, L. Wu, R. G. Bracho-Garillo, C. R. Penton, J. R. Cole, K. T. Konstantinidis, Y. Luo, E. A. G. Schuur, J. M. Tiedje, J. Zhou, Warming-induced permafrost thaw exacerbates tundra soil carbon decomposition mediated by microbial community. *Microbiome* **8**, 3 (2020).

16. K. Xue, M. M. Yuan, Z. J. Shi, Y. Qin, Y. Deng, L. Cheng, L. Wu, Z. He, J. D. Van Nostrand, R. Bracho, S. Natali, E. A. G. Schuur, C. Luo, K. T. Konstantinidis, Q. Wang, J. R. Cole, J. M. Tiedje, Y. Luo, J. Zhou, Tundra soil carbon is vulnerable to rapid microbial decomposition under climate warming. *Nat. Clim. Change* **6**, 595–600 (2016).

17. J. Curiel Yuste, A. J. Fernandez-Gonzalez, M. Fernandez-Lopez, R. Ogaya, J. Penuelas, J. Sardans, F. Lloret, Strong functional stability of soil microbial communities under semiarid Mediterranean conditions and subjected to long-term shifts in baseline precipitation. *Soil Biol. Biochem.* **69**, 223–233 (2014).

18. K. M. DeAngelis, G. Pold, B. D. Topçuoğlu, L. T. A. van Diepen, R. M. Varney, J. L. Blanchard, J. Melillo, S. D. Frey, Long-term forest soil warming alters microbial communities in temperate forest soils. *Front. Microbiol.* **6** (2015).

19. N. C. Dove, M. E. Barnes, K. Moreland, R. C. Graham, A. A. Berhe, S. C. Hart, Depth dependence of climatic controls on soil microbial community activity and composition. *ISME Commun.* **1**, 1–11 (2021).

20. J. L. M. Gutknecht, C. B. Field, T. C. Balser, Microbial communities and their responses to simulated global change fluctuate greatly over multiple years. *Glob. Change Biol.* **18**, 2256–2269 (2012).

21. S. Monteux, J. T. Weedon, G. Blume-Werry, K. Gavazov, V. E. J. Jassey, M. Johansson, F. Keuper, C. Olid, E. Dorrepaal, Long-term in situ permafrost thaw effects on bacterial communities and potential aerobic respiration. *ISME J.* **12**, 2129–2141 (2018).

22. K. Zhu, N. R. Chiariello, T. Tobeck, T. Fukami, C. B. Field, Nonlinear, interacting responses to climate limit grassland production under global change. *Proc. Natl. Acad. Sci.* **113**, 10589–10594 (2016).

23. F. De Vries, A. Shade, Controls on soil microbial community stability under climate change. *Front. Microbiol.* **4** (2013).

24. J. T. Weedon, G. A. Kowalchuk, R. Aerts, S. Freriks, W. F. M. Röling, P. M. van Bodegom, Compositional Stability of the Bacterial Community in a Climate-Sensitive Sub-Arctic Peatland. *Front. Microbiol.* **8** (2017).

25. J. B. Emerson, S. Roux, J. R. Brum, B. Bolduc, B. J. Woodcroft, H. B. Jang, C. M. Singleton, L. M. Solden, A. E. Naas, J. A. Boyd, S. B. Hodgkins, R. M. Wilson, G. Trubl, C. Li, S. Frolking, P. B. Pope, K. C. Wrighton, P. M. Crill, J. P. Chanton, S. R. Saleska, G. W. Tyson, V. I. Rich, M. B. Sullivan, Host-linked soil viral ecology along a permafrost thaw gradient. *Nat. Microbiol.* **3**, 870–880 (2018).

26. C. K. McCalley, B. J. Woodcroft, S. B. Hodgkins, R. A. Wehr, E.-H. Kim, R. Mondav, P. M. Crill, J. P. Chanton, V. I. Rich, G. W. Tyson, S. R. Saleska, Methane dynamics regulated by microbial community response to permafrost thaw. *Nature* **514**, 478–481 (2014).

27. R. Mondav, C. K. McCalley, S. B. Hodgkins, S. Frolking, S. R. Saleska, V. I. Rich, J. P. Chanton, P. M. Crill, Microbial network, phylogenetic diversity and community membership in the active layer across a permafrost thaw gradient. *Environ. Microbiol.* **19**, 3201–3218 (2017).

28. NOAA National Centers for Environmental Information, “NOAA National Centers for Environmental Information, Monthly Global Climate Report for Annual 2017” (Climate Monitoring Branch, DOC/NOAA/NESDIS/NCDC/, National Climatic Data Center, NESDIS, NOAA, U.S. Department of Commerce, 2018); https://www.ncei.noaa.gov/access/monitoring/monthly-report/global/201713.

29. S. Banerjee, K. Schlaeppi, M. G. A. van der Heijden, Keystone taxa as drivers of microbiome structure and functioning. *Nat. Rev. Microbiol.* **16**, 567–576 (2018).

30. J. C. Stegen, X. Lin, J. K. Fredrickson, X. Chen, D. W. Kennedy, C. J. Murray, M. L. Rockhold, A. Konopka, Quantifying community assembly processes and identifying features that impose them. *ISME J.* **7**, 2069–2079 (2013).

31. R. M. Wilson, M. M. Tfaily, M. Kolton, E. R. Johnston, C. Petro, C. A. Zalman, P. J. Hanson, H. M. Heyman, J. E. Kyle, D. W. Hoyt, E. K. Eder, S. O. Purvine, R. K. Kolka, S. D. Sebestyen, N. A. Griffiths, C. W. Schadt, J. K. Keller, S. D. Bridgham, J. P. Chanton, J. E. Kostka, Soil metabolome response to whole-ecosystem warming at the Spruce and Peatland Responses under Changing Environments experiment. *Proc. Natl. Acad. Sci.* **118**, e2004192118 (2021).

32. R. M. Wilson, M. A. Hough, B. A. Verbeke, S. B. Hodgkins, G. Tyson, M. B. Sullivan, E. Brodie, W. J. Riley, B. Woodcroft, C. McCalley, S. C. Dominguez, P. M. Crill, R. K. Varner, S. Frolking, W. T. Cooper, J. P. Chanton, S. D. Saleska, V. I. Rich, M. M. Tfaily, Plant organic matter inputs exert a strong control on soil organic matter decomposition in a thawing permafrost peatland. *Sci. Total Environ.* **820**, 152757 (2022).

33. A. M. Oliverio, A. B. Narrowe, J. A. Villa, C. Rinke, D. W. Hoyt, P. Liu, B. B. McGivern, E. K. Bechtold, J. B. Ellenbogen, R. A. Daly, G. J. Smith, J. C. Angle, R. M. Flynn, A. P. Freiburger, K. B. Louie, B. Stemple, T. R. Northen, C. Henry, C. S. Miller, T. H. Morin, G. Bohrer, M. A. Borton, K. C. Wrighton, Rendering the metabolic wiring powering wetland soil methane production. [Preprint] (2024). https://doi.org/10.1101/2024.02.06.579222.

34. A. T. Tveit, T. Urich, P. Frenzel, M. M. Svenning, Metabolic and trophic interactions modulate methane production by Arctic peat microbiota in response to warming. *Proc. Natl. Acad. Sci.* **112**, E2507–E2516 (2015).

35. S. B. Hodgkins, “Changes in organic matter chemistry and methanogenesis due to permafrost thaw in a subarctic peatland,” thesis, The Florida State University, United States -- Florida (2016).

36. E. Du, C. Terrer, A. F. A. Pellegrini, A. Ahlström, C. J. van Lissa, X. Zhao, N. Xia, X. Wu, R. B. Jackson, Global patterns of terrestrial nitrogen and phosphorus limitation. *Nat. Geosci.* **13**, 221–226 (2020).

37. J. J. Elser, M. E. S. Bracken, E. E. Cleland, D. S. Gruner, W. S. Harpole, H. Hillebrand, J. T. Ngai, E. W. Seabloom, J. B. Shurin, J. E. Smith, Global analysis of nitrogen and phosphorus limitation of primary producers in freshwater, marine and terrestrial ecosystems. *Ecol. Lett.* **10**, 1135–1142 (2007).

38. E. B. Graham, F. Yang, S. Bell, K. S. Hofmockel, High Genetic Potential for Proteolytic Decomposition in Northern Peatland Ecosystems. *Appl. Environ. Microbiol.* **85** (2019).

39. J. S. Norman, M. L. Friesen, Complex N acquisition by soil diazotrophs: how the ability to release exoenzymes affects N fixation by terrestrial free-living diazotrophs. *ISME J.* **11**, 315–326 (2017).

40. B. A. Lerch, D. A. Smith, T. Koffel, S. C. Bagby, K. C. Abbott, How public can public goods be? Environmental context shapes the evolutionary ecology of partially private goods. *PLOS Comput. Biol.* **18**, e1010666 (2022).

41. T. O. Delmont, C. Quince, A. Shaiber, Ö. C. Esen, S. T. Lee, M. S. Rappé, S. L. McLellan, S. Lücker, A. M. Eren, Nitrogen-fixing populations of Planctomycetes and Proteobacteria are abundant in surface ocean metagenomes. *Nat. Microbiol.* **3**, 804–813 (2018).

42. S. Beier, S. Bertilsson, Bacterial chitin degradation—mechanisms and ecophysiological strategies. *Front. Microbiol.* **4** (2013).

43. S. E. Belova, N. V. Ravin, T. A. Pankratov, A. L. Rakitin, A. A. Ivanova, A. V. Beletsky, A. V. Mardanov, J. S. Sinninghe Damsté, S. N. Dedysh, Hydrolytic Capabilities as a Key to Environmental Success: Chitinolytic and Cellulolytic Acidobacteria From Acidic Sub-arctic Soils and Boreal Peatlands. *Front. Microbiol.* **9** (2018).

44. C. De Tender, B. Mesuere, F. Van der Jeugt, A. Haegeman, T. Ruttink, B. Vandecasteele, P. Dawyndt, J. Debode, E. E. Kuramae, Peat substrate amended with chitin modulates the N-cycle, siderophore and chitinase responses in the lettuce rhizobiome. *Sci. Rep.* **9**, 9890 (2019).

45. M. B. Kaczmarek, K. Struszczyk-Swita, X. Li, M. Szczęsna-Antczak, M. Daroch, Enzymatic Modifications of Chitin, Chitosan, and Chitooligosaccharides. *Front. Bioeng. Biotechnol.* **7** (2019).

46. W. Lopes, D. R. Amor, J. Gore, Cooperative growth in microbial communities is a driver of multistability. *Nat. Commun.* **15**, 4709 (2024).

47. C. R. Perryman, C. K. McCalley, A. Malhotra, M. F. Fahnestock, N. N. Kashi, J. G. Bryce, R. Giesler, R. K. Varner, Thaw Transitions and Redox Conditions Drive Methane Oxidation in a Permafrost Peatland. *J. Geophys. Res. Biogeosciences* **125**, e2019JG005526 (2020).

48. V. Freire-Zapata, H. Holland-Moritz, D. R. Cronin, S. Aroney, D. A. Smith, R. M. Wilson, J. G. Ernakovich, B. J. Woodcroft, S. C. Bagby, EMERGE 2012 Field Team, S. B. Hodgkins, R. Mondav, EMERGE Biology Integration Coordinators, J. E. Cross, M. F. Fahnestock, R. Ferriere, M. Ibba, S. R. Saleska, R. K. Varner, A. A. Zayed, V. I. Rich, M. B. Sullivan, J. C. Stegen, M. M. Tfaily, Microbiome–metabolite linkages drive greenhouse gas dynamics over a permafrost thaw gradient. *Nat. Microbiol.*, doi: 10.1038/s41564-024-01800-z (2024).

49. D. E. Canfield, F. J. Stewart, B. Thamdrup, L. De Brabandere, T. Dalsgaard, E. F. Delong, N. P. Revsbech, O. Ulloa, A Cryptic Sulfur Cycle in Oxygen-Minimum–Zone Waters off the Chilean Coast. *Science* **330**, 1375–1378 (2010).

50. W. Helbert, Marine Polysaccharide Sulfatases. *Front. Mar. Sci.* **4** (2017).

51. D. M. Van Vliet, S. Palakawong Na Ayudthaya, S. Diop, L. Villanueva, A. J. M. Stams, I. Sánchez-Andrea, Anaerobic Degradation of Sulfated Polysaccharides by Two Novel Kiritimatiellales Strains Isolated From Black Sea Sediment. *Front. Microbiol.* **10**, 253 (2019).

52. D. Ciccarese, G. Micali, B. Borer, C. Ruan, D. Or, D. R. Johnson, Rare and localized events stabilize microbial community composition and patterns of spatial self-organization in a fluctuating environment. *ISME J.* **16**, 1453–1463 (2022).

53. M. Embree, J. K. Liu, M. M. Al-Bassam, K. Zengler, Networks of energetic and metabolic

interactions define dynamics in microbial communities. *Proc. Natl. Acad. Sci.* **112**, 15450–15455 (2015).

54. A. A. Ivanova, C.-E. Wegner, Y. Kim, W. Liesack, S. N. Dedysh, Identification of microbial populations driving biopolymer degradation in acidic peatlands by metatranscriptomic analysis. *Mol. Ecol.* **25**, 4818–4835 (2016).

55. H. Kang, C. Freeman, S. Soon park, J. Chun, N-Acetylglucosaminidase activities in wetlands: a global survey. *Hydrobiologia* **532**, 103–110 (2005).

56. S. Wörner, M. Pester, Microbial Succession of Anaerobic Chitin Degradation in Freshwater Sediments. *Appl. Environ. Microbiol.* **85**, e00963-19 (2019).

57. P. N. Evans, J. A. Boyd, A. O. Leu, B. J. Woodcroft, D. H. Parks, P. Hugenholtz, G. W. Tyson, An evolving view of methane metabolism in the Archaea. *Nat. Rev. Microbiol.* **17**, 219–232 (2019).

58. I. Sánchez-Andrea, I. A. Guedes, B. Hornung, S. Boeren, C. E. Lawson, D. Z. Sousa, A. Bar-Even, N. J. Claassens, A. J. M. Stams, The reductive glycine pathway allows autotrophic growth of Desulfovibrio desulfuricans. *Nat. Commun.* **11**, 5090 (2020).

59. S. D. Allison, J. B. H. Martiny, Resistance, resilience, and redundancy in microbial communities. *Proc. Natl. Acad. Sci.* **105**, 11512–11519 (2008).

60. T. H. Bell, T. Bell, Many roads to bacterial generalism. *FEMS Microbiol. Ecol.* **97**, fiaa240 (2020).

61. D. F. Doak, D. Bigger, E. K. Harding, M. A. Marvier, R. E. O'Malley, D. Thomson, The Statistical Inevitability of Stability-Diversity Relationships in Community Ecology. *Am. Nat.* **151**, 264–276 (1998).

62. L. M. Thibaut, S. R. Connolly, Understanding diversity–stability relationships: towards a unified model of portfolio effects. *Ecol. Lett.* **16**, 140–150 (2013).

63. J. HilleRisLambers, P. B. Adler, W. S. Harpole, J. M. Levine, M. M. Mayfield, Rethinking Community Assembly through the Lens of Coexistence Theory. *Annu. Rev. Ecol. Evol. Syst.* **43**, 227–248 (2012).

64. A. Shade, H. Peter, S. Allison, D. Baho, M. Berga, H. Buergmann, D. Huber, S. Langenheder, J. Lennon, J. Martiny, K. Matulich, T. Schmidt, J. Handelsman, Fundamentals of Microbial Community Resistance and Resilience. *Front. Microbiol.* **3** (2012).

65. C. Chang, J. HilleRisLambers, Integrating succession and community assembly perspectives. *F1000Research* **5**, 2294 (2016).

66. A. Fofana, D. Anderson, C. K. McCalley, S. Hodgkins, R. M. Wilson, D. Cronin, N. Raab, M. Torabi, R. K. Varner, P. Crill, S. R. Saleska, J. P. Chanton, M. M. Tfaily, V. I. Rich, Mapping substrate use across a permafrost thaw gradient. *Soil Biol. Biochem.* **175**, 108809 (2022).

67. K.-Y. Chang, W. J. Riley, E. L. Brodie, C. K. McCalley, P. M. Crill, R. F. Grant, Methane Production Pathway Regulated Proximally by Substrate Availability and Distally by Temperature in a High-Latitude Mire Complex. *J. Geophys. Res. Biogeosciences* **124**, 3057–3074 (2019).

Acknowledgments

Non-author contributions:

This study has been made possible by data provided by Abisko Scientific Research Station and the Swedish Infrastructure for Ecosystem Science (SITES) as well as the Swedish Polar Research Secretariat. We thank the Swedish Polar Research Secretariat and SITES for the support of the work done at the Abisko Scientific Research Station. A portion of this analysis and non-monetary technical support was also provided through the U.S. Department of Energy user facilities programs. Computational work was supported in part by an allocation of computing time from the Ohio Supercomputer Center. Lastly, we thank contracted science artist Elena Hartley for co-development of Figure 4.

Funding: We thank the many funding sources of this work, including:

- US National Science Foundation, Biology Integration Institutes Program, Award # 2022070 (VIR and RKV, with SH, MMT, GWT, BW, JE, SCB, and the EMERGE Institute Coordinators)
- Genomic Science Program of the United States Department of Energy Office of Biological and Environmental Research (BER), grants DE-SC0004632, DE-SC0010580 and DE-SC0016440 (SRS and VIR, with GWT, MMT). Associated with the third of these was a BER Support Science award (Proposal #503530 DOI: 10.46936/10.25585/60001148) for nucleic acid sequencing for a portion of these samples, conducted by the U.S. Department of Energy Joint Genome Institute (https://ror.org/04xm1d337), a DOE Office of Science User Facility supported by the Office of Science of the U.S. Department of Energy under Contract No. DE-AC02-05CH11231.
- US National Science Foundation MacroSystems Program, Award # NSF EF 1241037 (RV).
- US National Science Foundation Research for Undergraduates Program, the Northern Ecosystems Research for Undergraduates, Award # NSF REU EAR 1063037 (RV)
- Nucleic acid sequencing and and dissolved organic matter fourier transform ion cyclotron resonance mass spectrometry were partially supported by a Facilities Integrating Collaborations for User Science (FICUS) awards, DOI: 10.46936/fics.proj.2016.49521/60006018 and 503547, which used resources at the DOE Joint Genome Institute (https://ror.org/04xm1d337) and the Environmental Molecular Sciences Laboratory (https://ror.org/04rc0xn13), which are DOE Office of Science User Facilities. Both facilities are sponsored by the Office of Biological and Environmental Research and operated under Contract Nos. DE-AC02-05CH11231 (JGI) and DE-AC05-76RL01830 (EMSL).
- SITES is supported by the Swedish Research Council's grant 4.3-2021-00164

Author Contributions: DC, SA, DS, and HH-M all contributed equally to this work. Co-first authors have the right to list their name first in their CV. In addition, VR, SB, GT, BW, and JE are all co-senior authors and contributed equally to this work, order was paired with first author order and all may list their name last on their CV. Following the CRediT model, authors made the following contributions

Conceptualization - VR, CM, SH, RV, EMERGE Institute Coordinators, DC, HH-M, DS, SA, JE, SB, BW, MT, PC
Data Curation - DC, HH-M, DS, SA, VR, BW, SH, FL, RV
Formal Analysis - DC, HH-M, DS, SA, CM, KW, MB, IsoGenie Field & Analytic Teams 2011-2017
Funding acquisition - VR, JE, SB, BW, GT, KW, SH, RV, EMERGE Institute Coordinators, MT, PC
Investigation - DC, HH-M, DS, SA, CM, SH, FL, RV, IsoGenie Field & Analytic Teams 2011-2017, PC
Methodology Development - DC, HH-M, DS, SA, VR, PC
Project Administration - DC, HH-M, DS, SA, VR, JE, SB, BW, GT, KW, SH, RV, EMERGE Institute Coordinators, PC
Resources Provision - VR, KW, SH, RV, EMERGE Institute Coordinators, PC
Software Programming - DC, HH-M, SA, KW, MB, SH
Supervision Oversight - VR, JE, KW, RV, MT
Validation Verification- SA, DC, HH-M
Visualization - DC, HH-M, DS, SA, VR, SB, KH
Writing - DC, HH-M, DS, SA, VR, JE, SB, BW, GT, CM, KW, MB, SH, FL, RV, IsoGenie Field & Analytic Teams 2011-2017, EMERGE Institute Coordinators, KH, MT, PC

Competing interests: Authors declare that they have no competing interests.

Data and materials availability:
Sample Metadata Sheet v1.0.0, containing field sample information and geochemical measurements are available on Zenodo at https://zenodo.org/records/12827096. Gas flux measurements are available on Zenodo at https://doi.org/10.5281/zenodo.13377109 and https://emerge-db.asc.ohio-state.edu/datasources/0138_DailyFlux_20122018. Temperature and water table summary for lagged effects analysis are available on Zenodo at https://doi.org/10.5281/zenodo.14189390. Water table depth measurements used for determining lagged effects are available on Zenodo at https://doi.org/10.5281/zenodo.10420396. ANS temperature measurements used in supplemental (figS2) were recorded at the Abisko Scientific Research Station (ANS), Sveriges meteorologiska och hydrologiska institut (SMHI). (2024). Meteorological data from Abisko Observatory (Abisko: station 188800), daily mean air temperatures, 2011-2017. Retrieved [05/30/2024], from https://www.smhi.se/data/meteorologi/ladda-ner-meteorologiska-observationer#stationid=188800.

All metagenomes and metatranscriptomes used in this study are available in NCBI under the umbrella BioProject PRJNA888099. SRA accessions for the reads used for the interannual microbiome comparisons are listed in SuppTable_temporal-paper_reads, and those used to generate the MAGs are listed in the metadata table accompanying those MAGs (https://doi.org/10.5281/zenodo.13901514). Metagenome-assembled genomes (MAGs) are

available in Zenodo at https://doi.org/10.5281/zenodo.13901514.

Figures

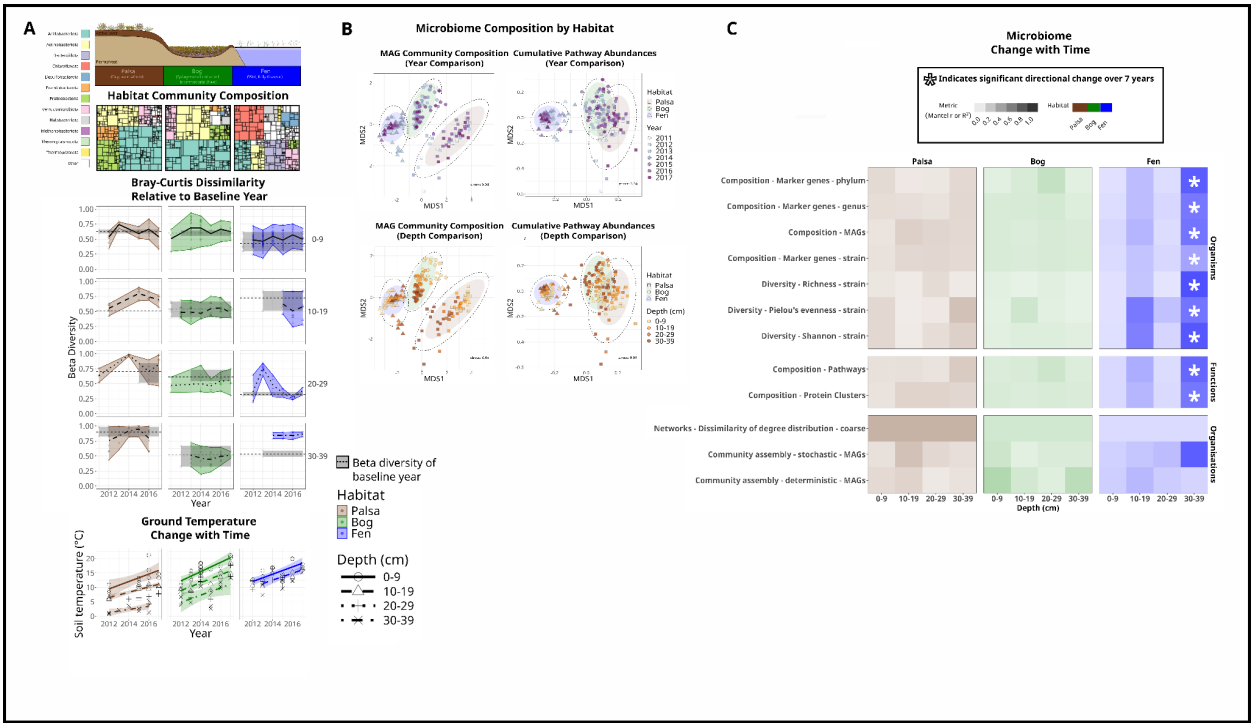

Figure 1: Stordalen Mire microbiomes resist temporal change. A) The three main thaw-gradient habitats (palsas, bogs, and fens; colored throughout as brown, green and blue, respectively) host microbiomes with distinct taxonomy (treemap with dereplicated MAGs as rectangles, colored by phyla and sized proportional to relative abundance). Microbiome beta diversity did not change significantly with time (middle panels); each point is one microbiome's average Bray-Curtis dissimilarity to those at the same depth for the earliest baseline year (2011, or the first year for which at least two depth-matched microbiomes were available). Black lines are the running dissimilarity average. Reference-year microbiomes' within-year dissimilarities are indicated by gray dots, with their ranges and averages extended as shaded gray bars and dashed lines, respectively. Soil temperatures increased significantly with time (lines indicate significant linear relationships, $p<0.05$, lowest panel). **B)** Habitat and depth structure microbiome beta diversity data more strongly than year, observed in non-metric multidimensional scaling (NMDS) ordinations of each sample's MAG-based taxonomic (left

767 panels) and functional (right panels) composition, colored by year (upper panel) or depth (lower
768 panel). Habitats are denoted by shape (palsa, square; bog, circle; fen, triangle) and demarcated
769 by ellipses (dashed-line ellipses reflect each habitat's multivariate normal distribution, while
770 shaded ellipses are the multivariate t-distribution). Functions are cumulative pathway
771 abundances: each complete pathway observed in a MAG was weighted by that MAG's relative
772 abundance, then all occurrences are summed for each pathway. **C)** Granular heatmap of
773 microbiome temporal change, in each habitat and depth. Change was assessed spanning
774 organisms (from phylum to strains diversity metrics, both single copy marker genes and MAGs),
775 functions (from pathways to protein clusters, both annotatable and non-annotatable), and
776 organization (both network structure and community assembly metrics of stochasticity and
777 determinism). The amount of variation explained by time (as Mantel R or R^2 depending on
778 statistical test appropriate for each data type; see Methods) is indicated with the intensity of the
779 shaded color; white asterisks denote significant correlations to time. Across all granularities
780 surveyed only deeper fen (30-39 cm) showed significant change over time.
781
782
783
784
785
786
787
788

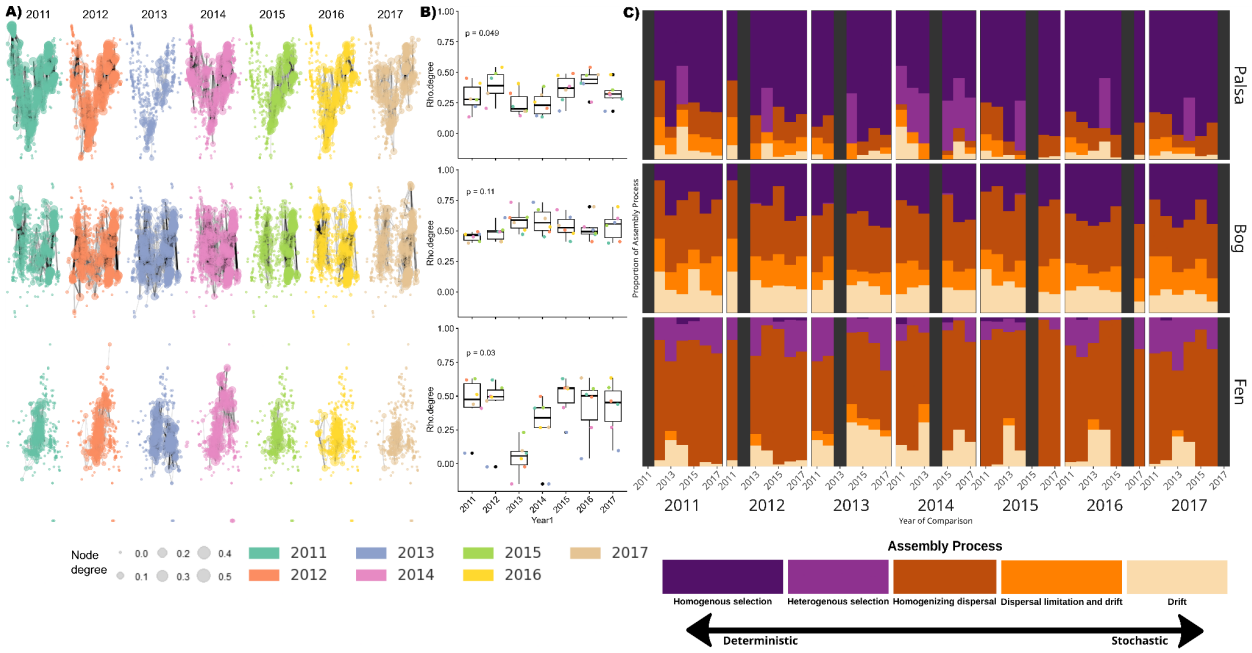

Figure 2: Microbiome organization is consistent within habitats over time. A) Multilayer temporal networks depict correlations between MAGs within annual networks for each habitat. Each network layer corresponds to a specific year, with nodes representing MAGs. Black edges represent significant ($p < 0.05$) correlations (>0.3) between MAGs within the same habitat and year, while node size reflects node degree (the number of connections for that node) within its respective layer (year). **B)** Pairwise interyear correlations (Spearman's rho) in network node degree (x-axis, base year; colored points, comparison years) within each habitat. Note that the fen's recovery to a near-stable state after 2013 suggests strong resilience in this habitat. **C)** Assembly processes detected within each habitat (rows) by βNTI and RCBC modeling in interyear comparisons. For each year, columns show pairwise comparisons to all other years (self-comparisons are obscured by black bars). Stacked bar colors denote the proportion of different assembly processes detected in each pairwise comparison, revealing overall stability in assembly within habitats over time.

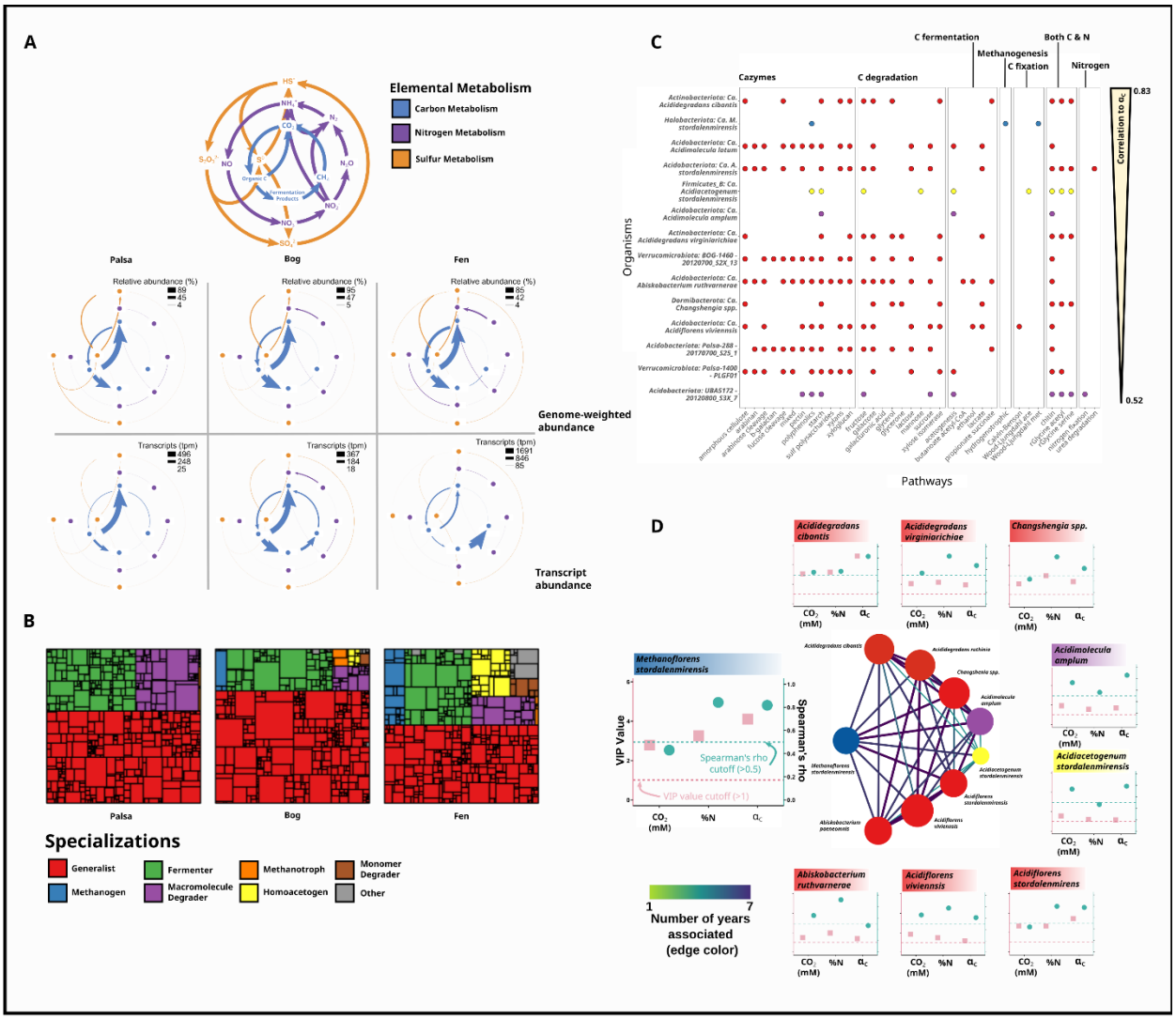

806

807 **Figure 3: Microbiome metabolisms across the thaw gradient are interlinked by carbon,**
808 **nitrogen, and sulfur cycling. A)** Aggregated over the study period, key pathways in carbon,
809 nitrogen, and sulfur metabolism (top center), metagenomic (middle row) and metatranscriptomic
810 (bottom row) data show differences in microbial investment in methanotrophy and carbon
811 fixation, nitrogen fixation, and sulfur redox cycling. **B)** Functional composition of palsa, bog, and
812 fen communities. Treemap rectangles are MAGs colored by carbon metabolic specialization and
813 scaled by relative abundance. **C)** Metabolic capabilities of MAGs belonging to the weighted
814 genome correlation network analysis (WGCNA) module correlated with the isotopic fractionation
815 of carbon between carbon dioxide and methane carbon ($\alpha_{CO2\text{-}CH4}$) in the bog. Carbon and

816 nitrogen-related metapathways present in these MAGs. MAGs are colored by carbon metabolic
817 specialization (see panel B) and ordered by VIP score. **D)** Bog network structure of the
818 persistent subcommunity of MAGs connected to *Ca.* 'M. stordalenmirensis' in multi-layer
819 temporal network (MTN) modeling. MAGs were included if they maintained a connection to *Ca.*
820 'M. stordalenmirensis' for at least six years and had a VIP score > 1 and a correlation > 0.5 in at
821 least one metric. MAGs are colored by carbon metabolic specialization (see panel B). Edge
822 color represents the number of years MAGs were connected to *Ca.* 'M. stordalenmirensis'.
823 Subplots show the Spearman correlation coefficient (rho) of each MAG to key environmental
824 variables (teal) and their VIP value (pink).

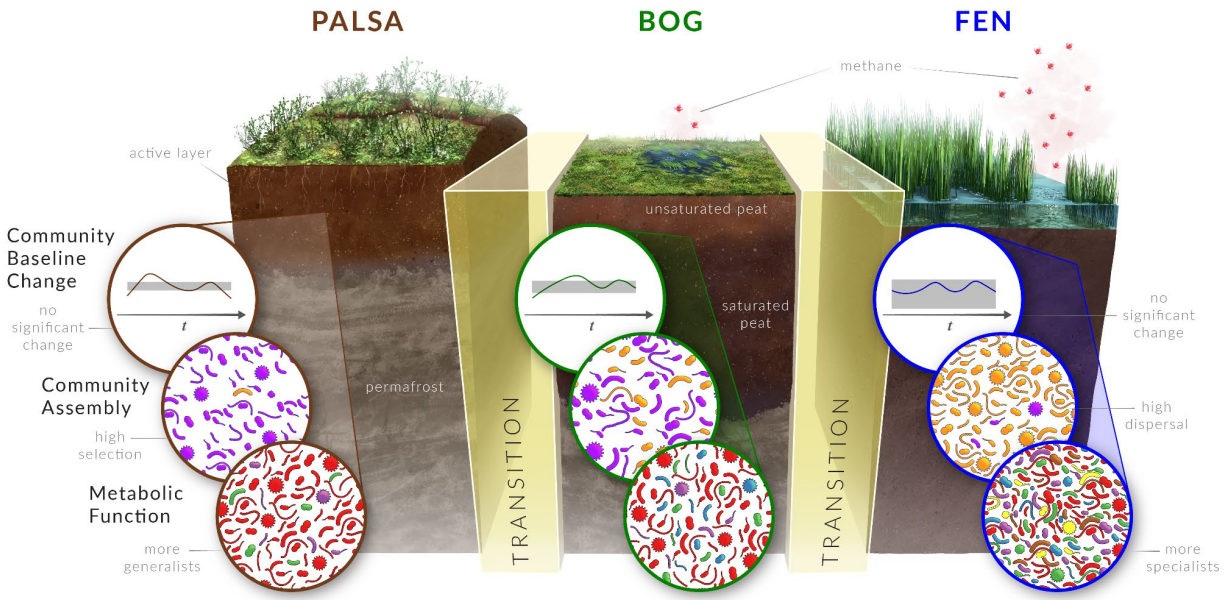

Figure 4: Within-habitat communities resist change until increasing environmental pressures trigger a concerted transition along the thaw gradient. Community composition fluctuates but does not change steadily with time in each habitat. Population density increases in tandem with water saturation (*9*). Across the thaw gradient, ecological assembly shifts from predominantly deterministic processes in the palsa (community assembly, purple) to predominantly stochastic processes in the fen (orange), while the balance of functional specializations shifts from predominantly generalists (red) to a more metabolically diverse range of specialists. We hypothesize that functional redundancy, dispersal (bog, fen), and metabolic versatility (palsa, bog) drive within-habitat ecological resistance.

Supplemental Text

Supplemental Note 1: In-depth literature review on microbial community responses to warming and climate forcings
Supplemental Note 2: Literature-based definitions of resistance, resilience and stability
Supplemental Note 3: Site description of the model permafrost peatland ecosystem, Stordalen Mire
Supplemental Note 4: The peat of the fen at deeper depths are more variable, which might explain why this is the sole depth and habitat that shows directional microbiome change with time rather than just fluctuation.
Supplemental Note 5: Further analyses on stability with time and temperature
Supplemental Note 6: Carbon generalist genomes are significantly larger in size than specialists, which supports ecological literature, linking genome size to metabolic flexibility and functional redundancy
Supplemental Note 7: Methanogens have simplistic and specialized metabolic calls oftentimes with limited to no recognized nitrogen capabilities, which leads to a larger number of associations with other organisms.
Supplemental Note 8: Etymology.

Supplemental Figures

Supplemental Text

***Supplemental Note 1*: In-depth literature review on microbial community responses to warming and climate forcings**

In order to observe significant change in the soil microbial community or structure, some studies have required large pressed and/or pulsed disturbances with experimental climate forcings (e.g. increased temperature, precipitation, N addition, etc.) (e.g. ref (*1*) and/or shorter time scales (<3 years) of observation (*2*, *3*), however there are inconsistencies across the literature and longer-term (>5 years) studies. In a 12-year grassland study, it took 8 years for the effects of enhanced CO_2 exposure to significantly alter soil respiration rates and community function. These 8 years of data were not reported on in the main text of that study due in part to no functional genes involved in C degradation or N cycling being significantly correlated with soil CO_2 efflux rates, however the second phase of the experiment (years 9 to 12) showed significant correlations and were highlighted (*4*). In anaerobic microcosms from the Spruce and Peatland Responses Under Changing Environments (SPRUCE) site incubated at 6°C and 15°C going down to 2 m over 70 days, temperature did not significantly alter the relative abundance of the predominant taxa, alpha diversity metrics, or bacterial and archaeal 16S rRNA gene copies (*5*). At the Harvard Forest Long-Term Ecological Research (LTER) project, where soils were warmed 5°C above ambient for 5, 8, and 20 years, only at the 20-year site in the organic and mineral soil horizons had the community structure and Shannon H diversity been significantly altered (*6*).

881 Natural variation and variability in environmental conditions and the microbial community
882 can outweigh observed perturbations due to climate change. This suggests that communities
883 may maintain some baseline amount of natural functional stability and metabolic flexibility that
884 can be on par with the magnitudes required to respond to climate-change induced perturbation.
885 Soil depth and pH can be two of the largest effectors on microbial community diversity and
886 structure and are often more significant effectors than climate change forcings (*7*–*9*). Seasonal
887 variation in sampling date, attributed to short-term variations in environmental parameters, was
888 more important than 10 years of shifted baseline precipitation in a Mediterranean climate, which
889 led to the conclusion that the functional stability of these particular communities is key (*10*).
890 There were inconsistent and non-unidirectional yearly temporal trends in the community
891 response in the Jasper Ridge Global Change Experiment (JRGCE), a 17-year multifactorial
892 [warming, added rainfall, elevated CO_2 and additional nitrogen] experiment. The natural inter-
893 annual variability of the microbial community was more significant than any treatment effect (*11*,
894 *12*), which might suggest this community possessed the metabolic flexibility to deal with even
895 large pressed climate forcings.
896
897 Yet, individual metabolic processes and pathways, particularly in the case of nitrogen
898 fixation and methanogenesis, have shown significant response to climate change-associated
899 effects, even when the overall community structure or diversity remained unchanged. At
900 JRGCE, individual metabolic processes were linked to specific forcings, for example enzymes
901 related to carbon degradation (starch, hemicellulose, chitin, pectinase, and aromatics) showed a
902 response to elevated CO_2, however the direction and magnitude of these responses was
903 variable and carbon fixation related genes remained unchanged (*13*). Across study sites, N-
904 fixation and methanogenesis (measured via abundance of *nifH* and *mcrA*, respectively) are two
905 of the more commonly reported pathways that show significant change with increased heating
906 or other climate-change environmental factors (*3*, *7*, *14*). However, this pattern is not consistent
907 across all sites, since at the SPRUCE site in a 5-year study where deep peat experienced
908 intense heating (up to +9°C over ambient), neither a significant change in methanogen-related
909 genes at 40-50 cm nor a significant change in carbon substrate preference were observed (*15*,
910 *16*).
911
912 The consequences of pulsed vs. pressed disturbances and the sensitivity and response
913 of the microbial community to those disturbances varies and is seen over timeframes that can
914 range from hours to multiple decades, due in part to the resistance and resiliency of the
915 microbial community (*17*, *18*). The diversity and functional stability of the peatlands may arise
916 from strong filtering by the environment (low pH, oligotrophy, metabolite, and plant exudate
917 concentrations) which promotes a community that is resistant, or resilient, to change (*19*, *20*). At
918 Abisko in northern Sweden, a temperature experiment, raising growing period ambient
919 conditions by ~1°C for more than 10 years, did cause alterations in the phylogenetic
920 composition of the bacterial community despite documented changes in gas fluxes (*20*). In a
921 similarly established warming-focused decadal experiment nearby Abisko at Storflaket, while
922 the microbial community composition was dependent on depth and decadal heating, the overall
923 community structure was not different in the thawed layers, and the active layer community
924 structure was not significantly altered between treatments (*21*). Given these observations, we

advocate a change in focus: from examining whether microbial function can be directly associated with modifications of community composition associated with climate change forcings to exploring under what specific contexts functional alterations agree with compositional alterations (in accordance with refs (*20*, *22*)).

***Supplemental Note 2*: Literature-based definitions of resistance, resilience and stability**

Resistance is the insensitivity of a community to a disturbance or stressor, or the ability to withstand change (*17*, *23*, *24*). Resilience is the rate at which a community is able to return to its original state after disturbance (*17*, *23*, *24*). Both resistance and resilience must address the natural variability that exists in a community's mean state. This is important as stability, defined as little or no difference between a community's average state before and after disturbance, has factors of both resistance and resilience and can be assessed through the persistence of microbial taxa and metabolic functions with time (*18*, *25*). It is worth noting that one aspect of ecological stability depends on the community's ability to coexist in various stable states (*18*, *26*).

***Supplemental Note 3*: Site description of the model permafrost peatland ecosystem, Stordalen Mire**

Stordalen Mire, in arctic Sweden, located at 68°20'N 19°03'E, is a permafrost peatland complex underlain by discontinuous permafrost. The presence or absence of permafrost determines microtopography and hydrology, creating three thaw stages, palsa, bog and fen (Fig. 4), with distinct biogeochemistry and plant communities. These three distinct sub-habitats have been utilized for more than 60 years for plant ecology studies ranging from the Swedish IBP/PT tundra biome project 1968-1974 to more recent dynamic landscape studies of climate sensitive arctic atmosphere-biosphere interactions (*27*–*29*).

Palsa are common in the zone of discontinuous permafrost. The largest central area of Stordalen Mire is a palsa underlain and elevated 1-2 m above the surrounding landscape and ponds by continuous ice-rich permafrost (*30*). Palsa is underlain by continuous ice-rich permafrost with a shallow seasonal active layer (20-50 cm) and unsaturated peats. It is dominated by cryptogams and low form ericoid shrubs such as those from the genera *Andromeda*, *Vaccinium*, and *Rubus*. Permafrost becomes unstable at ambient annual air temperatures above 0°C. The mean annual air temperatures (MAATs) at the Abisko Research Station (ANS), ca. 10 km west of Stordalen Mire, have mostly been above 0°C since ca.1995 (*31*) and averaged +0.7°C for the duration of this study, 2011-2017 (SMHI 2024). The Stordalen Mire palsa is maintained by strong bidirectional winds (*32*) which keeps the snow cover minimal and allows deep penetration of the winter frost. Wind will also drift snow into surface depressions and the palsa edges, which change the thermal structure, increasing the heat capacities of the now wet peat causing the underlying ice-rich permafrost to thaw, further collapsing the surface and changing the plant community (*33*).

Bogs are found in the intermediate state of the thaw gradient if the permafrost is not entirely lost. Bogs remain perched above the local water table. The bogs are ombrotrophic collecting water from limited runoff from surrounding palsa, snow melt and rain, and are dominated by *Sphagnum* spp.. Bogs are also intermediate between the palsa and fen sites in

their productivity and carbon gas exchange rates (*34*). The seasonal active layer in the bog is deeper (50-90 cm) than that of the palsa and the water table can vary substantially during the year but the bog sites remain wet with the deeper peats above the permafrost remaining saturated.

Fens are the lowest and wettest areas in Stordalen Mire and lack discernible underlying permafrost. They are connected to the regional water table flowing from the surrounding watershed and, more immediately from shallow post-glacial lakes to the east and south of the Mire with a slow flow towards Lake Tornetrask to the north. The water table is usually at or above the fen surface (*35*): The persistent supply of relatively nutrient rich lake and groundwater supports productive communities of emergent macrophytes such as *Equisetum* spp. and graminoids such as *Eriophorum angustifolium* and *Carex rostrata* that grow to heights >1 m in a single growth season

***Supplemental Note 4*: The peat of the fen at deeper depths are more variable, which might explain why this is the sole depth and habitat that shows directional microbiome change with time rather than just fluctuation.**

The deeper fen peats are different and more prone to variability because of more, fresh, annual inputs of belowground litter due to macrophyte productivity combined with higher rates of lateral hydrologic transport (lower porewater residence times) because of their local water table connectivity. As illustrated in Supplemental Note 3, the habitat-specific plant communities have different productivities (*34*) that are reflected in and are integrally linked to the microbial communities in the peat below. There are distinct microbial communities and specific metabolisms in the peats coincident with the obvious surface plant communities (*36*). Aboveground productivity of these plant communities is affected by abiotic factors such as temperature, water, and belowground litter inputs (*37*) which in turn will likely affect belowground microbial and plant activity and variability. Palsa and bog peats are likely to have more stable conditions in the deeper peat layers. Both of those habitats have lower productivity of recalcitrant organic matter and restricted seasonal active layers. Palsa has the shallowest active layer with colder drained peats and woody litter inputs. *Sphagnum* dominated bogs grow from the top with less variability in belowground litter input into recalcitrant *Sphagnum* peat. Because bogs are perched there is minimal or no water flow in the deeper, more decomposed catotelm with longer porewater residence times. Fens, on the other hand, are more productive with high water conductivity. The roots of the graminoids in the fen will extend through the peat profile to the basement depth providing substantial amounts of seasonally fresh belowground litter input.

The MAAT and precipitation at ANS (SMHI 2024) and the CO_2/CH_4 flux rates (*34*) measured in the Stordalen Mire during 2013 were not anomalous for the study period. Two events related to the hydrology and temperatures occurred during the 2012 to 2013 winter that may particularly have affected the deep fen peat communities (Figs 1a and 2a). Pascual and Johansson (*38*), using meteorological data from ANS, calculated a larger number of melt days and positive degree days at the Storflaket (7 km west of Stordalen). Thaw days may have affected the input of the quantity and quality of fresh belowground litter. It was also noted that

the post-glacial ponds lost their ice cover earlier in the spring of 2013 (*39*) which would have also provided more fen waterflow earlier in the season affecting productivity. Both processes would have provided more and earlier substrate and water supply potentially affecting the microbial community structure specifically in the fens.

<u>Supplemental Note 5</u>: There is little compelling evidence non-linear responses to time or temperature for microbial community composition, function, or assembly.

The data shows little to no evidence of a linear relationship with time or temperature for the microbial community composition, function, or assembly. There is still a possibility of a significant non-linear relationship between community composition and time or temperature, or individual metabolic pathways or organisms that show relationships to temperature. At the community scale non-linearity may occur since temperature or time could have non-linear dynamics that create inflection points or other complex structures in the data. Furthermore, individual pathways or organisms may show more sensitivity than the whole community. Therefore, we performed several tests for non-linear responses of the community and taxa to time and temperature.

To investigate non-linear relationships between the microbial community and time or temperature, we ran generalized additive models (GAMs) to better understand if complex non-linear dynamics of the microbial community (represented by the first two principle coordinate axes) could predict year or temperature. To mirror our tests for linear relationships we ran the models both with and without the effects of habitat and depth. We found no evidence that microbial composition had a significant non-linear relationship to either time or temperature. Microbial community composition was a poor, non-significant predictor of year both when differences due to depth and habitat were not included in the model (GAM; $R^2 = 6.5 \times 10^{-3}$, microbial smooth term p-value = 0.4, deviance explained = 2.02%) and when they were included as covariates (GAM $R^2 = 5.6 \times 10^{-2}$, microbial smooth term p-value = 0.142, deviance explained = 12.3%). For temperature, microbial community was a good predictor of ground temperature only when the model did not account for habitat and depth (GAM $R^2 = 0.34$, microbial smooth term p-value = 1.64×10^{-16}, deviance explained = 40.5%). When habitat and depth were included in the model, the explanatory power of the model increased (GAM $R^2 = 0.6$, deviance explained = 63.7%, microbial smooth term p-value = 0.38), but the significance of the terms containing the microbial community principle coordinate axes were rendered non-significant. Taken together these results support our findings that microbial community composition was remarkably insensitive over time and to fluctuations in temperature.

To investigate the sensitivity of particular organisms and pathways to temperature we first chose organisms and pathways of interest to minimize the chance of inflating error rates due to multiple comparisons. In the case of organisms, we selected those that were present in WGCNA modules that showed >0.5 correlation coefficients with ground temperature and further selected only organisms within those modules that had the highest variable importance in projection (VIP) score (VIP > 1.5). We reasoned that these organisms would be the most likely to exhibit a strong population-level response to temperature change in our dataset. We then ran linear models to the relative importance of ground temperature and depth (as well as their interaction) on the centered log-ratio (CLR)-transformed abundance of each organism within a particular habitat (model formulas took the form: $\text{GenomeAbundance}_{ij} \sim \text{SoilTemperature}_j +$

$Depth_j$ + $SoilTemperature_j$:$Depth_j$, where $GenomeAbundance_{ij}$ is the CLR-transformed genome abundance of taxon *i* in habitat *j*). In some cases, $GenomeAbundance_{ij}$ was log-transformed to meet the assumptions of linear regression. Of the 109 organisms tested, only 14 showed any significant effect of temperature (linear regression, R^2 range: 0.11-0.57, $p<0.05$), and in all 14 cases, temperature had a minor negative effect on abundance (standardized effects size ranged from -0.079 to -0.036).

In the case of metabolic pathways, sixteen pathways of the 48 pathways analyzed, selected for their central contributions to carbon, nitrogen, and sulfur cycling in Stordalen Mire, were chosen for temperature analysis. We reasoned that temperature sensitivity in these sixteen critical pathways were most likely to have downstream effects in the community-level metabolism due to their centrality to key processes such as methanogenesis, or nitrogen and sulfur acquisition. The temperature sensitivity of pathways was analyzed similarly as for organisms, substituting cumulative weighted pathway abundance for genome abundance. Of the sixteen pathways only CAZymes for xyloglucan degradation in the fen showed any significant effect of temperature (R^2 = 0.57, temperature effect p-value < 0.05, standardized temperature effect size = -0.097). Collectively, these results support our findings that even at the granular level of individual organisms and pathways, the microbes and metabolisms in these communities are resistant to fluctuations in temperature over the 7 years, and that differences in habitat and depth have a larger effect on community variation in abundance of organisms and pathways than temperature.

<u>Supplemental Note 6</u>: Carbon generalist genomes are significantly larger in size than specialists, which supports ecological literature, linking genome size to metabolic flexibility and functional redundancy.

To date, research on microbial generalism has focused more often on “habitat generalism” than on the metabolic generalism we investigate here (*40*, *41*). In these studies, the breadth of an organism’s niche has typically been inferred through measurements of abundance across different habitats (*42*, *43*). Organisms occupying narrow or broad fundamental niches have then been taken to be specialists or generalists, respectively, with functional inferences occurring only downstream of this classification (*40*, *44*, *45*). Because generalism is expected to come at a cost (e.g., lower catalytic efficiency; higher maintenance costs for larger genomes; competitive exclusion), specialists have been hypothesized to dominate in many habitats (*46*, *47*). Alternatively, ecological theory suggests that broader niches should allow generalists to maintain more stable populations, while narrow-niche specialists should be less able to withstand environmental variation. Ready access to a broad pan-genome has been hypothesized to support the production of metabolic generalists (*48*), which should then succeed under selection in dynamic environments (*45*). It is not clear what aspects of environmental variability at Stordalen Mire drive the abundance of metabolic generalists. Furthermore, depending on the strength and ordering of substrate preferences in different organisms, apparent metabolic generalism may effectively be specialization in disguise (*48*).

To define specialists and generalists on the basis of function rather than habitat range, we first annotated genomes for metabolic functioning and then grouped by specialization (see Methods). We did not consider genome size in our classification of metabolic specialists and

generalists. We then hypothesized, in accordance with genome streamlining and ecological inference (*49–51*), that generalist organisms encoding more metabolic pathways would have larger genomes than methanogens and other metabolic specialists (figS23). Consistent with this prediction, our carbon generalists had significantly larger genomes (mean 5.00 ± 1.63 Mb, Tukey test, $p < 7.85 \times 10^{-12}$) than methanogens (mean 2.30 ± 0.45 Mb) and most other carbon specialists (Tukey test, *p*-values range from $<7.78 \times 10^{-12}$ to $<1.48 \times 10^{-4}$). Among specialists, homoacetogen genome sizes (mean 4.06 ± 1.70 Mb) were indistinguishable from those of methanotrophs or fermenters (mean 3.50 ± 1.28 Mb) but significantly larger than the macromolecule degraders (mean 3.36 ± 1.36 Mb, Tukey test, $p < 0.039$). Monomer degraders (mean 2.75 ± 0.97 Mb) were indistinguishable in genome size from both these larger specialists and from methanogens. Methanotrophs were the sole exception (mean 4.25 ± 0.64 Mb, Tukey test, not significant) to the finding that generalists had larger genomes than specialists. The methanotrophs identified here are aerobic, which might partially explain why their genomes are larger than those of other specialists (*52*); moreover, we found that these methanotrophs typically encoded chemotaxis, various CAZyme and carbon fermentation pathways, and nitrogen, sulfur and phosphate metabolic capabilities. Collectively, this pattern of genome size differentiation between generalists and specialists across metabolism types provides confidence in our pathway annotation-based calls of carbon generalists and specialists.

Functional generalism, observed within individual organisms, can lead to functional redundancy in the community (*41*, *43*, *53*). Functional redundancy, defined here and elsewhere as the ability of taxonomically distinct organisms to encode the same dissimilatory metabolic capabilities (*44*), is a common observation in microbial soil systems across global latitudes (*54*). Consistent with the observations throughout this work, functional redundancy that results in taxonomic differences in intermediate reactions of the metabolic network is unlikely to affect the endpoints of dissimilatory metabolic pathways (*44*), e.g., methane production in anaerobic digesters (*55*).

<u>Supplemental Note 7</u>: Methanogens have simplistic and specialized metabolic calls often with limited to no recognized nitrogen capabilities, which leads to a larger number of associations with other organisms.

The methanogens with a high importance to the overall structure and number of connections in WGCNA and MTN networks, respectively, were highly specialized with few annotated metabolisms. Hydrogenotrophic methanogens, dominant in the bog, were quite specialized with simplified carbon and nitrogen metabolic calls. There was greater versatility and diversity in methanogenic metabolisms in the fen with more variations of carbon fixation and degradation pathways, and more types of methanogenesis. Two of the most crucial organisms in the bog and fen networks, the hydrogenotrophic methanogens *Ca*. 'M. stordalenmirensis' (bog) and *Ca*. 'M. crilli' (fen), lacked recognizable nitrogen metabolism calls (figS34). Methanogens capable of nitrogen fixation had fewer connections in the MTN and lesser influence (via degree centrality and betweenness metrics) in WGCNA networks (figS34; figS35; figS36). These observations, along with those discussed in association with Fig 3c&d of the main text, led us to propose the hypothesis that if a methanogen has nitrogen-fixation or other

nitrogen-linked decomposition pathways it will have fewer temporal connections since it is less likely to need additional nitrogen inputs from other members of the community.

To further assess this hypothesis we examined whether we could identify other genes and functions, not directly addressed in our metabolic annotations, that could differentiate the methanogens with more connections from those with fewer connections (See Methods section on Genome Annotation for more details). Those methanogens that tended to be more independent with fewer associations to other organisms had five different functions that were either significantly enriched (adjusted q-value ≤ 0.05) or nearly significant (q-value < 0.055). Four of the functions (K02586, K02587, K02591, K02592) pertained to nitrogenase and nitrogen fixation, and one (COG1048) was involved in lysine biosynthesis, a critical amino acid. That a group of nitrogen-fixing methanogens were enriched in genes that pertain to nitrogen cycling and fixation, when compared to non-nitrogen fixing methanogens, was not unexpected but was consistent with our hypothesis. The only nearly significant (q value < 0.054) functions that were enriched in the methanogenic group with more connections and associates with time (“less independent” methanogens) were COG4656 and COG1035 which encode Na+ translocating ferredoxin: NADH oxidoreductase (Rnf). This Na^+ pump and Rnf complex have been found to play important roles in energy conservation, ATP generation and electron shuttling (*56*, *57*). Perhaps, the highly reducing conditions of the anoxic environment and reliance on reverse electron transport could be beneficial to those organisms, but the precise reason why an energy conservation function would be enriched in an apparent more collaborative group of methanogens is not entirely clear. Collectively, these results support the hypothesis and trends seen in the metabolic, MTN and WGCNA analysis that if a methanogen isn’t clearly limited in nitrogen capabilities they have fewer associations and alternatively when there isn’t a known nitrogen pathway those methanogens likely need external sources of nitrogen from surrounding community members.

***Supplemental Note 8*: Etymology.**

‘Acidi’ from Latin noun neuter acidum an acid, adj. acidus, sour.

Description of ‘Candidatus Acididegradans cibantis’ sp. nov.
Classification and differentiation based on average nucleotide identity (ANI). ‘degradans’ Latin verb neuter present active participle: degrade. ‘Cibantis’ Latin verb neuter present active participle: to feed. This organism is of the order Acidimicrobiales in the Actinobacteriota phylum, was classified as a carbon generalist and proposed to be providing key substrates to other organisms, including methanogens.

Description of ‘Candidatus Acididegradans virginiarichiae’ sp. nov.
Classification and differentiation based on ANI. ‘degradans’ Latin verb neuter present active participle: degrade. ‘virginiarichiae’, New Latin noun feminine, named after Virginia Rich, the Ohio State University, USA, in recognition of her pioneering efforts on deciphering the controls that climate change has from scales of genes to ecosystems in thawing permafrost. This organism is of the order Acidimicrobiales in the Actinobacteriota phylum, and was classified as a carbon generalist.

1183
1184 Description of ‘Candidatus Acidimolecula latum’ sp. nov.
1185 Classification and differentiation based on topology and ANI. ‘molecula’ Latin noun feminine:
1186 molecule. ‘latum’ Latin adjective neuter: broad. This organism is of the genus Terracidiphilus in
1187 the Acidobacteriota phylum, was classified as a carbon generalist and possessed a broad range
1188 of the carbon metabolisms considered.
1189
1190 Description of ‘Candidatus Acidimolecula amplum’ sp. nov.
1191 Classification and differentiation based on ANI. ‘molecula’ Latin noun feminine: molecule.
1192 ‘amplum’ Latin adjective neuter: large. This organism is of the genus Terracidiphilus in the
1193 Acidobacteriota phylum and was classified as a carbon macro-molecule degrader.
1194
1195 Description of ‘Candidatus Acidiacetogenum stordalenmirensis’ sp. nov.
1196 Classification and differentiation based on ANI. ‘acetogenum’ New Latin noun neuter: acetogen.
1197 ‘stordalenmirensis’ New Latin adjective masculine, of or belonging to Stordalen Mire, Sweden
1198 from where the species was characterized. This organism belongs to the family
1199 Thermacetogeniaceae in the Firmicutes phylum and was classified as a homoacetogen.
1200
1201 Description of ‘Candidatus Abiskobacterium ruthvarnerae’ sp. nov.
1202 Classification and differentiation based on ANI. ‘Abiskobacterium’ New Latin noun neuter:
1203 bacterium from Abisko, Sweden from the surrounding area where the species was
1204 characterized. ‘ruthvarnerae’ New Latin noun feminine, named after Ruth Varner, University of
1205 New Hampshire, USA in recognition of her pioneering efforts on deciphering the controls that
1206 climate change has from scales of genes to ecosystems in thawing permafrost. This organism
1207 belongs to the family of Bryobacteraceae, was classified as a carbon generalist and possessed
1208 nearly all of the carbon metabolisms considered.
1209
1210 Description of ‘Candidatus Acidiflorens viviennsis’ and ‘Candidatus Acidiflorens anabellensis’,
1211 sp. nov.
1212 Classification and differentiation based on ANI and topology, and ANI, respectively.
1213 ‘Acidiflorens’, New Latin an organism that blooms in acid (*58*). ‘viviennsis’ and ‘anabellensis’
1214 New Latin adjective feminine, of or belonging to Vivien and Annabelle, respectively, the mothers
1215 of Virginia Rich, the Ohio State University, USA and Ruth Varner, University of New Hampshire,
1216 USA, respectively, whom they wish to be honored.
1217
1218 Description of ‘Candidatus Acidiaspiraculum latum’ sp. nov.
1219 Classification and differentiation based on topology and ANI. ‘a’ Latin preposition: away from.
1220 ‘spiraculum’ Latin noun neuter: air. ‘‘latum’ Latin adjective neuter: broad. This organism belongs
1221 to Verrucomicrobiota, found to be important in the anoxic fen habitat and was classified as a
1222 carbon generalist and possessed a broad range of the carbon metabolisms considered.
1223
1224 Description of ‘Candidatus Acidiaspiraculum fermentum’ sp. nov.
1225 Classification and differentiation based on topology and ANI. ‘a’ Latin preposition: away from.
1226 ‘spiraculum’ Latin noun neuter: air. ‘‘fermentum’ Latin noun neuter: fermentation. This organism

1227 belongs to Verrucomicrobiota, found to be important in the anoxic fen habitat and was classified
1228 as a fermenter.
1229
1230
1231
1232
1233
1234
1235
1236
1237
1238
1239
1240
1241
1242
1243
1244
1245
1246
1247
1248
1249
1250
1251

Supplemental Figures

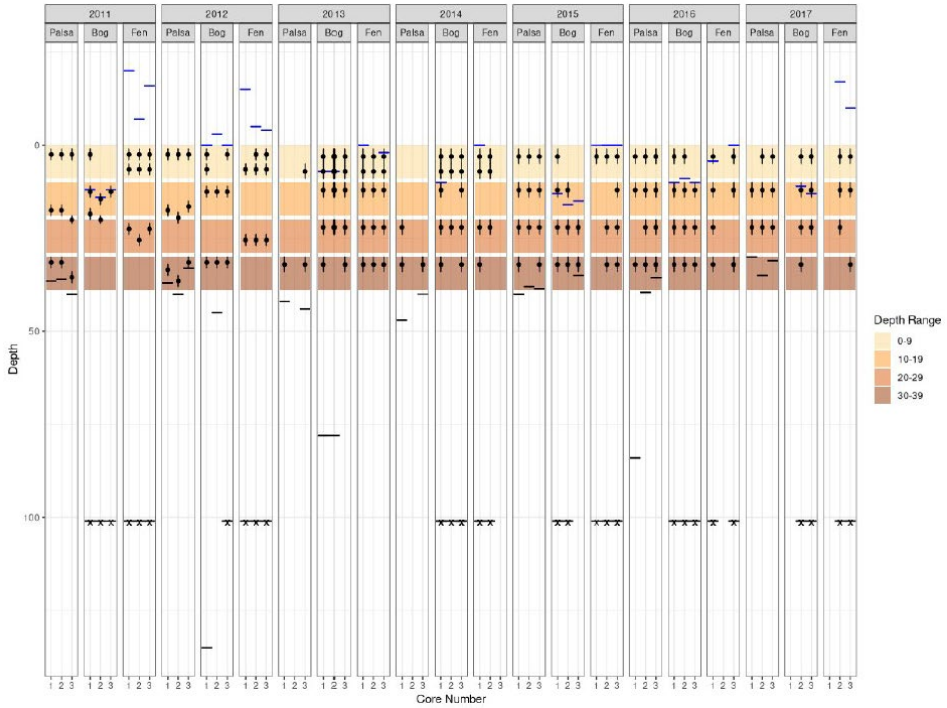

Supplemental Figure 1: Overview of samples included in this study. Each point represents the average depth of a sample (cm) with error bars showing the minimum and maximum depth of the sample. Blue lines represent water table depth where appropriate, black lines show active layer depth, black lines with x's show the maximum depth of the active-layer probe (where the permafrost was not reached). We note that in 2012, a deeper probe was used but broke during sampling of the first bog core, after which a standard 1 m probe was used.

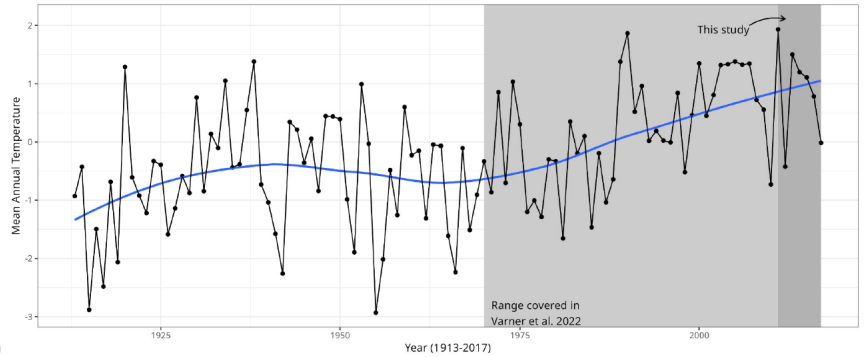

A)

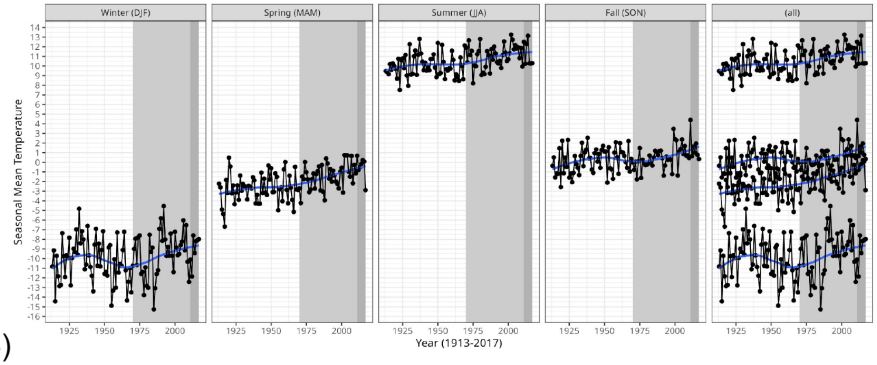

B)

<u>Supplemental Figure 2:</u> A) The trends of mean annual temperature at Stordalen Mire (as measured by the Abisko weather station SMHI) have been increasing for over fifty years (light grey, C-losses and associated habitat conversion discussed in ref *<u>29</u>*), despite large inter-annual fluctuations. Our study captures the recent period from 2011-2017 (dark grey). **B)** There are important seasonal differences in the temperature change over the last fifty years. The summer, which represents the time of peak emissions, is one of the more stable times of year, while the winters and shoulder seasons have been experiencing the most rapid increases in temperature. Panels are presented in the following order: winter, spring, summer, fall, all seasons.

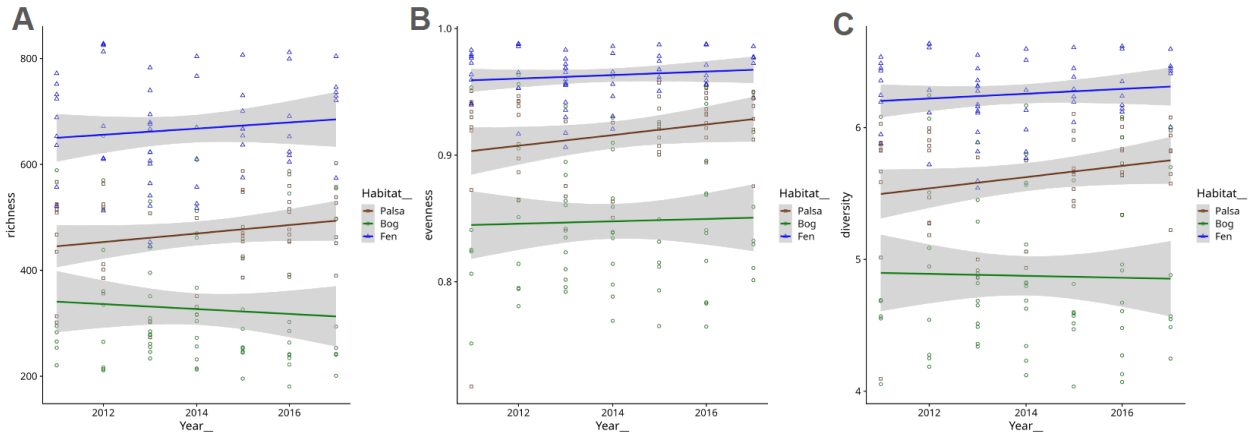

Supplemental Figure 3: There are no significant relationships between SingleM based alpha diversity metrics and time as a continuous variable. Alpha diversity, as measured as richness **(A)**, Pielou's evenness **(B)**, and Shannon diversity **(C)** for SingleM results rarefied to 1000 sequence hits per marker gene and averaged across marker genes with linear model significance testing against time (in years) as a continuous variable.

SingleM based Alpha Diversity for each habitat by depth against continuous time (as year)

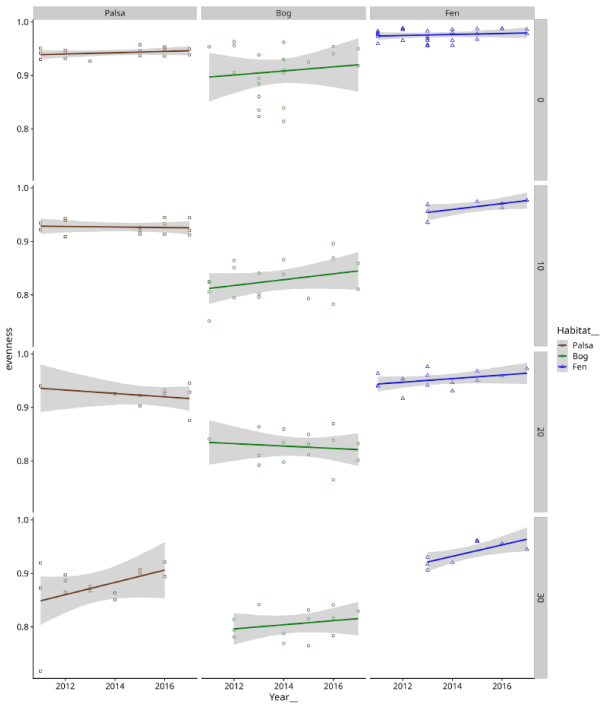

Habitat	Depth	Alpha	R^2	p-value
Fen	10-19	diversity	0.52	0.043
Fen	10-19	richness	0.57	0.031
Fen	30-39	evenness	0.58	0.017
Fen	30-39	diversity	0.58	0.017
Fen	30-39	richness	0.54	0.023

Supplemental Figure 4: The only significant relationships between SingleM based alpha diversity metrics and time as a continuous variable occurred in the fen (10-19 cm and 30-39 cm). Alpha diversity (measured as richness, Pielou's evenness, and Shannon diversity) for SingleM results rarefied to 1000 sequence hits per marker gene and averaged across marker genes by depth across habitats with linear model significance testing against time (in years) as a continuous variable.

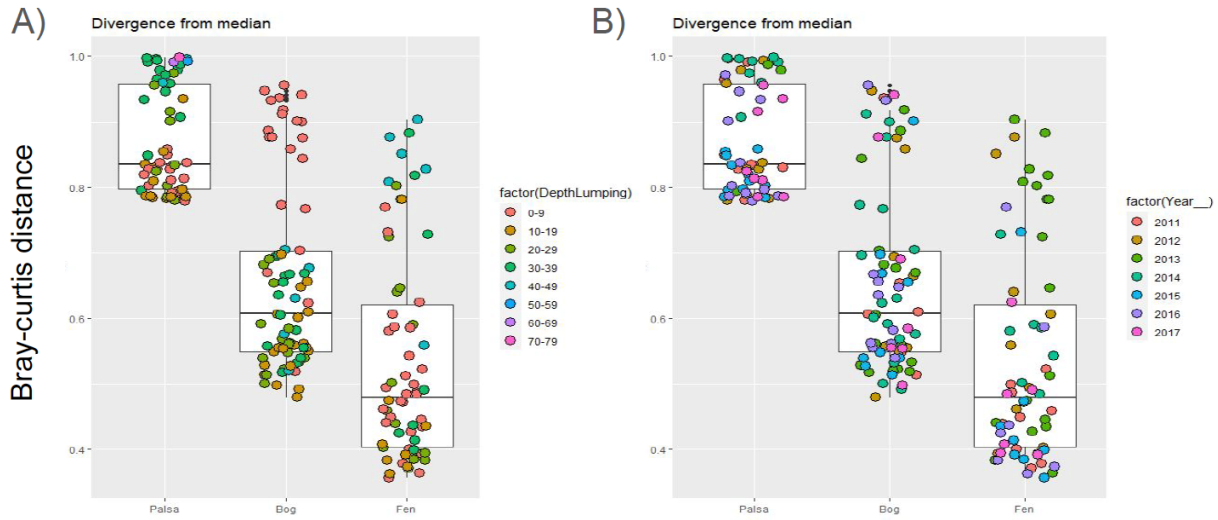

<u>Supplemental Figure 5:</u> Divergence of each sample from the median community profile in each habitat. Points within each boxplot are jittered to represent individual samples, with the Bray-Curtis distance (determined from MAG abundances) indicating the divergence of each sample from the median profile. The data is plotted in two panels: **(a)** samples are colored by depth, and **(b)** samples are colored by year. This allows for comparison of divergence patterns across different depths and years within each habitat.

Supplemental Figure 6: Comparing pairwise sample distances within year and between years for each habitat (palsa, bog, and fen). Points represent individual pairwise comparisons between samples, with the year differential between the two samples indicated by a gradient color scale. The Wilcoxon ranked sum test p value is displayed on the plots, comparing within-year versus between-year groups. This provides statistical insights into the temporal variability of samples within each habitat type.

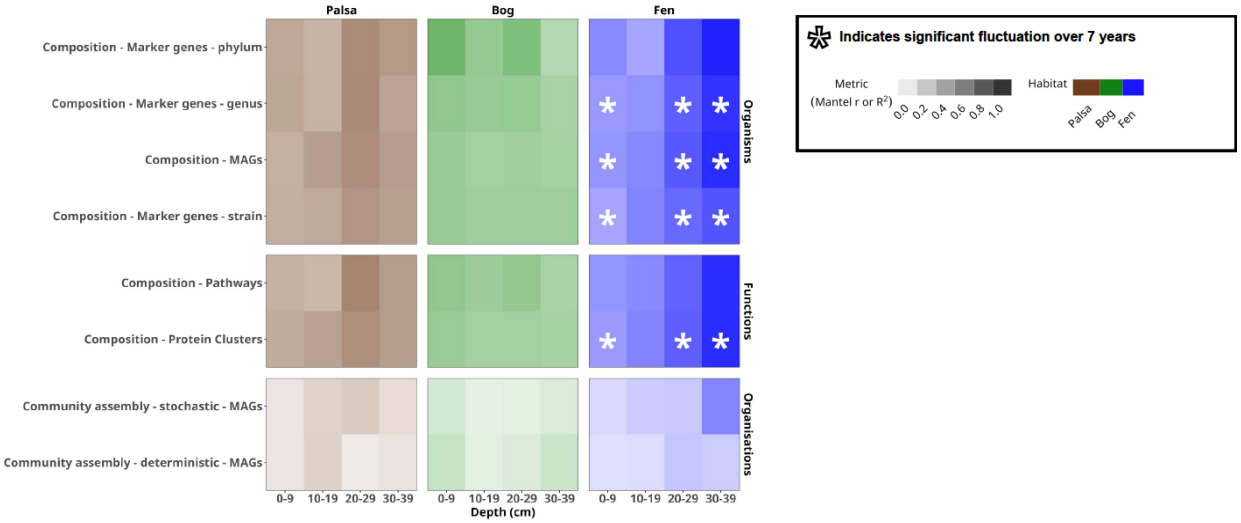

Supplemental Figure 7: Fluctuation over time was assessed by using time as an unordered categorical variable. Heatmap visualization of microbiome temporal fluctuation at different levels of granularity, spanning organisms (from phylum to strains to diversity metrics, via single copy marker genes and MAGs), functions (from pathways to protein clusters, both annotatable and non-annotatable), and organization (community assembly metrics of stochasticity and determinism), in each habitat and depth. The amount of variation explained by time (as Mantel R or R^2 depending on statistical test appropriate for each data type; see Methods) is indicated with the intensity of the shaded color; white asterisks denote significant correlations to time. Different statistical tests were used to test structure with time depending on the data type (e.g. multivariate vs. single variate data). Change in community phylogenetic and stochastic assembly data was tested with a Mantel test. Change in organisms and functions metrics was tested with a redundancy analysis with time as an explanatory factor.

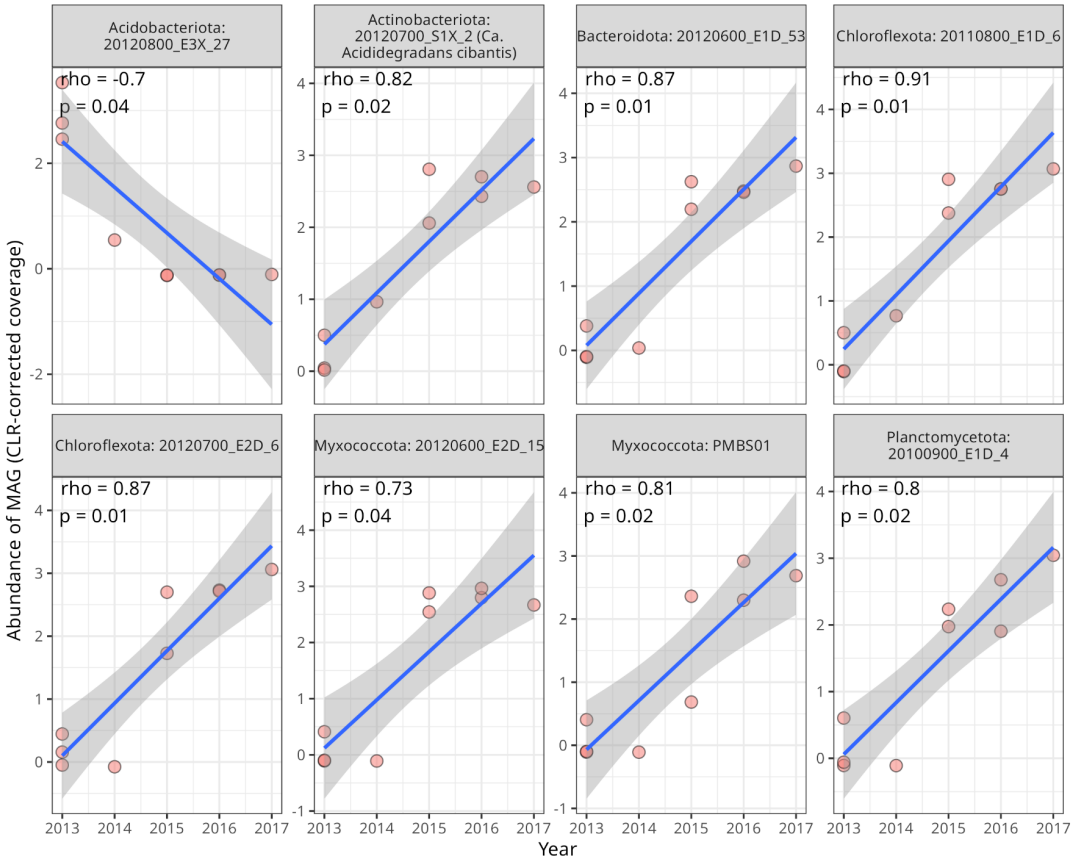

Supplemental Figure 8:

8 MAGs from the fen at 30-39 cm depth showed both significant differential centered log-ratio (CLR) abundances across years and significant correlations to time. Lines of best fit are shown in blue with standard error indicated in gray. Spearman rho and false discovery rate (FDR) adjusted p-values for each test are displayed in the top left-hand corner of each subplot. Each organism is designated at the top of the plot by its phylum and unique genome identifier.

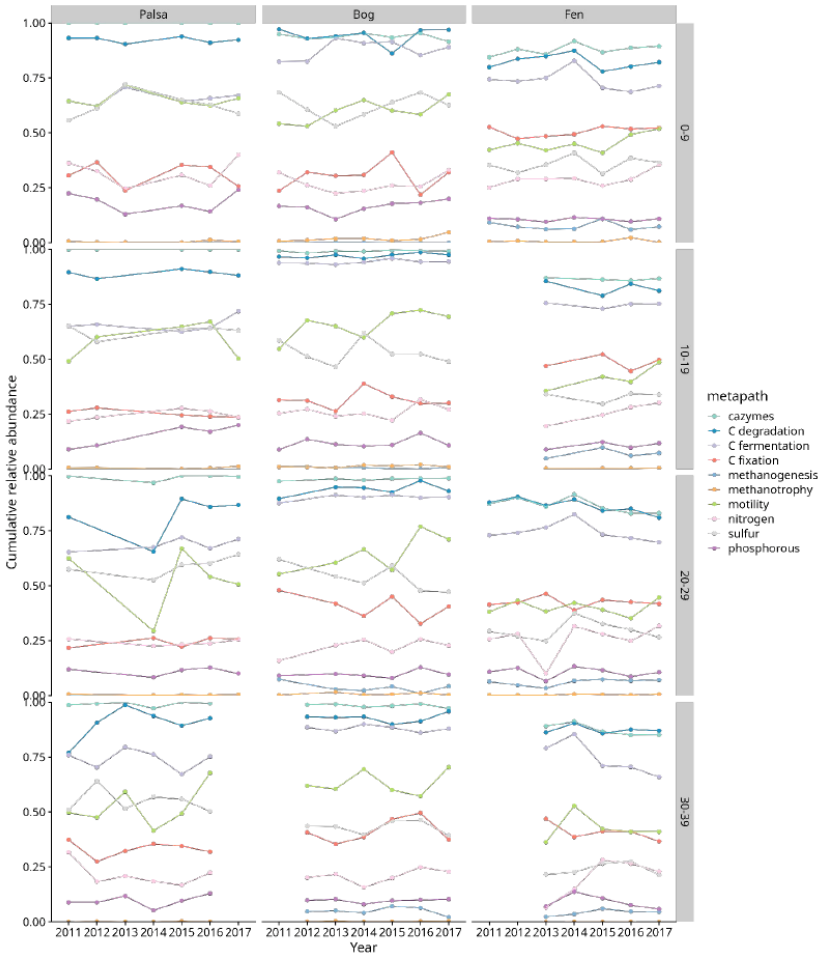

Supplemental Figure 9: Encoded cumulative relative abundance of meta-pathways with depth and time across habitats. Each point represents the cumulative relative abundance of all species that encode a pathway within the given meta-pathway.

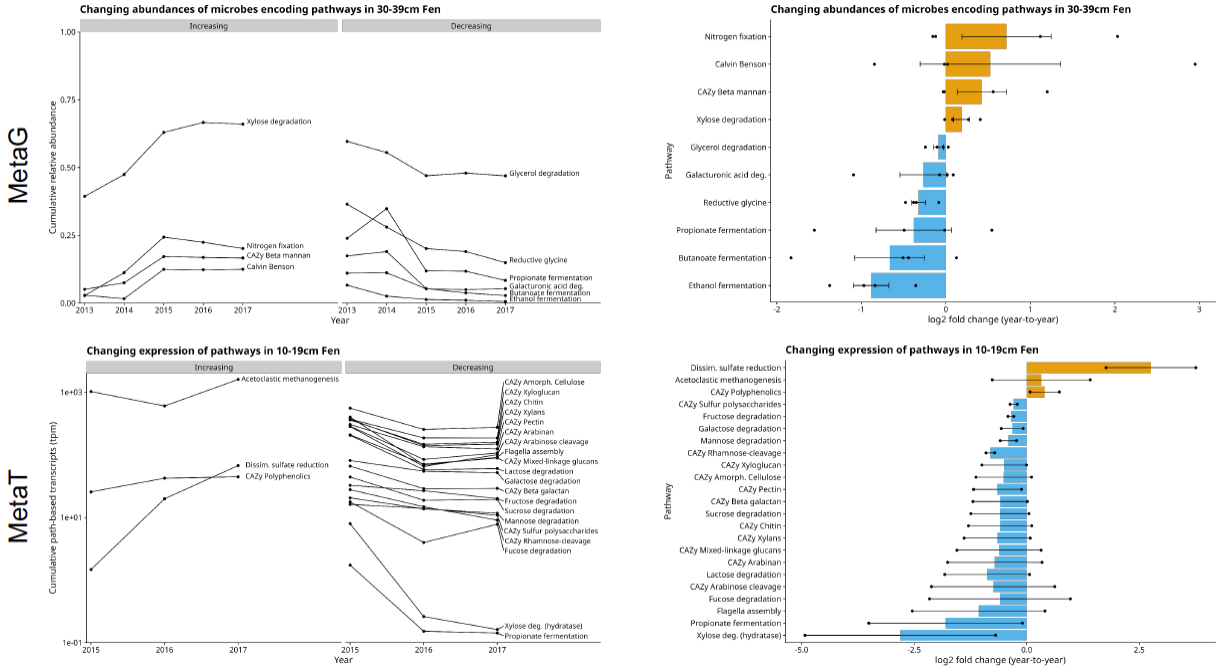

Supplemental Figure 10: Metabolic pathways that significantly change over time. Pathways with changing cumulative abundance across years in metagenomes (top), in 30-39cm Fen, representing 10/13 of the significantly changing pathways; and metatranscriptomes (bottom), in the 10-19cm Fen, representing 34/132 of the significantly changing pathways. Left column represents cumulative abundances over time for significantly changing pathways, right column represents year-to-year log2 fold-change. Error bars represent standard error. All pathways were significant $p<0.05$ in Likelihood-ratio test of beta-regression (logit) with and without Year parameter.

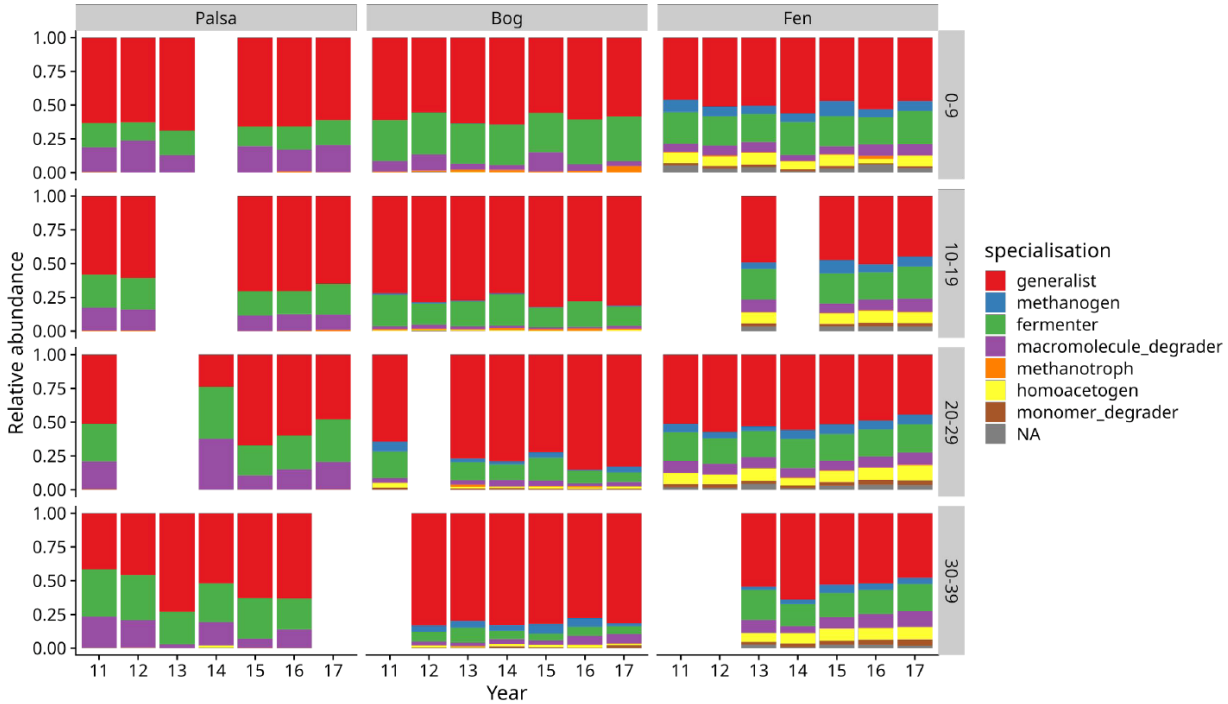

Supplemental Figure 11: Relative abundance of each group of carbon specializations across habitats, depths and years and averaged across samples. “NA” represents genomes that were unable to be assigned to a specialization.

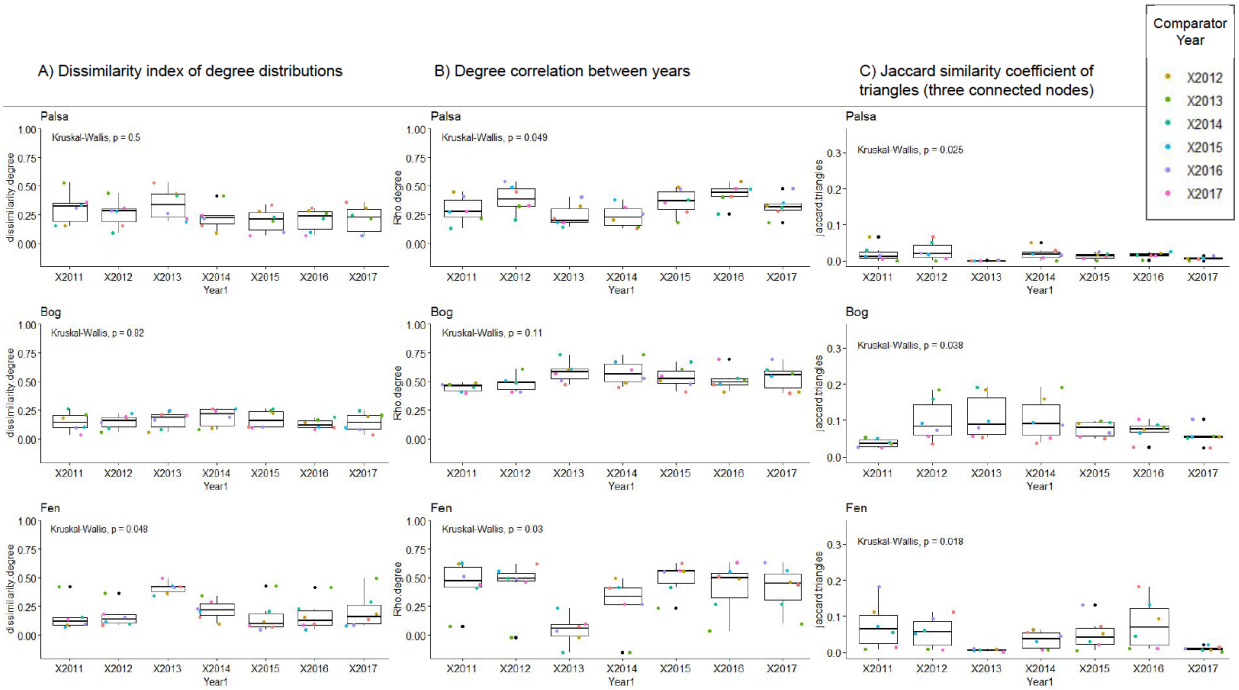

<u>Supplemental Figure 12:</u> Temporal comparison of network structures across habitats.

This figure examines year-to-year variations in network metrics for the three habitats: Palsa, Bog, and Fen. Multilayer networks (MTN) were constructed for each year and habitat, and metrics were calculated to compare network structure over time. Pairwise comparisons are shown using boxplots, with individual data points jittered and color-coded to indicate the comparator year. Statistical significance is indicated above each boxplot through a Kruskal-Wallis test. (A) Dissimilarity index of degree distributions. The dissimilarity in degree distributions between years within each habitat. The degree distribution reflects the frequency of nodes having a specific number of connections. A higher dissimilarity index indicates greater differences in connectivity patterns between years. (B) Degree correlation (ρ\rhoρ). Pairwise correlations of node connectivity patterns across years. (C) Jaccard similarity coefficient of triangles. Pairwise comparisons of triangle connectivity (three connected nodes) between years. The coefficient measures the proportion of shared triangles relative to the total number of unique triangles across the years, indicating the stability or change in triadic structures over time.

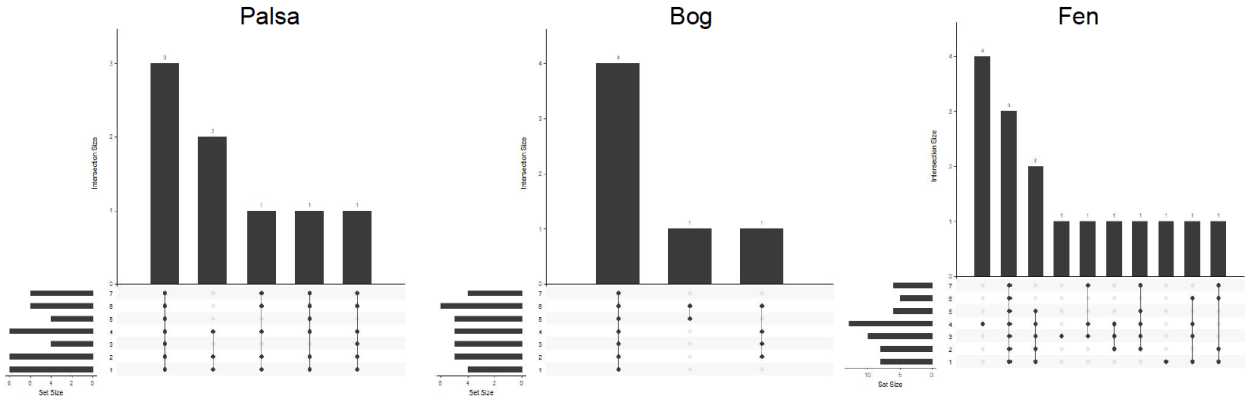

Supplemental Figure 13: This figure shows upset plots of clustered modules, generated by selecting the highest possible likelihood of clustering across layers, based on varying the interlayer edge weights. The y-axis represents the number of modules present in the years indicated by the bolded points below the x-axis. The values below the x-axis indicate the year where a module was present (1-7 is 2011-2017). Generally, the plots reveal higher levels of module persistence in the Palsa and Bog compared to the Fen, where ephemeral modules are more prevalent.

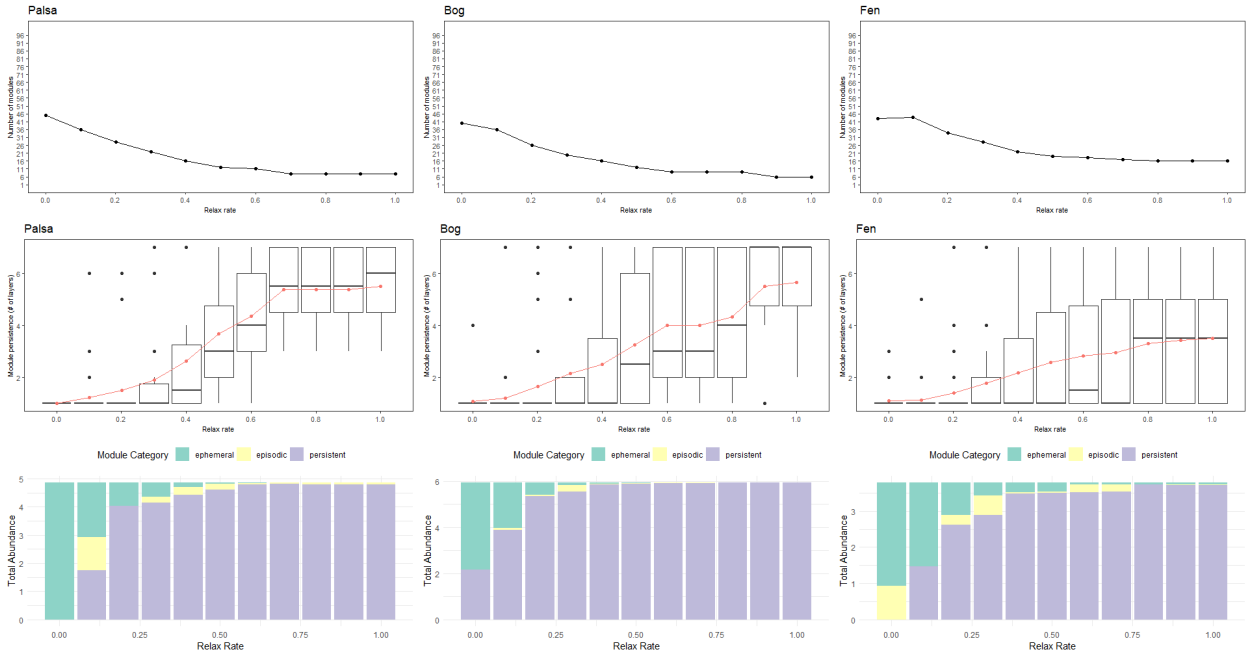

Supplemental Figure 14: Since we have no direct measurement of interlayer edge weight (which roughly corresponds how strongly one year's network influences the subsequent year's community), we tested a variety of interlayer edge weights (ranging from 0 to 1 with 0 being the least relationship between years) to assess the impact on the clustering of modules. The top row of panels shows how many modules formed across the range of relax rates (the change in interlayer edge weight). The middle row shows the distribution of the persistence of modules (the number of layers where a module is present) at various relax rates. The bottom row shows the average relative abundance of organisms within each kind of module. Modules are grouped into three categories: ephemeral (present in 1 layer), episodic (present in 2–3 layers), and persistent (present in ≥ 4 layers). At higher relax rates, fewer modules are detected but have higher persistence over time. Compared to the bog and palsa, the fen shows a higher abundance of episodic and ephemeral modules across all relax rates.

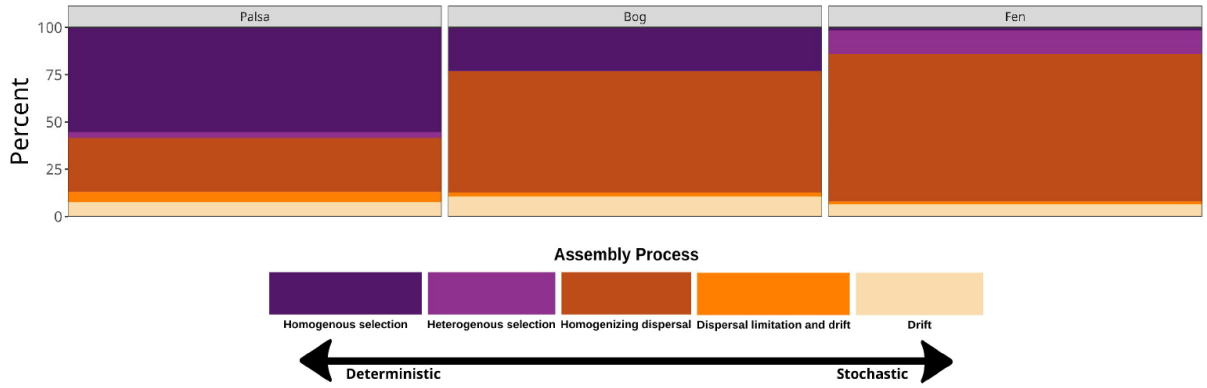

Supplemental Figure 15: The proportion of assembly processes in each habitat. To control for depth, cross-depth sample-to-sample comparisons have been filtered out. The proportion of sample-to-sample comparisons within each habitat whose assembly processes were characterized as homogenous selection, heterogenous selection, homogenizing dispersal, dispersal limitation and drift, or pure drift are indicated on the y-axis. While each depth interval is indicated on the x-axis. Purple-tinted colors are indicative of deterministic assembly processes, orange-tinted colors are indicative of stochastic assembly processes.

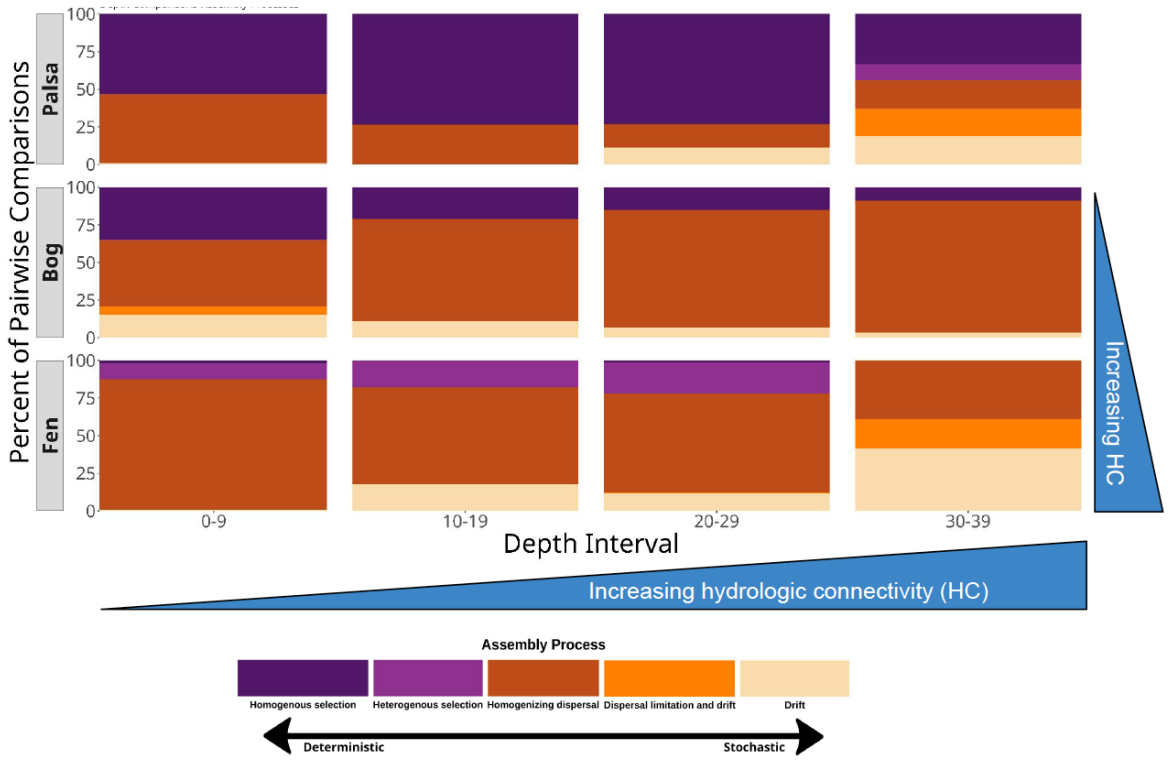

Supplemental Figure 16: The proportion of assembly processes in each habitat as a function of depth (in 10-cm intervals). The proportion of sample-to-sample comparisons whose assembly processes were characterized as homogenous selection, heterogenous selection, homogenizing dispersal, dispersal limitation and drift, or pure drift are indicated on the y-axis. Each depth interval is indicated on the x-axis. Each row of plots represents a different habitat across the thaw gradient. Hydrologic connectivity as measured by time below the water table during the growing season prior to sampling increases with thaw (bogs are sometimes waterlogged and fens are nearly always waterlogged) and time below the water table increases with depth, particularly in the bog.

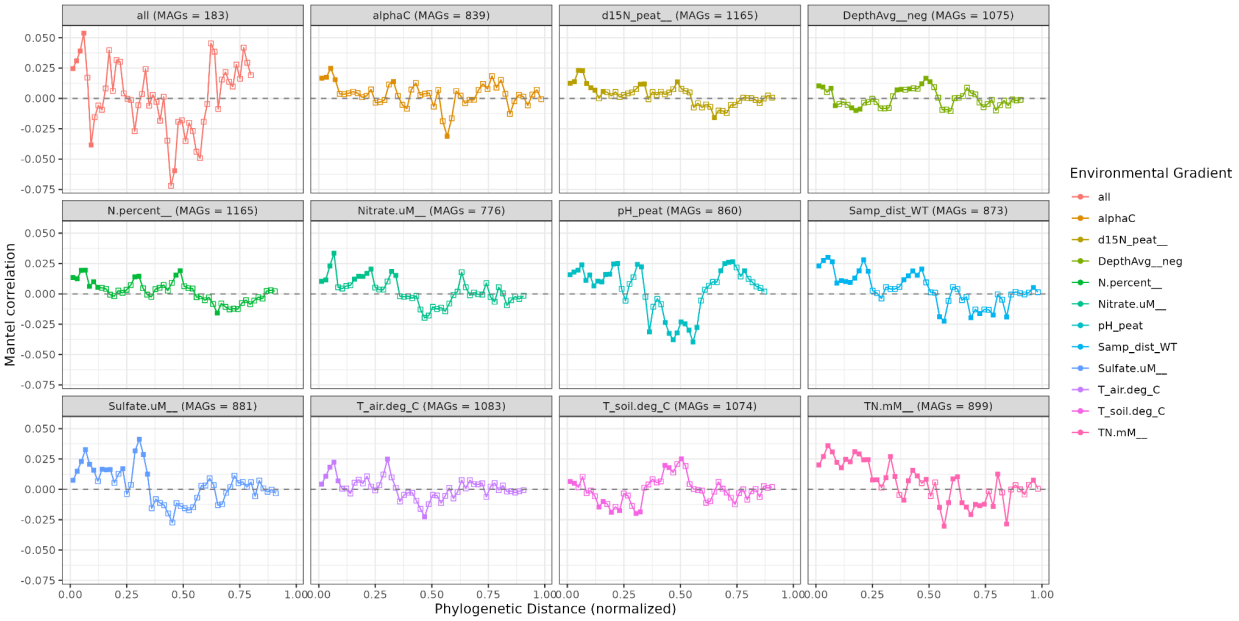

Supplemental Figure 17: Mantel correlograms showing the Pearson correlation between between-MAG environmental optima and between-MAG phylogenetic distance for a number of environmental gradients at the site. Significant correlations ($P < 0.05$, filled points) indicate that a phylogenetic signal in MAG ecological niche for the associated distance class. Significant positive correlations indicate ecological similarity among MAGs is higher than expected for the associated distance class. Gradients summarized from left to right and top to bottom: all - composite of all site environmental data distances summarized by gower distance, alphaC - fractionation coefficient, d15N_peat - delta 15N value of peat N, DepthAvg_neg - the depth optima of each MAG, N.percent - the % N in peat (by weight), Nitrate.uM - Nitrate concentrations (uM), pH_peat - pH of peat, samp_dist_WT - typical distance of a MAG from the water table, Sulfate.uM - sulfate concentration (uM), T_air_deg_C - air temperature, T_soil_deg_C - soil temperature, TN.mM - total nitrogen concentration (organic and inorganic).

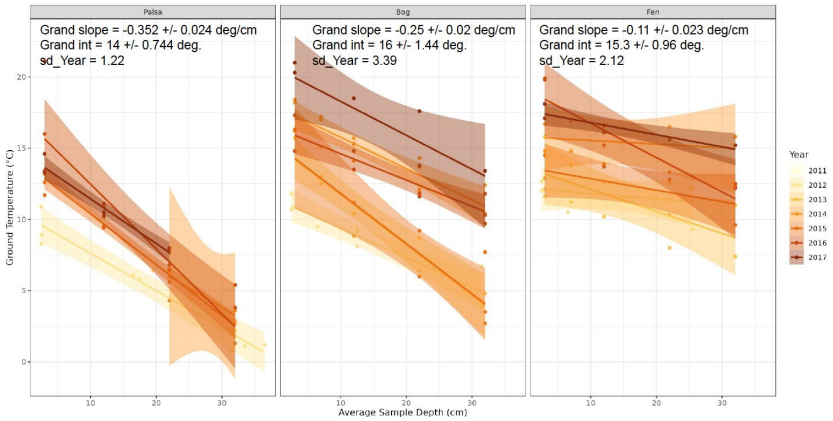

Supplemental Figure 18: Depth-dependent temperature decreases for all habitats across years. We ran several different mixed effects models to understand the effect of year on the relationship between ground temperature and depth, we tested year as both a random slope and a random intercept, as well as running the model without year as a random effect. The best model (as determined by Akaike and Bayesian information criterion, AIC and BIC, respectively) was one in which year was a random intercept, indicating that while the surface temperature does vary from year to year, the relationship (slope) between temperature and depth is fairly consistent within habitat from year to year. Soil temperature (y-axis) was most strongly related to depth (x-axis) in the palsa (slope = -0.352 +/- 0.024 deg/cm), and more weakly related in the bog and fen (slope = -0.25 +/- 0.02 and -0.11 +/- 0.02 deg/cm, respectively). Here, “grand slope” and “grand intercept” represent the best fit pooled mean estimate of the relationship between temperature and depth (slope), and average temperature at the surface (intercept) over the seven years. sd_Year shows the variation among years around that mean. Year-to-year differences in surface temperature were most variable in the bog (sd_Year = 3.39), and least variable in the Palsa (sd_Year = 1.22).

Habitat	Not Depth Corrected		Depth-Corrected (partial mantel)	
	Rho	Significance	Rho	Significance
All	0.126	0.001	0.106	0.001
Palsa	0.314	0.001	-0.129	0.978 (NS)
Bog	0.269	0.001	0.152	0.003
Fen	0.24	0.004	0.24	0.005

<u>Supplemental Table 2</u>: Mantel tests of the relationship between community composition and temperature. Ground temperatures show low-to-moderate positive relationships with community composition (rho ranges 0.106-0.31). When depth-corrected (via partial Mantel tests) the relationship weakens but is mostly still significant except in palsa where the depth-temperature relationship is strongest.

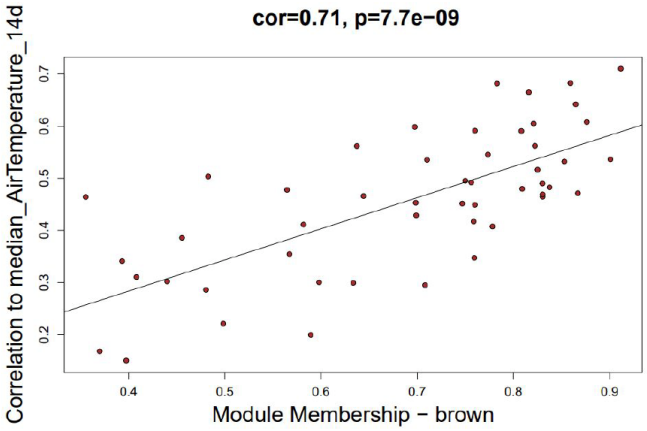

Supplemental Figure 19: A single WGCNA module showed a relationship to temperature that was greater than its relationship to depth. The 'brown' module from the fen samples was strongly correlated to the 2-week average air temperature leading to sample collection date. Each data point represents one MAG within the brown module, where the x-axis shows the correlation between the MAG shown and the representative eigenvector of the module. Additionally, each MAG is also correlated to the air temperature on the y-axis.

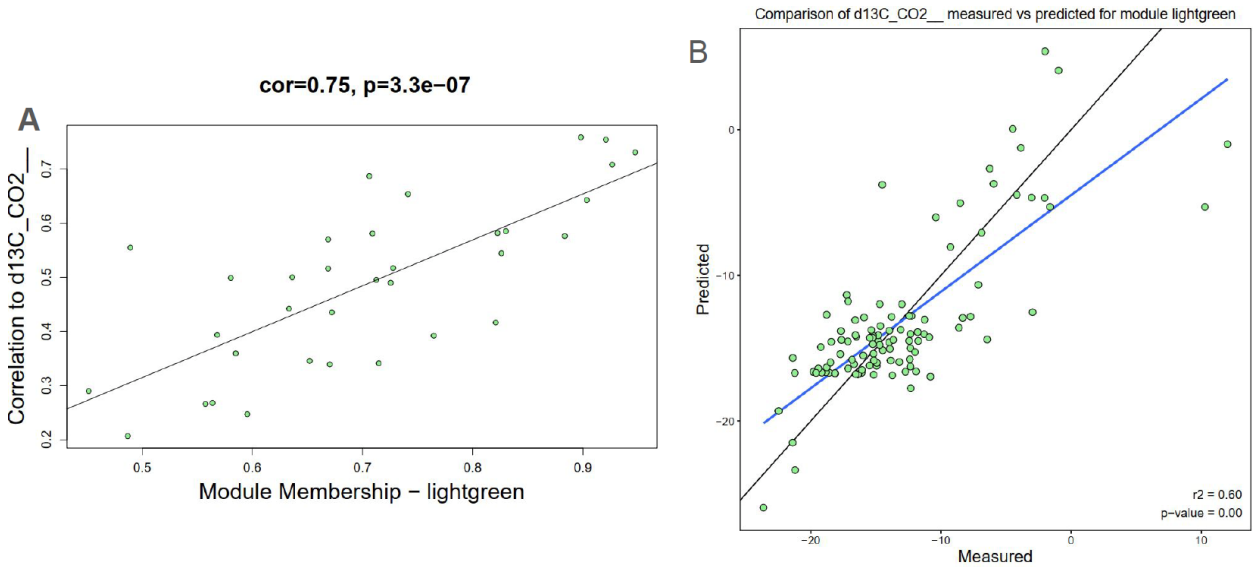

<u>Supplemental Figure 20:</u> (a) The WGCNA module containing the MAGs from all habitats most highly correlated to $\delta^{13}C_{CO2}$ of porewater (y-axis) over seven years of data with the relationship of the MAG to the module representative (x-axis), where stronger relationships between the environmental variable and the module representative eigenvector indicate a robust relationship. **(b)** Measured vs predicted values of $\delta^{13}C_{CO2}$ porewater values using partial least squares regression with leave-one-out cross validation.

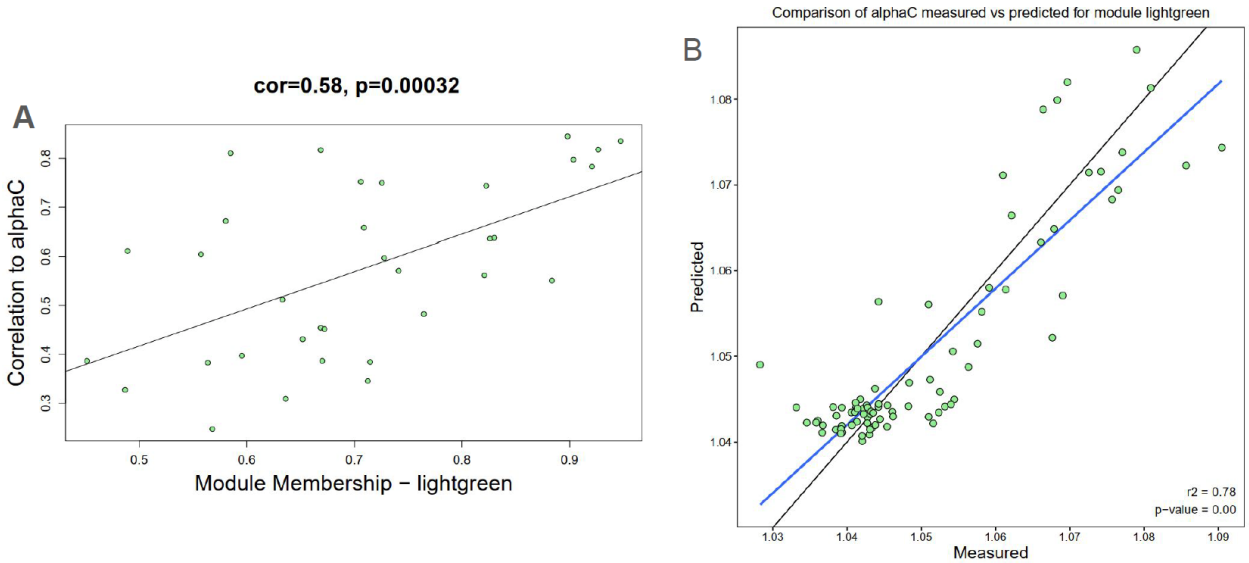

<u>Supplemental Figure 21:</u> (a) The WGCNA module containing the MAGs from all habitats most highly correlated to $\alpha_{CO2\text{-}CH4}$ of porewater (y-axis) over seven years of data with the relationship of the MAG to the module representative eigenvector (x-axis), where stronger relationships between the environmental variable and module representative indicate a robust relationship. **(b)** Measured vs predicted values of $\alpha_{CO2\text{-}CH4}$ of porewater values using partial least squares regression with leave-one-out cross validation.

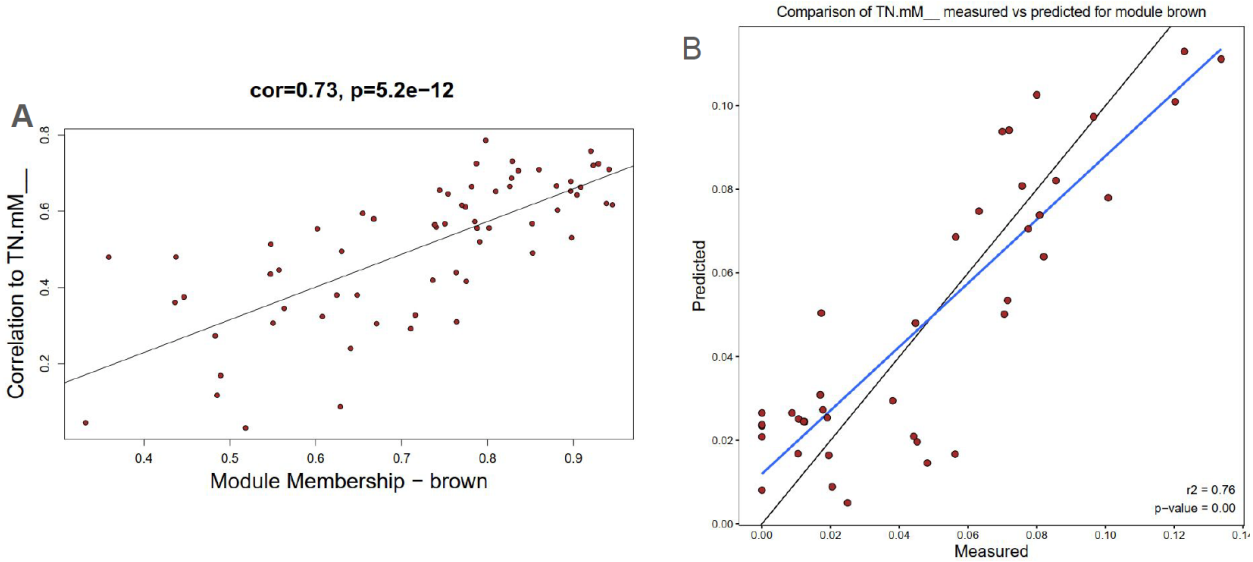

<u>Supplemental Figure 22:</u> (a) The WGCNA module containing the MAGs from all habitats most highly correlated to total nitrogen concentration (TN.mM) of porewater (y-axis) over seven years of data with the relationship of the MAG to the module representative (x-axis), where stronger relationships between the environmental variable and module representative indicate a robust relationship. **(b)** Measured vs predicted values of TN.mM porewater values using partial least squares regression with leave-one-out cross validation.

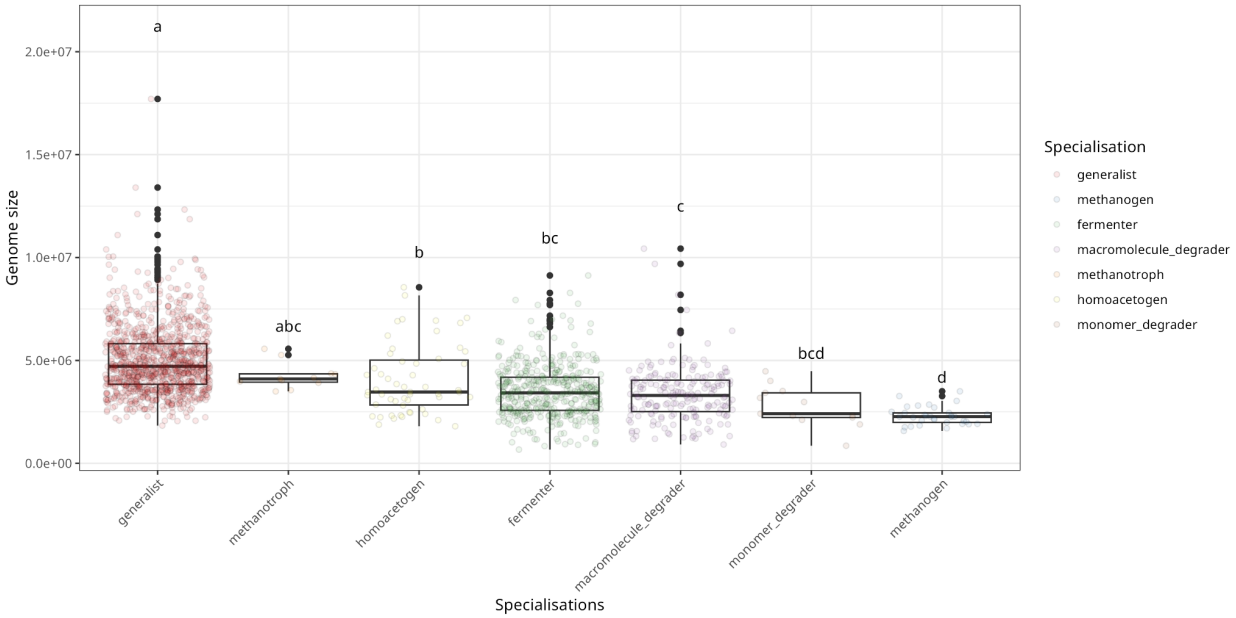

Supplemental Figure 23: Genome size for each of the different carbon specializations. Carbon generalists had significantly larger genomes (mean 5.00 ± 1.63 Mb, Tukey test, $p < 7.85 \times 10^{-12}$) than methanogens (mean 2.30 ± 0.45 Mb) and most other carbon specialists (Tukey test, *p*-values range from $<7.78 \times 10^{-12}$ to $<1.48 \times 10^{-4}$).

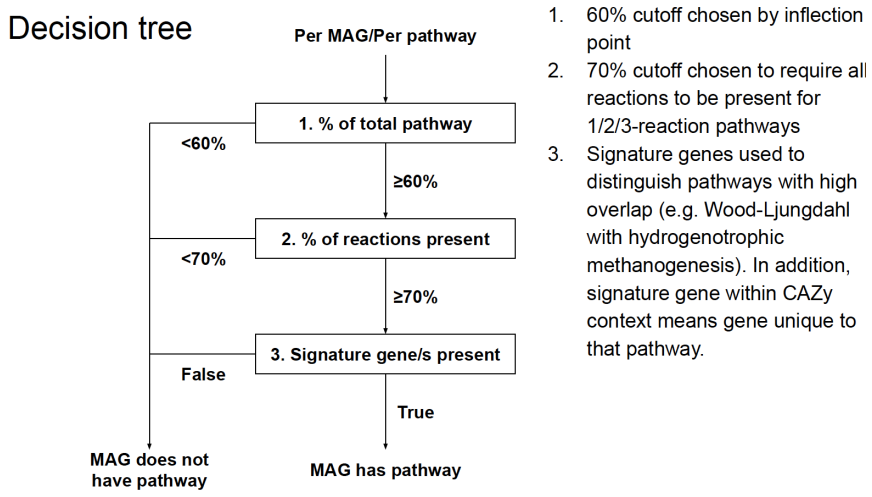

Supplemental Figure 24: A conservative decision tree for positive functional pathway calls: genomes had to contain ≥60% of the total genes in a pathway, ≥70% of the total reactions in a pathway, and the 'signature' gene(s) of a pathway to be positively identified. The 70% cutoff was chosen to require all reactions to be present for pathways with 3 or fewer reactions, and inclusion of signature genes helped distinguish between pathways with high overlap (e.g. Wood-Ljungdahl and hydrogenotrophic methanogenesis). In most cases, signature genes are those typically used in the literature to identify a pathway's presence (e.g. *acsBCD* for Wood-Ljungdahl). See Methods section on Genome Annotation for more details.

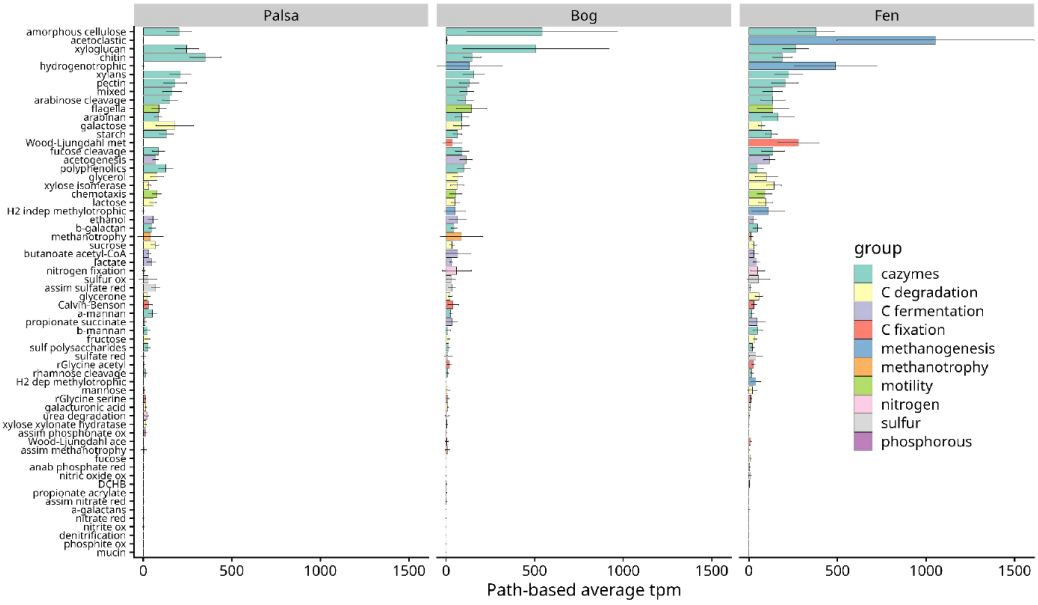

Supplemental Figure 25: Metabolic pathway expression, determined as pathway-based averaged transcripts per million (tpm), across habitats. Transcripts were averaged across reaction proteins and reactions, and summed across parallel reactions. Each bar represents the mean ± SD of pathway-averaged expression, summed across genomes and averaged across samples.

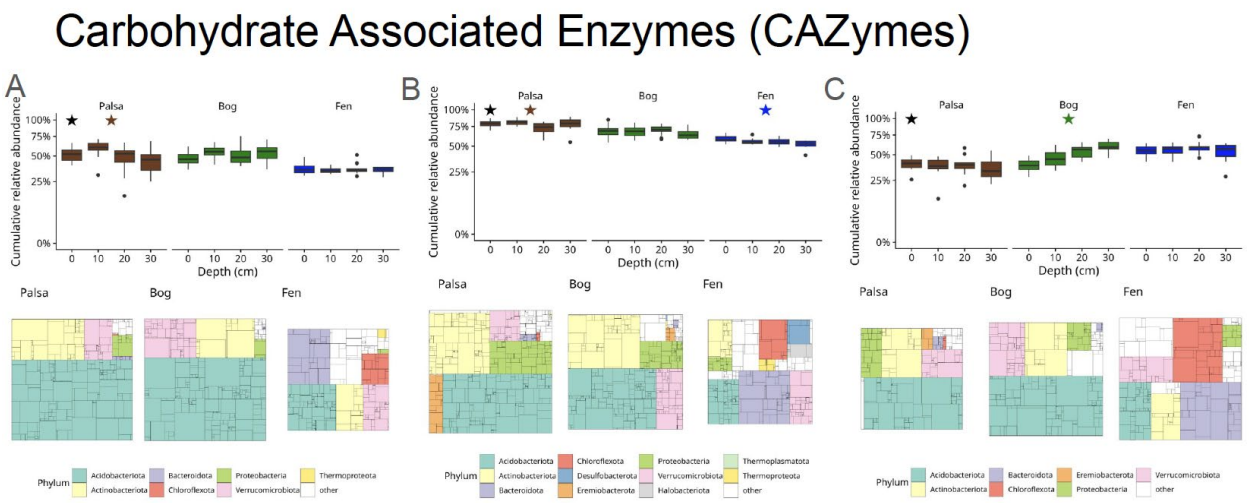

Supplemental Figure 26: The abundance and taxonomy of the MAGs across habitats that encode xylan **(a)**, starch **(b)**, and amorphous cellulose **(c)** CAZymes: box plots of encoded cumulative relative abundance over 7 years for each habitat with depth lumping of 0-9, 10-19, 20-29 and 30-39cm. Black stars represent significant differences between habitat and specific colored stars represent significant differences between depths within that habitat ($p<0.05$, Likelihood-ratio test of beta-regression (logit) with and without Habitat parameter). Treemap taxonomy where rectangles represent dereplicated MAGs, colored according to phylum and sized proportional to relative abundance.

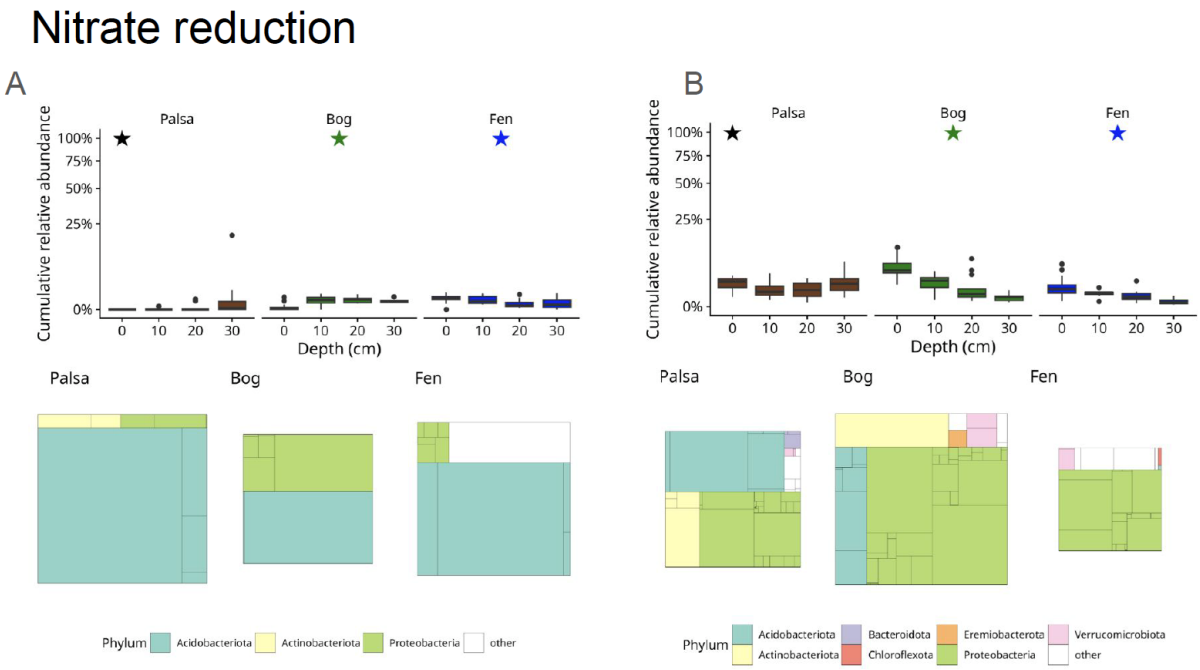

<u>Supplemental Figure 27:</u> Dissimilatory **(a)** and assimilatory **(b)** nitrate reduction: box plots of encoded cumulative relative abundance over 7 years for each habitat with depth lumping of 0-9, 10-19, 20-29 and 30-39cm. Black stars represent significant difference between habitat, and specific colored stars represent significant difference between depths within that habitat ($p<0.05$, Likelihood-ratio test of beta-regression (logit) with and without Habitat parameter). Treemap taxonomy where rectangles represent dereplicated MAGs, colored according to phylum and sized proportional to relative abundance.

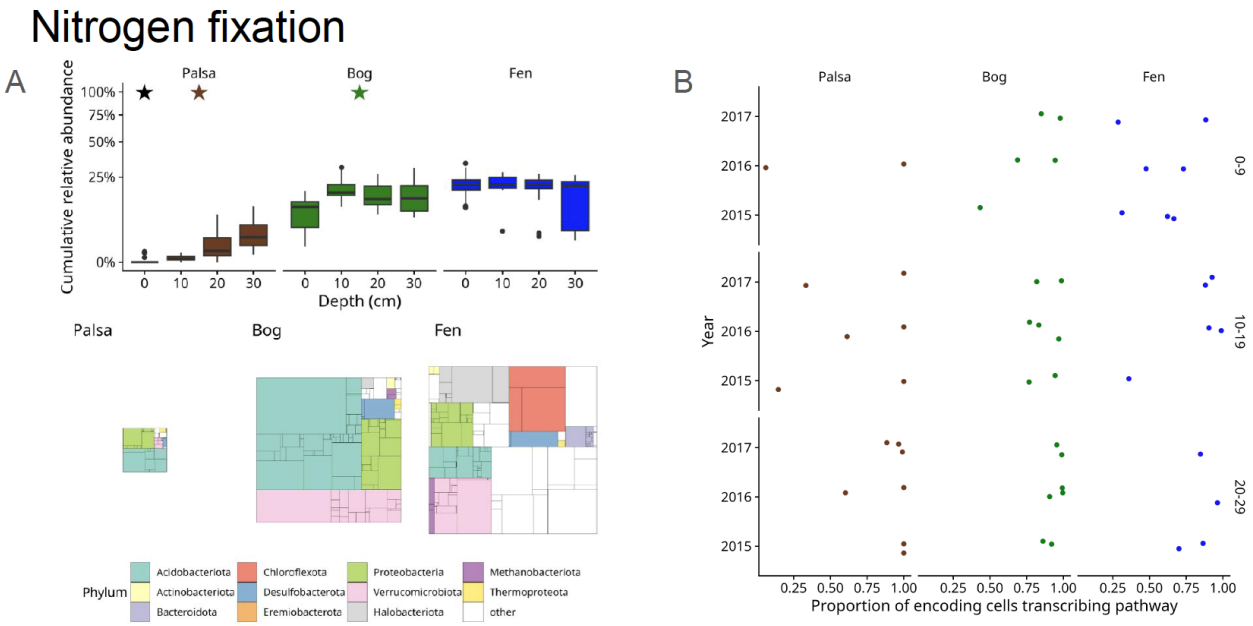

Supplemental Figure 28: The abundance and taxonomy of the MAGs that encode and transcribe nitrogen fixation across habitats. **a)** Box plots of encoded cumulative relative abundance over 7 years for each habitat with depth lumping of 0-9, 10-19, 20-29 and 30-39cm. Black stars represent significant differences between habitat and specific colored stars represent significant differences between depths within that habitat ($p<0.05$, Likelihood-ratio test of beta-regression (logit) with and without Habitat parameter). Treemap taxonomy where rectangles represent dereplicated MAGs, colored according to phylum and sized proportional to relative abundance. **b)** Taxonomic expression, averaged over specific metabolic pathway, across habitats and with depth.

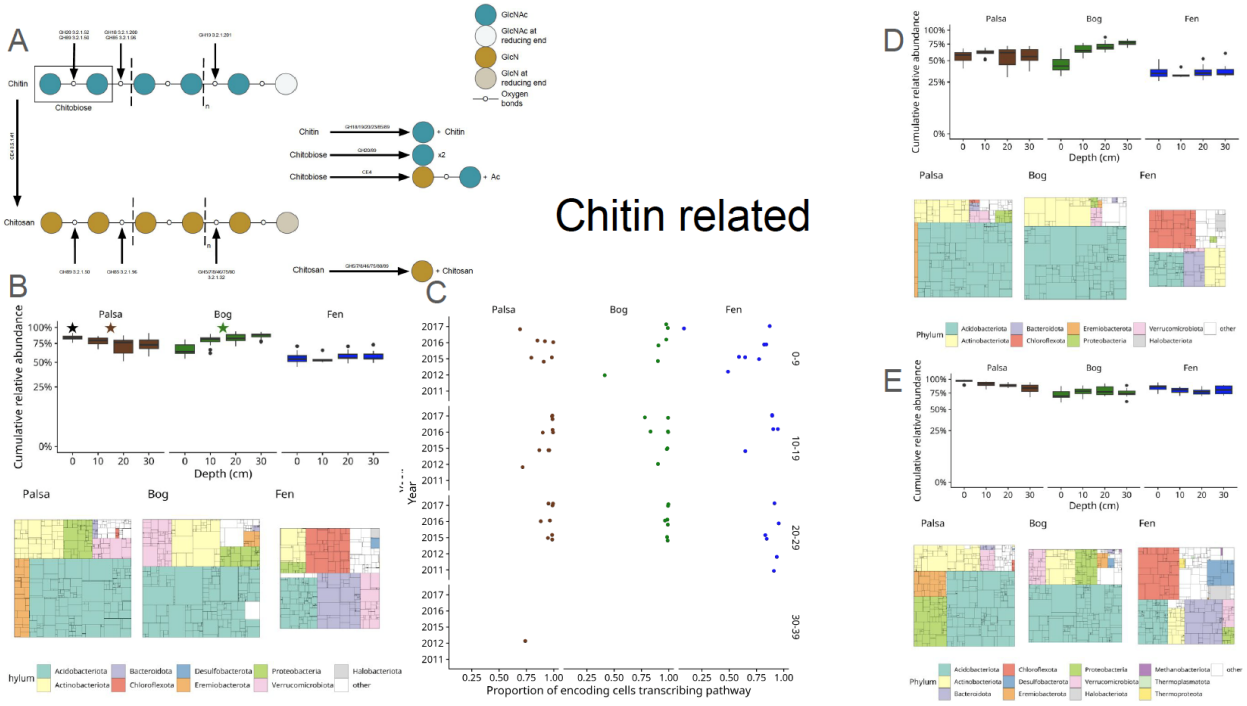

<u>Supplemental Figure 29:</u> (a) Various possible degradation pathways of chitin as determined via KEGG and CAZy.org databases. Overall positive pathway call for chitin **(b)**, specific glycoside hydrolase (GH) 18 exo-chitinase (non-reducing end), *chiB*, EC: 3.2.1.200 **(d)**, and carbohydrate esterase (CE)4 **(e)**: box plots of encoded cumulative relative abundance over 7 years for each habitat with depth lumping of 0-9, 10-19, 20-29 and 30-39cm. Black stars represent significant differences between habitat and specific colored stars represent significant differences between depths within that habitat ($p<0.05$, Likelihood-ratio test of beta-regression (logit) with and without Habitat parameter). Treemap taxonomy where rectangles represent dereplicated MAGs, colored according to phylum and sized proportional to relative abundance. **(c)** Proportion of cells transcribing positive pathway call for chitin **(b)**, as determined by dividing the number of MAGs encoding the pathway that had expression by the total number of MAGs encoding the specific pathway across habitats and with depth.

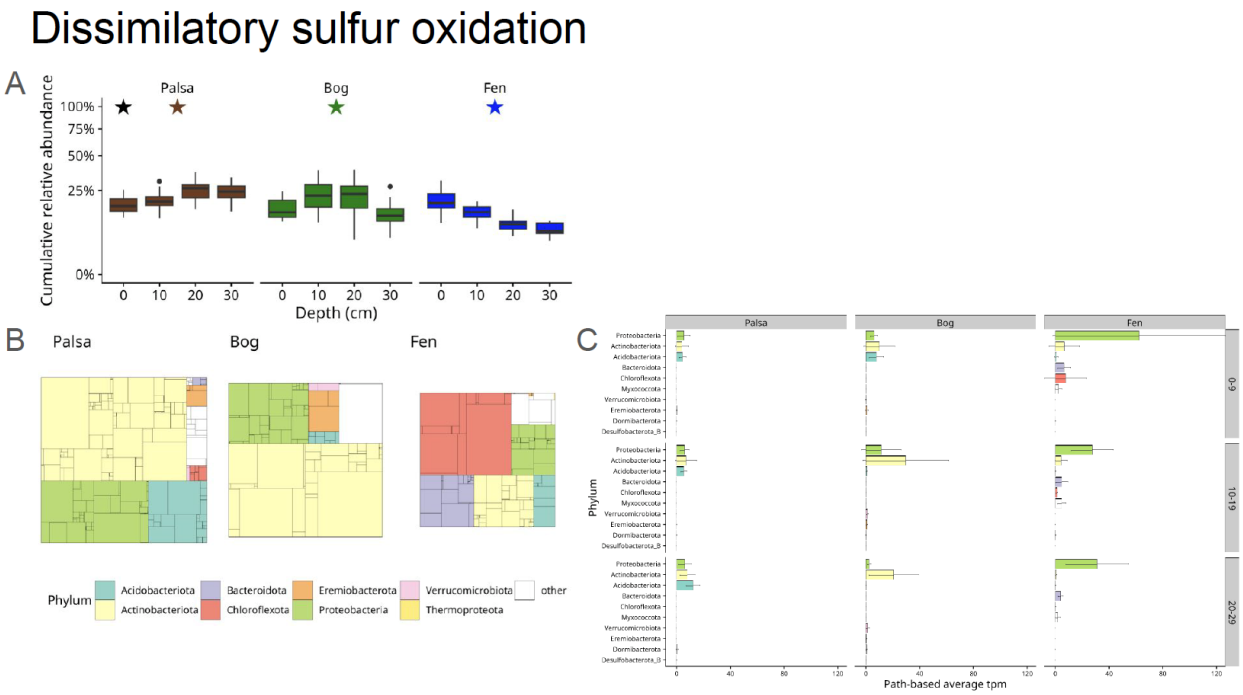

Supplemental Figure 30: The abundance and taxonomy of the MAGs that encode and transcribe dissimilatory sulfur oxidation across habitats. **a)** Box plots of encoded cumulative relative abundance over 7 years for each habitat with depth lumping of 0-9, 10-19, 20-29 and 30-39cm. Black stars represent significant differences between habitat and specific colored stars represent significant differences between depths within that habitat ($p<0.05$, Likelihood-ratio test of beta-regression (logit) with and without Habitat parameter). **b)** Treemap taxonomy where rectangles represent dereplicated MAGs, colored according to phylum and sized proportional to relative abundance. **c)** Taxonomic expression, averaged over specific metabolic pathway, across habitats and with depth.

Dissimilatory sulfate reduction

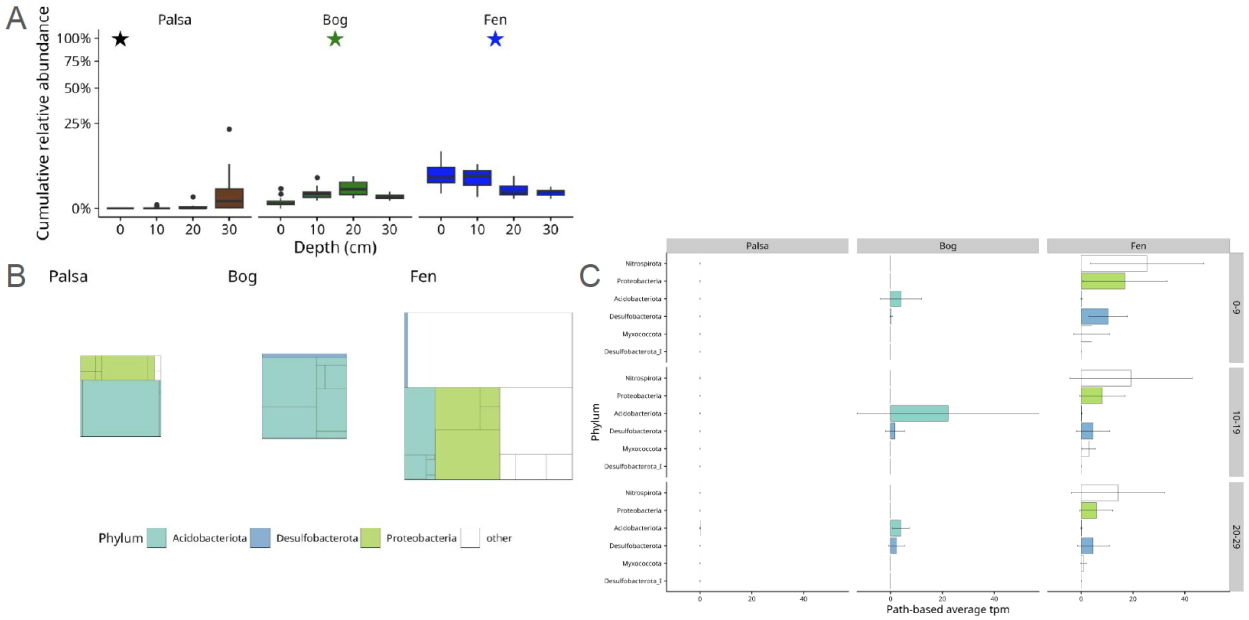

Supplemental Figure 31: The abundance and taxonomy of the MAGs that encode and transcribe dissimilatory sulfate reduction across habitats. **a)** Box plots of encoded cumulative relative abundance over 7 years for each habitat with depth lumping of 0-9, 10-19, 20-29 and 30-39cm. Black stars represent significant differences between habitat specific colored stars represent significant differences between depths within that habitat ($p<0.05$, Likelihood-ratio test of beta-regression (logit) with and without Habitat parameter). **b)** Treemap taxonomy where rectangles represent dereplicated MAGs, colored according to phylum and sized proportional to relative abundance. **c)** Taxonomic expression, averaged over specific metabolic pathway, across habitats and with depth.

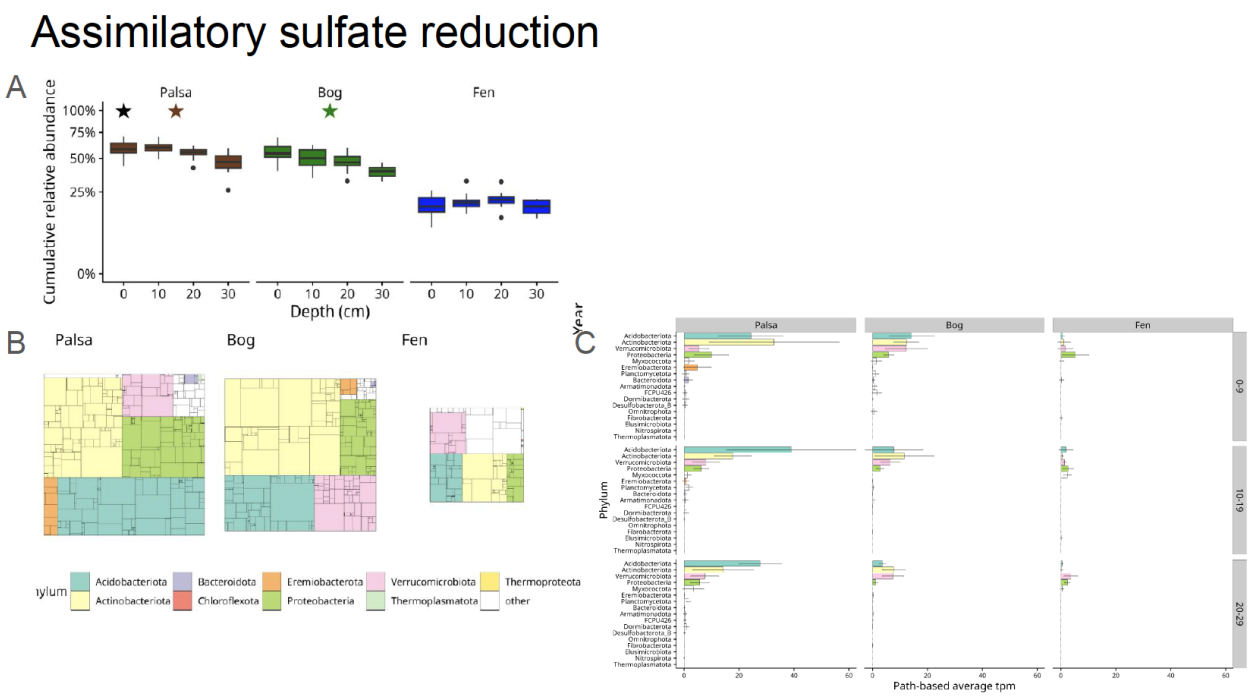

Supplemental Figure 32: The abundance and taxonomy of the MAGs that encode and transcribe assimilatory sulfate reduction across habitats. **a)** Box plots of encoded cumulative relative abundance over 7 years for each habitat with depth lumping of 0-9, 10-19, 20-29 and 30-39cm. Black stars represent significant differences between habitat and specific colored stars represent significant differences between depths within that habitat ($p<0.05$, Likelihood-ratio test of beta-regression (logit) with and without Habitat parameter). **b)** Treemap taxonomy where rectangles represent dereplicated MAGs, colored according to phylum and sized proportional to relative abundance. **c)** Taxonomic expression, averaged over specific metabolic pathway, across habitats and with depth.

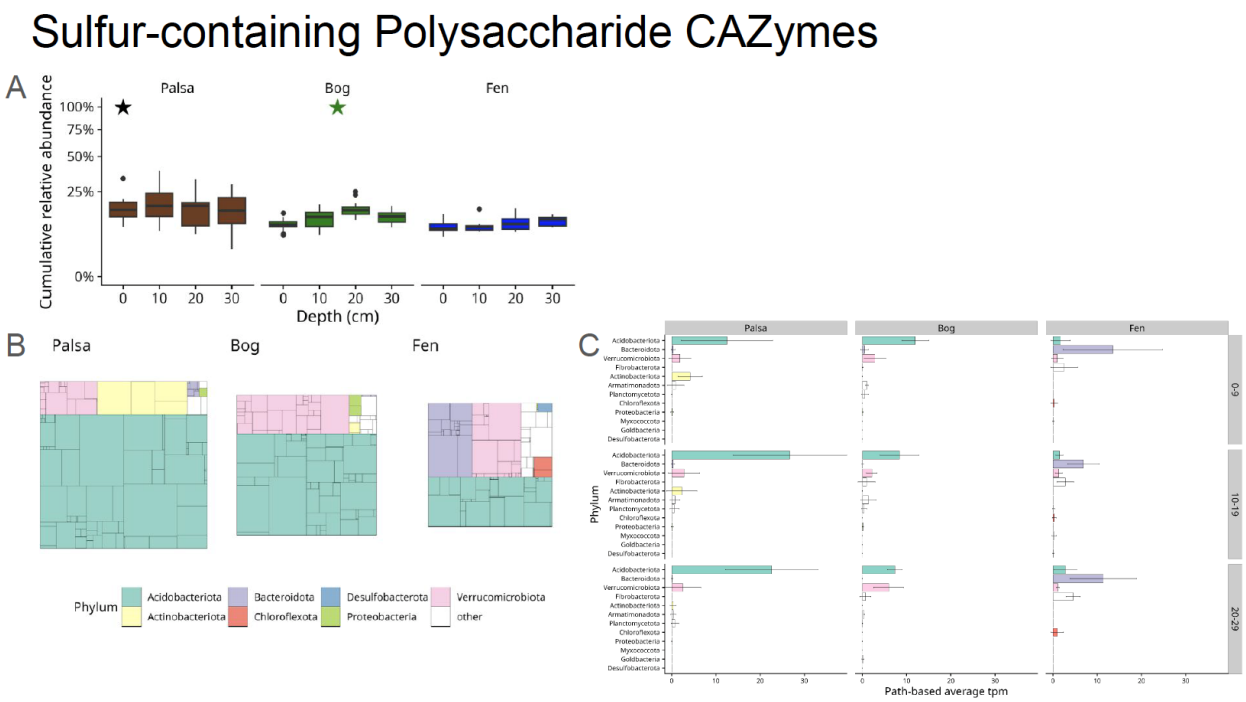

Supplemental Figure 33: The abundance and taxonomy of the MAGs that encode and transcribe the genes necessary to degrade sulfur-containing polysaccharides across habitats. a) Box plots of encoded cumulative relative abundance over 7 years for each habitat with depth lumping of 0-9, 10-19, 20-29 and 30-39cm. Black stars represent significant differences between habitat and specific colored stars represent significant differences between depths within that habitat ($p<0.05$, Likelihood-ratio test of beta-regression (logit) with and without Habitat parameter). b) Treemap taxonomy where rectangles represent dereplicated MAGs, colored according to phylum and sized proportional to relative abundance. c) Taxonomic expression, averaged over specific metabolic pathway, across habitats and with depth.

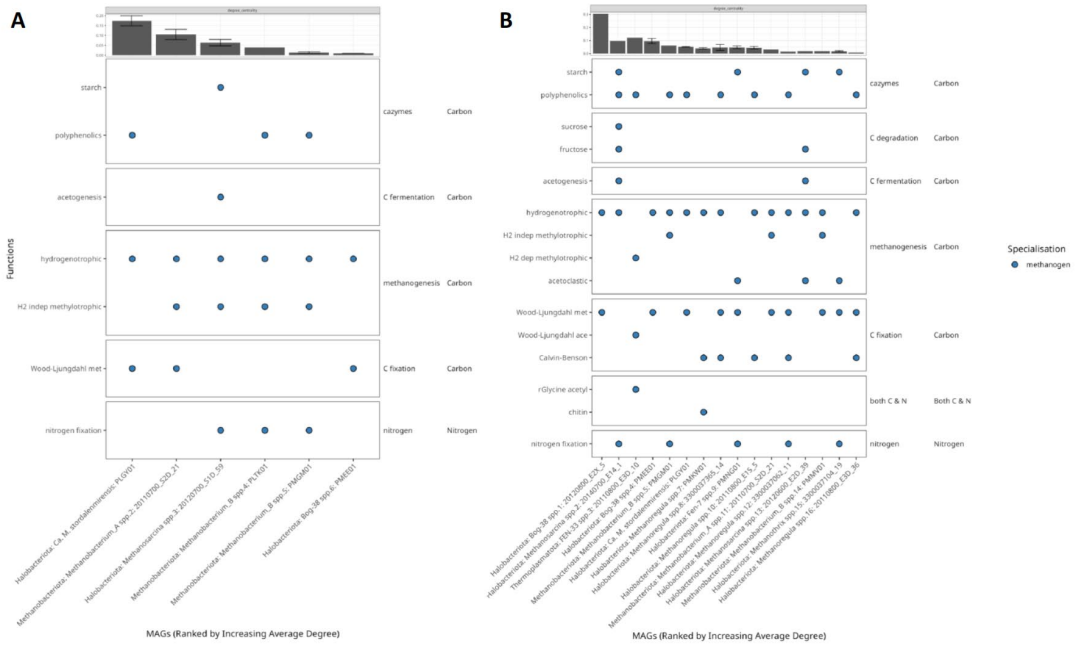

<u>Supplemental Figure 34:</u> The average degree centrality of methanogens, and their carbon and nitrogen related metabolic pathway calls from genome annotations for the **(a)** bog and **(b)** fen habitats.

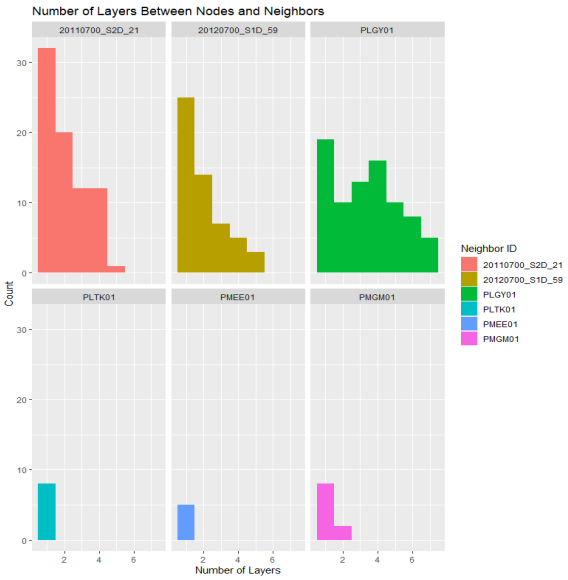

Supplemental Figure 35: The number of yearly connections in the bog habitat, derived from MTN, that exist between methanogens and other community members. The x-axis ("number of layers") is the number of years that specific neighbors persist (significant correlation exists). The y-axis (count) is the number of lineages positively correlated to each methanogen for each number of years.

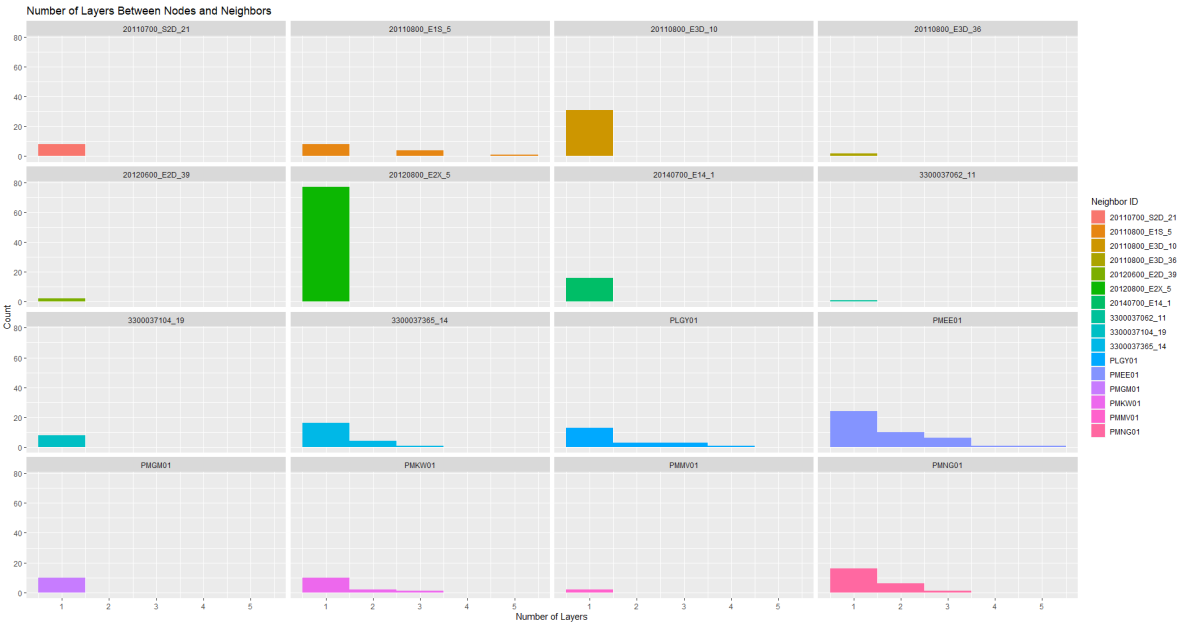

Supplemental Figure 36: The number of yearly connections in the fen habitat, derived from MTN, that exist between methanogens and other community members. The x-axis ("number of layers") is the number of years that specific neighbors persist (significant correlation exists). The y-axis (count) is the number of lineages positively correlated to each methanogen for each number of years.

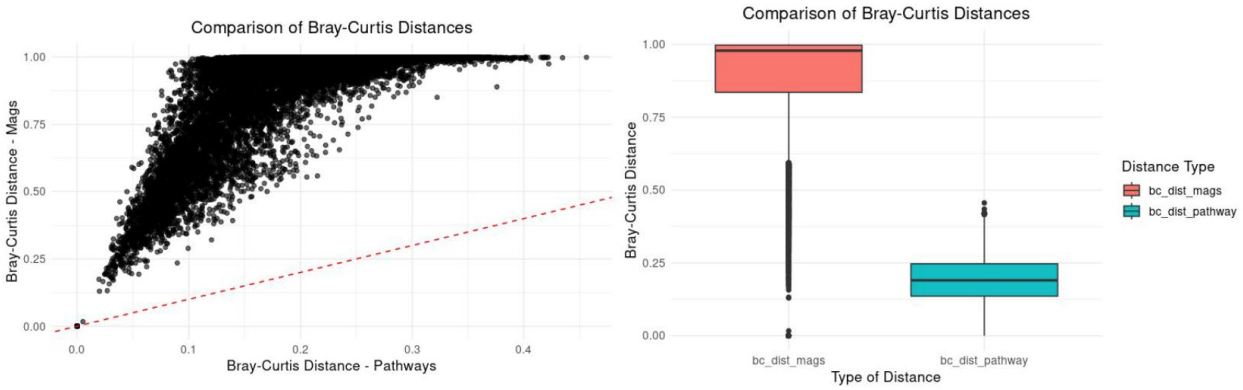

Supplemental Figure 37: The specific genes that encode the carbon, nitrogen and sulfur pathways annotated in this work show functional redundancy. The difference in community composition changes (as measured by the MAG-resolved community Bray-Curtis distance) more rapidly than changes in genes encoding annotated functional pathways ("Bray-Curtis Distance - Pathways"). This means that as new MAGs are added to the community, new pathways accumulate more slowly; stated differently, as every new MAG is added to the community, it is more likely to have the same pathways as are already observed.

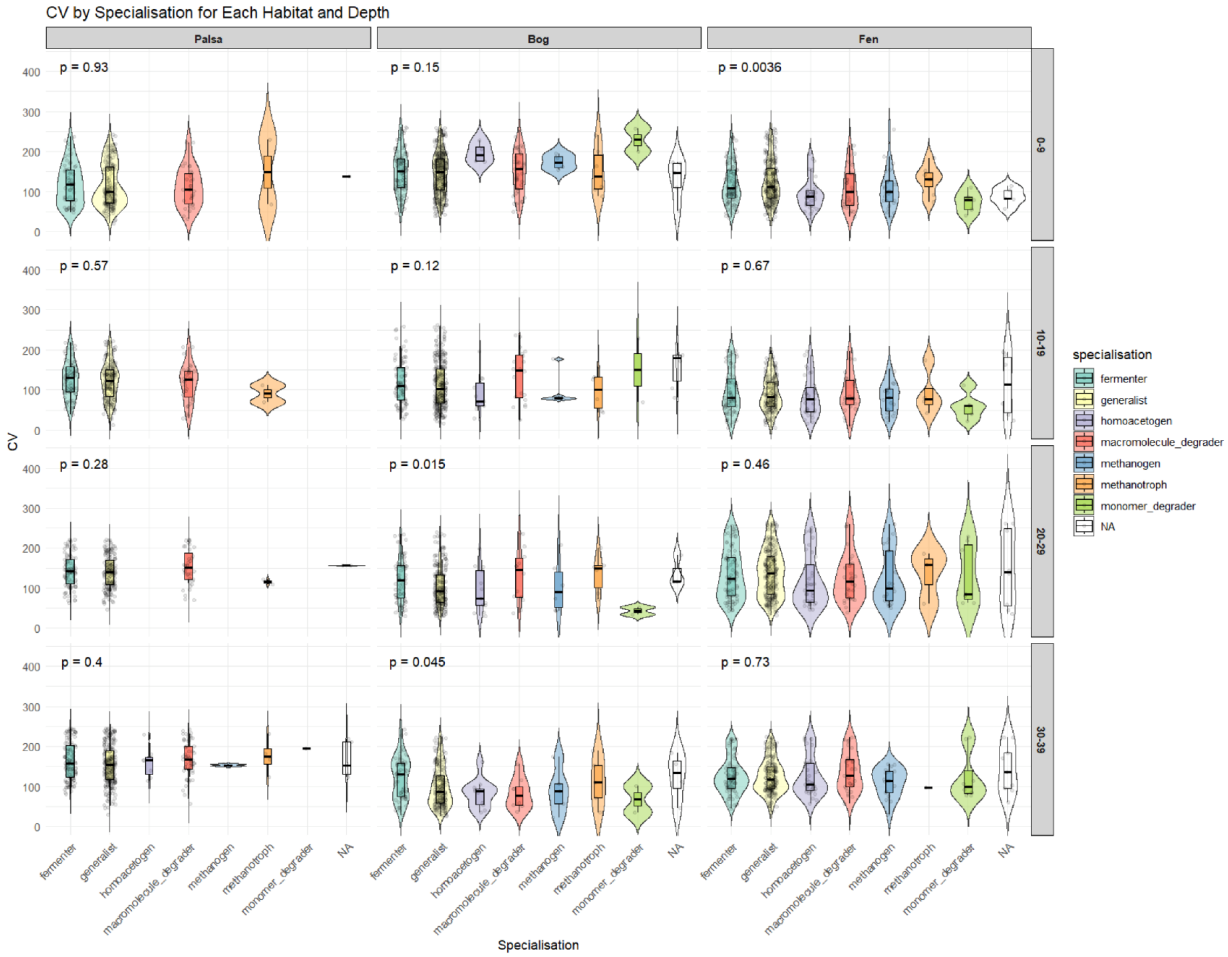

Supplemental Figure 38: Temporal variation in carbon specialization of MAGs across habitats and depths. Violin plots display the coefficient of variation (CV) over time for approximately 1,800 dereplicated MAGs (metagenome-assembled genomes), categorized by metabolic specialization across three habitats and four depth intervals. Each panel represents a depth interval, with the y-axis showing the CV and each data point corresponding to an individual MAG. The x-axis and colors indicate the metabolic specialization categories, allowing for comparisons of CV across specializations within and between habitats. Temporal variation in specialization suggests overall habitat stability but also reveals potential inconsistencies with traditional generalist-specialist definitions, particularly in the context of carbon metabolism.

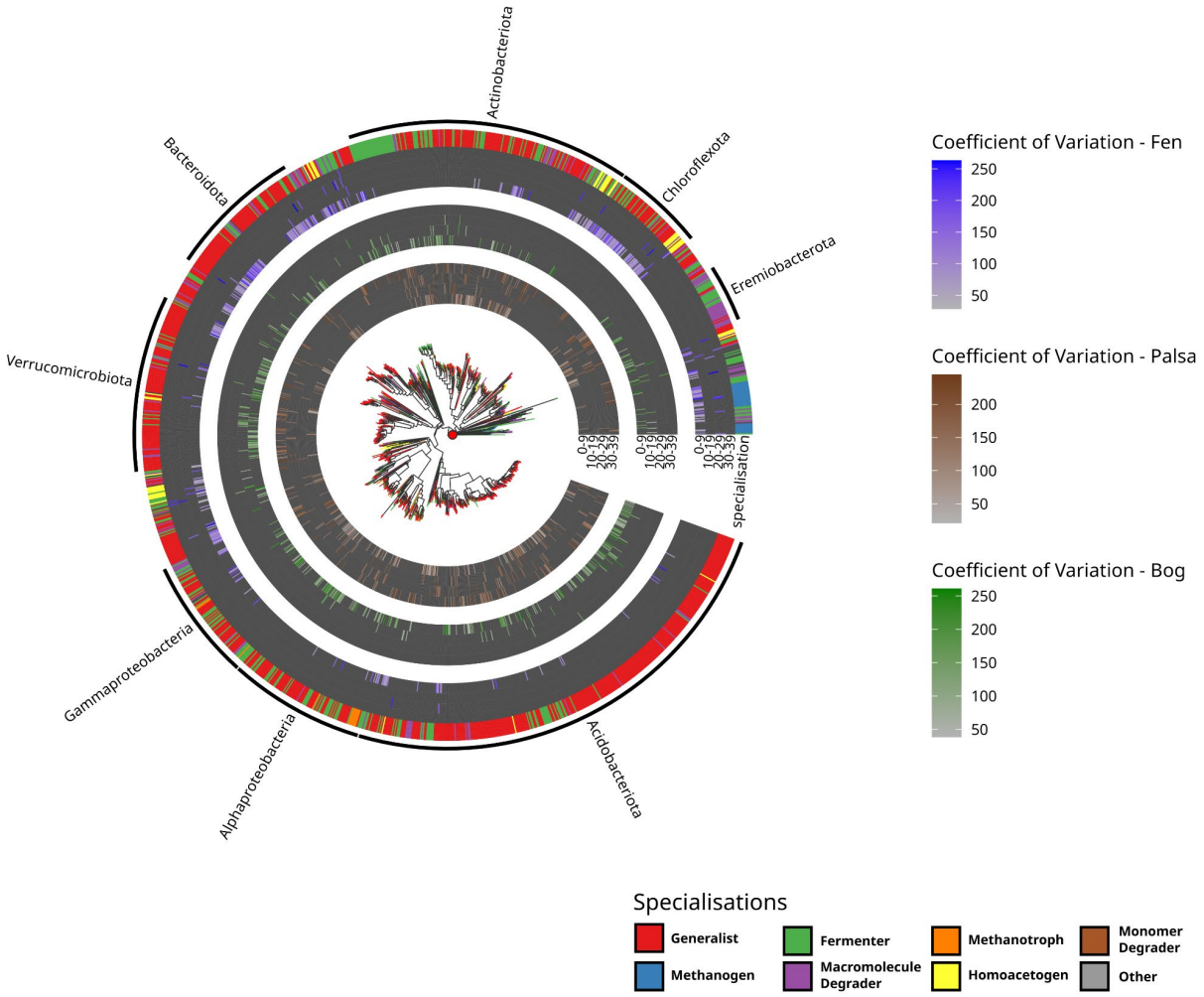

Supplemental Figure 39: Phylogenetic tree of the dereplicated ~1,800 MAGs across habitat, depth interval, shaded by habitat and the coefficient of variation, color coded by carbon specialization.

References

1. L. Wu, Y. Zhang, X. Guo, D. Ning, X. Zhou, J. Feng, M. M. Yuan, S. Liu, J. Guo, Z. Gao, J. Ma, J. Kuang, S. Jian, S. Han, Z. Yang, Y. Ouyang, Y. Fu, N. Xiao, X. Liu, L. Wu, A. Zhou, Y. Yang, J. M. Tiedje, J. Zhou, Reduction of microbial diversity in grassland soil is driven by long-term climate warming. *Nat. Microbiol.* **7**, 1054–1062 (2022).

2. K. Xue, M. M. Yuan, Z. J. Shi, Y. Qin, Y. Deng, L. Cheng, L. Wu, Z. He, J. D. Van Nostrand, R. Bracho, S. Natali, E. A. G. Schuur, C. Luo, K. T. Konstantinidis, Q. Wang, J. R. Cole, J. M. Tiedje, Y. Luo, J. Zhou, Tundra soil carbon is vulnerable to rapid microbial decomposition under climate warming. *Nat. Clim. Change* **6**, 595–600 (2016).

3. J. Feng, C. Wang, J. Lei, Y. Yang, Q. Yan, X. Zhou, X. Tao, D. Ning, M. M. Yuan, Y. Qin, Z. J. Shi, X. Guo, Z. He, J. D. Van Nostrand, L. Wu, R. G. Bracho-Garillo, C. R. Penton, J. R. Cole, K. T. Konstantinidis, Y. Luo, E. A. G. Schuur, J. M. Tiedje, J. Zhou, Warming-induced permafrost thaw exacerbates tundra soil carbon decomposition mediated by microbial community. *Microbiome* **8**, 3 (2020).

4. Q. Gao, G. Wang, K. Xue, Y. Yang, J. Xie, H. Yu, S. Bai, F. Liu, Z. He, D. Ning, S. E. Hobbie, P. B. Reich, J. Zhou, Stimulation of soil respiration by elevated CO2 is enhanced under nitrogen limitation in a decade-long grassland study. *Proc. Natl. Acad. Sci.* **117**, 33317–33324 (2020).

5. L. A. Kluber, E. R. Johnston, S. A. Allen, J. N. Hendershot, P. J. Hanson, C. W. Schadt, Constraints on microbial communities, decomposition and methane production in deep peat deposits. *PLOS ONE* **15**, e0223744 (2020).

6. K. M. DeAngelis, G. Pold, B. D. Topçuoğlu, L. T. A. van Diepen, R. M. Varney, J. L. Blanchard, J. Melillo, S. D. Frey, Long-term forest soil warming alters microbial communities in temperate forest soils. *Front. Microbiol.* **6** (2015).

7. J. Feng, C. R. Penton, Z. He, J. D. Van Nostrand, M. M. Yuan, L. Wu, C. Wang, Y. Qin, Z. J. Shi, X. Guo, E. A. G. Schuur, Y. Luo, R. Bracho, K. T. Konstantinidis, J. R. Cole, J. M. Tiedje, Y. Yang, J. Zhou, Long-Term Warming in Alaska Enlarges the Diazotrophic Community in Deep Soils. *mBio* **10**, e02521-18 (2019).

8. J. Seward, M. A. Carson, L. J. Lamit, N. Basiliko, J. B. Yavitt, E. Lilleskov, C. W. Schadt, D. S. Smith, J. Mclaughlin, N. Mykytczuk, S. Willims-Johnson, N. Roulet, T. Moore, L. Harris, S. Bräuer, Peatland Microbial Community Composition Is Driven by a Natural Climate Gradient. *Microb. Ecol.* **80**, 593–602 (2020).

9. N. C. Dove, M. E. Barnes, K. Moreland, R. C. Graham, A. A. Berhe, S. C. Hart, Depth dependence of climatic controls on soil microbial community activity and composition. *ISME Commun.* **1**, 1–11 (2021).

10. J. Curiel Yuste, A. J. Fernandez-Gonzalez, M. Fernandez-Lopez, R. Ogaya, J. Penuelas, J. Sardans, F. Lloret, Strong functional stability of soil microbial communities under semiarid Mediterranean conditions and subjected to long-term shifts in baseline precipitation. *Soil Biol. Biochem.* **69**, 223–233 (2014).

11. J. L. M. Gutknecht, C. B. Field, T. C. Balser, Microbial communities and their responses to

simulated global change fluctuate greatly over multiple years. *Glob. Change Biol.* **18**, 2256–2269 (2012).

12. K. Zhu, N. R. Chiariello, T. Tobeck, T. Fukami, C. B. Field, Nonlinear, interacting responses to climate limit grassland production under global change. *Proc. Natl. Acad. Sci.* **113**, 10589–10594 (2016).

13. S. Yang, Q. Zheng, M. Yuan, Z. Shi, N. R. Chiariello, K. M. Docherty, S. Dong, C. B. Field, Y. Gu, J. Gutknecht, B. A. Hungate, X. Le Roux, X. Ma, A. Niboyet, T. Yuan, J. Zhou, Y. Yang, Long-term elevated CO2 shifts composition of soil microbial communities in a Californian annual grassland, reducing growth and N utilization potentials. *Sci. Total Environ.* **652**, 1474–1481 (2019).

14. A. A. Carrell, M. Kolton, J. B. Glass, D. A. Pelletier, M. J. Warren, J. E. Kostka, C. M. Iversen, P. J. Hanson, D. J. Weston, Experimental warming alters the community composition, diversity, and N2 fixation activity of peat moss (Sphagnum fallax) microbiomes. *Glob. Change Biol.* **25**, 2993–3004 (2019).

15. R. M. Wilson, M. M. Tfaily, M. Kolton, E. R. Johnston, C. Petro, C. A. Zalman, P. J. Hanson, H. M. Heyman, J. E. Kyle, D. W. Hoyt, E. K. Eder, S. O. Purvine, R. K. Kolka, S. D. Sebestyen, N. A. Griffiths, C. W. Schadt, J. K. Keller, S. D. Bridgham, J. P. Chanton, J. E. Kostka, Soil metabolome response to whole-ecosystem warming at the Spruce and Peatland Responses under Changing Environments experiment. *Proc. Natl. Acad. Sci.* **118**, e2004192118 (2021).

16. M. R. Baysinger, R. M. Wilson, P. J. Hanson, J. E. Kostka, J. P. Chanton, Compositional stability of peat in ecosystem-scale warming mesocosms. *PLOS ONE* **17**, e0263994 (2022).

17. S. D. Allison, J. B. H. Martiny, Resistance, resilience, and redundancy in microbial communities. *Proc. Natl. Acad. Sci.* **105**, 11512–11519 (2008).

18. A. Shade, H. Peter, S. Allison, D. Baho, M. Berga, H. Buergmann, D. Huber, S. Langenheder, J. Lennon, J. Martiny, K. Matulich, T. Schmidt, J. Handelsman, Fundamentals of Microbial Community Resistance and Resilience. *Front. Microbiol.* **3** (2012).

19. R. Andersen, S. J. Chapman, R. R. E. Artz, Microbial communities in natural and disturbed peatlands: A review. *Soil Biol. Biochem.* **57**, 979–994 (2013).

20. J. T. Weedon, G. A. Kowalchuk, R. Aerts, S. Freriks, W. F. M. Röling, P. M. van Bodegom, Compositional Stability of the Bacterial Community in a Climate-Sensitive Sub-Arctic Peatland. *Front. Microbiol.* **8** (2017).

21. S. Monteux, J. T. Weedon, G. Blume-Werry, K. Gavazov, V. E. J. Jassey, M. Johansson, F. Keuper, C. Olid, E. Dorrepaal, Long-term in situ permafrost thaw effects on bacterial communities and potential aerobic respiration. *ISME J.* **12**, 2129–2141 (2018).

22. F. De Vries, A. Shade, Controls on soil microbial community stability under climate change. *Front. Microbiol.* **4** (2013).

23. S. Pimm, The complexity and stability of ecosystems. *Nature* **307**, 321–326 (1984).

24. J. W. Sorensen, A. Shade, Dormancy dynamics and dispersal contribute to soil microbiome resilience. doi: https://doi.org/10.1098/rstb.2019.0255 (2020).

25. B. Worm, J. E. Duffy, Biodiversity, productivity and stability in real food webs. *Trends Ecol. Evol.* **18**, 628–632 (2003).

26. C. Chang, J. HilleRisLambers, Integrating succession and community assembly perspectives. *F1000Research* **5**, 2294 (2016).

27. M. Sonesson, S. Jonsson, T. Rosswall, B. E. Rydén, The Swedish IBP/PT Tundra Biome Project Objectives-Planning-Site. *Ecol. Bull.*, 7–25 (1980).

28. T. Johansson, N. Malmer, P. M. Crill, T. Friborg, J. H. Åkerman, M. Mastepanov, T. R. Christensen, Decadal vegetation changes in a northern peatland, greenhouse gas fluxes and net radiative forcing. *Glob. Change Biol.* **12**, 2352–2369 (2006).

29. R. K. Varner, P. M. Crill, S. Frolking, C. K. McCalley, S. A. Burke, J. P. Chanton, M. E. Holmes, null null, S. Saleska, M. W. Palace, Permafrost thaw driven changes in hydrology and vegetation cover increase trace gas emissions and climate forcing in Stordalen Mire from 1970 to 2014. *Philos. Trans. R. Soc. Math. Phys. Eng. Sci.* **380**, 20210022 (2021).

30. K. Kujala, M. Seppälä, T. Holappa, Physical properties of peat and palsa formation. *Cold Reg. Sci. Technol.* **52**, 408–414 (2008).

31. T. V. Callaghan, F. Bergholm, T. R. Christensen, C. Jonasson, U. Kokfelt, M. Johansson, A new climate era in the sub-Arctic: Accelerating climate changes and multiple impacts. *Geophys. Res. Lett.* **37** (2010).

32. P. Łakomiec, J. Holst, T. Friborg, P. Crill, N. Rakos, N. Kljun, P.-O. Olsson, L. Eklundh, A. Persson, J. Rinne, Field-scale CH_4 emission at a subarctic mire with heterogeneous permafrost thaw status. *Biogeosciences* **18**, 5811–5830 (2021).

33. M. Johansson, T. V. Callaghan, J. Bosiö, H. J. Åkerman, M. Jackowicz-Korczynski, T. R. Christensen, Rapid responses of permafrost and vegetation to experimentally increased snow cover in sub-arctic Sweden. *Environ. Res. Lett.* **8**, 035025 (2013).

34. M. E. Holmes, P. M. Crill, W. C. Burnett, C. K. McCalley, R. M. Wilson, S. Frolking, K. -Y. Chang, W. J. Riley, R. K. Varner, S. B. Hodgkins, IsoGenie Project Coordinators, IsoGenie Field Team, A. P. McNichol, S. R. Saleska, V. I. Rich, J. P. Chanton, Carbon Accumulation, Flux, and Fate in Stordalen Mire, a Permafrost Peatland in Transition. *Glob. Biogeochem. Cycles* **36**, e2021GB007113 (2022).

35. D. Olefeldt, N. T. Roulet, Effects of permafrost and hydrology on the composition and transport of dissolved organic carbon in a subarctic peatland complex. *J. Geophys. Res. Biogeosciences* **117** (2012).

36. M. Hough, A. McClure, B. Bolduc, E. Dorrepaal, S. Saleska, V. Klepac-Ceraj, V. Rich, Biotic and Environmental Drivers of Plant Microbiomes Across a Permafrost Thaw Gradient. *Front. Microbiol.* **11**, 796 (2020).

37. S. Frolking, N. T. Roulet, T. R. Moore, P. J. H. Richard, M. Lavoie, S. D. Muller, Modeling Northern Peatland Decomposition and Peat Accumulation. *Ecosystems* **4**, 479–498 (2001).

38. D. Pascual, M. Johansson, Increasing impacts of extreme winter warming events on permafrost. *Weather Clim. Extrem.* **36**, 100450 (2022).

39. B. F. Thornton, M. Wik, P. M. Crill, Climate-forced changes in available energy and methane bubbling from subarctic lakes. *Geophys. Res. Lett.* **42**, 1936–1942 (2015).

40. T. H. Bell, T. Bell, Many roads to bacterial generalism. *FEMS Microbiol. Ecol.* **97**, fiaa240 (2020).

41. L. A. Malard, A. Guisan, Into the microbial niche. *Trends Ecol. Evol.* **38**, 936–945 (2023).

42. N. Fierer, M. A. Bradford, R. B. Jackson, TOWARD AN ECOLOGICAL CLASSIFICATION OF SOIL BACTERIA. *Ecology* **88**, 1354–1364 (2007).

43. A. Barberán, K. S. Ramirez, J. W. Leff, M. A. Bradford, D. H. Wall, N. Fierer, Why are some microbes more ubiquitous than others? Predicting the habitat breadth of soil bacteria. *Ecol. Lett.* **17**, 794–802 (2014).

44. S. Louca, M. F. Polz, F. Mazel, M. B. N. Albright, J. A. Huber, M. I. O'Connor, M. Ackermann, A. S. Hahn, D. S. Srivastava, S. A. Crowe, M. Doebeli, L. W. Parfrey, Function and functional redundancy in microbial systems. *Nat. Ecol. Evol.* **2**, 936–943 (2018).

45. Y.-J. Chen, P. M. Leung, J. L. Wood, S. K. Bay, P. Hugenholtz, A. J. Kessler, G. Shelley, D. W. Waite, A. E. Franks, P. L. M. Cook, C. Greening, Metabolic flexibility allows bacterial habitat generalists to become dominant in a frequently disturbed ecosystem. *ISME J.* **15**, 2986–3004 (2021).

46. M. Mariadassou, S. Pichon, D. Ebert, Microbial ecosystems are dominated by specialist taxa. *Ecol. Lett.* **18**, 974–982 (2015).

47. E. E. L. Muller, Determining Microbial Niche Breadth in the Environment for Better Ecosystem Fate Predictions. *mSystems* **4**, e00080-19 (2019).

48. D. Bajic, A. Sanchez, The ecology and evolution of microbial metabolic strategies. *Curr. Opin. Biotechnol.* **62**, 123–128 (2020).

49. K. T. Konstantinidis, J. M. Tiedje, Trends between gene content and genome size in prokaryotic species with larger genomes. *Proc. Natl. Acad. Sci.* **101**, 3160–3165 (2004).

50. B. Guieysse, S. Wuertz, Metabolically versatile large-genome prokaryotes. *Curr. Opin. Biotechnol.* **23**, 467–473 (2012).

51. S. J. Giovannoni, J. Cameron Thrash, B. Temperton, Implications of streamlining theory for microbial ecology. *ISME J.* **8**, 1553–1565 (2014).

52. D. A. Nielsen, N. Fierer, J. L. Geoghegan, M. R. Gillings, V. Gumerov, J. S. Madin, L. Moore, I. T. Paulsen, T. B. K. Reddy, S. G. Tetu, M. Westoby, Aerobic bacteria and archaea tend to have larger and more versatile genomes. *Oikos* **130**, 501–511 (2021).

53. D. R. Johnson, F. Goldschmidt, E. E. Lilja, M. Ackermann, Metabolic specialization and the assembly of microbial communities. *ISME J.* **6**, 1985–1991 (2012).

54. H. Chen, K. Ma, C. Lu, Q. Fu, Y. Qiu, J. Zhao, Y. Huang, Y. Yang, C. W. Schadt, H. Chen, Functional Redundancy in Soil Microbial Community Based on Metagenomics Across the Globe. *Front. Microbiol.* **13**, 878978 (2022).

55. I. Vanwonterghem, P. D. Jensen, K. Rabaey, G. W. Tyson, Genome-centric resolution of microbial diversity, metabolism and interactions in anaerobic digestion. *Environ. Microbiol.* **18**, 3144–3158 (2016).

56. R. K. Thauer, A.-K. Kaster, H. Seedorf, W. Buckel, R. Hedderich, Methanogenic archaea: ecologically relevant differences in energy conservation. *Nat. Rev. Microbiol.* **6**, 579–591 (2008).

57. D. Gupta, K. Chen, S. J. Elliott, D. D. Nayak, MmcA is an electron conduit that facilitates both intracellular and extracellular electron transport in Methanosarcina acetivorans. *Nat. Commun.* **15**, 3300 (2024).

58. B. J. Woodcroft, C. M. Singleton, J. A. Boyd, P. N. Evans, J. B. Emerson, A. A. F. Zayed, R. D. Hoelzle, T. O. Lamberton, C. K. McCalley, S. B. Hodgkins, R. M. Wilson, S. O. Purvine, C. D. Nicora, C. Li, S. Frolking, J. P. Chanton, P. M. Crill, S. R. Saleska, V. I. Rich, G. W. Tyson, Genome-centric view of carbon processing in thawing permafrost. *Nature* **560**, 49–54 (2018).